ISBN 978-82-326-4050-8 (printed ver.)
ISBN 978-82-326-4051-5 (electronic ver.)
ISSN 1503-8181

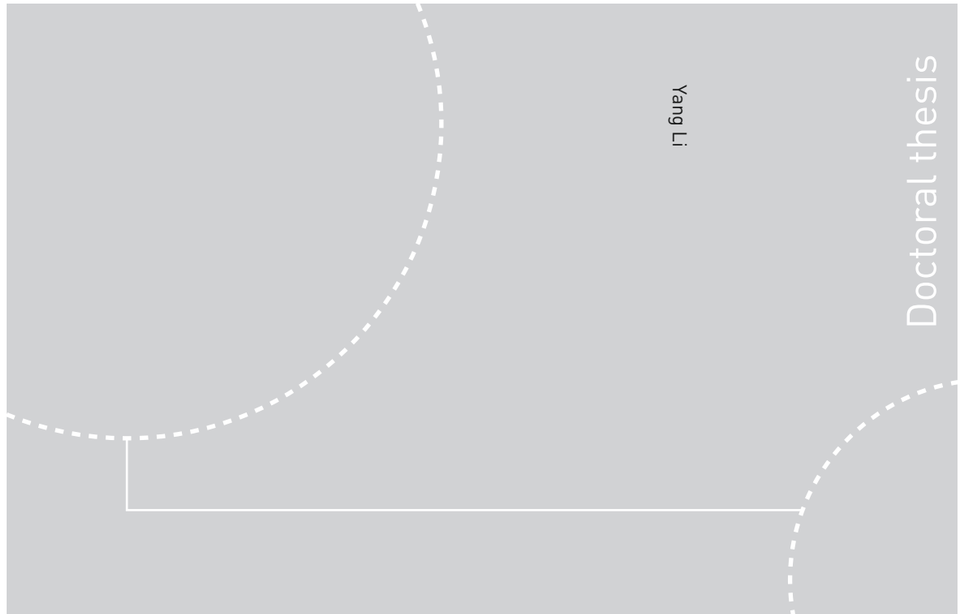

Doctoral theses at NTNU, 2019: 227

Yang Li

Numerical Study on Ductile-to-Brittle Transition of Steel and its Behavior under Residual Stresses

NTNU
Norwegian University of Science and Technology
Thesis for the Degree of
Philosophiae Doctor
Faculty of Engineering
Department of Structural Engineering

NTNU
Norwegian University of
Science and Technology

Doctoral theses at NTNU, 2019:227

NTNU

NTNU
Norwegian University of
Science and Technology

Yang Li

Numerical Study on Ductile-to-Brittle Transition of Steel and its Behavior under Residual Stresses

Thesis for the Degree of Philosophiae Doctor

Trondheim, August 2019

Norwegian University of Science and Technology
Faculty of Engineering
Department of Structural Engineering

NTNU
Norwegian University of
Science and Technology

NTNU
Norwegian University of Science and Technology

Thesis for the Degree of Philosophiae Doctor

Faculty of Engineering
Department of Structural Engineering

ISBN 978-82-326-4050-8 (printed ver.)
ISBN 978-82-326-4051-5 (electronic ver.)
ISSN 1503-8181

Doctoral theses at NTNU, 2019: 227

Printed by NTNU Grafisk senter

This PhD thesis is dedicated to my beloved mother, father and daughter.

Preface

This thesis is submitted to the Norwegian University of Science and Technology (NTNU) for partial fulfilment of the requirements for the degree of philosophiae doctor.

This doctoral work has been carried out at NTNU Nanomechanical lab, Department of Structural Engineering, Faculty of Engineering, Norwegian University of Science and Technology, Trondheim, Norway, in the period between September 2014 and April 2019. The work is mainly supervised by Prof. Zhiliang Zhang at Department of Structural Engineering of NTNU, and also by Senior Research Scientist Dr. Xiaobo Ren at SINTEF of Norway and Prof. Jianying He at Department of Structural Engineering of NTNU.

The thesis was financially supported by the Research Council of Norway through the project 'Petromaks 2 Programme', Contract No.228513/E30. And the thesis was also financially supported from Eni, Statoil, Lundin, Total, JFE Steel Corporation, Posco, Kobe Steel, SSAB, Bredero Shaw, Borealis, Trelleborg, Nexans, Aker Solutions, FMC Kongsberg Subsea, Kværner Verdal, Marine Aluminium, Hydro and Sapa. All supports are greatly acknowledged.

Yang Li

Trondheim, April, 2019

Abstract

The transition of fracture mode from ductile to brittle (DBT) is a crucial phenomenon of structural materials, e.g. body centered cubic (BCC) metals, which are normally brittle at low temperatures or high loading rates, become ductile at high temperatures or low loading rates. The DBT has aroused great concerns in science and engineering in the past years. The prediction of DBT will benefit for the application of materials in arctic engineering, particularly where avoiding the occurrence of catastrophic brittle fracture is one of the major concerns for the material or structures working at the low temperature. To this end, some important aspects pertaining to the DBT will be addressed in the present PhD thesis: (i) revealing the intrinsic mechanisms of DBT and searching a physically-motivated variable to capture the temperature dependent fracture toughness in the transition regime, (ii) exploring a framework for the modelling of DBT by implementing the micromechanical approach with this physically-based variable, (iii) studying the DBT of material or components under an important circumstance, e.g., residual stresses, through applying this framework.

The mechanism of DBT can be fundamentally discovered by studying its reverse process, e.g., brittle-to-ductile transition (BDT), in which an intrinsically brittle material fractures in a ductile manner. The BDT is not an intrinsic phenomenon of material, and depends not only on the strain rate but also on the constraint at crack tip. However, few work has been performed on studying the effect of constraint on BDT. A dislocation mobility based continuum model is employed to model the BDT behavior of single-crystal iron under different loading rates. Two scenarios of T-stress implementation in the model have been adopted to study the constraint effect on the BDT. It is found that the change of the stress distribution ahead of crack tip due to the T-stress dictates the fracture toughness in the BDT transition region. Lower constraint leads to a higher fracture toughness in the transition region, a smoother transition curve and a lower critical BDT temperature, and also a higher fracture toughness at the critical BDT temperature. A quantitative relation between fracture toughness and T-stress has been established such that the BDT curve with constraint can be estimated from a reference BDT curve. A solution to build a temperature-dependent effective surface energy law has been proposed, which could facilitate the understanding of the change of the fracture toughness in the transition region.

It is still a challenge to numerically achieve the interactive competition between ductile damage and brittle fracture in transition region. In addition, since two types of fracture occur

at two independent material length scales, it is difficult to process them with the same mesh size by using finite element method. A framework of modelling DBT of a thermal mechanical controlled-rolling (TMCR) steel is explored by using the cellular automata finite element (CAFE) method. The statistical feature of material's microstructure is incorporated in the modelling. It is found that DBT curve cannot be reproduced with only one temperature dependent flow property, for which another temperature dependent variable must be considered. A temperature dependent effective surface energy based on typical cleavage fracture stage is proposed and obtained through a continuum approach. The DBT of TMCR steel is simulated by using CAFE method implemented with a temperature dependent effective surface energy. It is found that numerical simulation is able to produce a full transition curve, especially with scattered absorbed energies in the transition region represented. It is also observed that simulation results can reproduce a comparable DBT curve contrasting to the experimental results.

The effect of residual stresses on fracture of materials or structures has been widely studied. However, its influence on DBT has rarely been investigated so far. Employing the eigenstrain method residual stresses are introduced into a bi-material specimen, where two configurations of crack and interface, e.g., one with interface perpendicular and one parallel to the crack extension, are designed to study the influence of residual stress. The DBT of the bi-material specimen in the presence of residual stresses is numerically studied by using the CAFE method where temperature dependent surface energy is implemented. It is found that residual stresses generated in the two configurations affect the DBT with a similar manner. The DBT curves generally shift to higher temperature due to the decrease of absorbed energy with the increase of residual stress. Residual stress induces a significant change of the DBT curve at higher temperature, e.g., the upper-shelf, however its influence decays with the decrease of temperature. It is found that the decrease of absorbed energy in both configurations is caused by the additional constraint on the notch root induced by the residual stress, which can facilitates the fracture.

Acknowledgement

At the moment of the first word written on this thesis, more than 4 years has elapsed since I started my PhD journey. I had to postpone the time for the accomplishment of my PhD project again and again in my time schedule. Sometimes it looked endless and hopeless like the darkness in the winter of Trondheim when I sat in front of the computer to wait for the satisfied results. I was absent in the most valuable time in the growing of my dear daughter, from an eight-month baby to a five-year girl. And, I missed so much time of staying with my family. However, like the thing you want most, the harder it is, the more it is worth being cherished. I am so lucky to have chance making my dream come true. At times I took this sentence to comfort myself when I was upset, while it is true for me. Otherwise, I would be a negligible engineer in a small company just as I had been for 9 years before I came to Norway.

The person most deserved my gratitude is my supervisor, Prof. Zhiliang Zhang, a wise, knowledgeable, humble and diligent person. I got to firstly know Prof. Zhiliang Zhang in 2011 when he visited the TGRI of CNPC where I was working for. At that time, although I was an engineer in materials field, I was eager to know something related to fracture mechanics to solve technical problems related to dynamic ductile fracture propagation and its arrest in pipeline engineering. The presentation of his achievements in fracture mechanics opened a new window to me. I was invited to visit Nano mechanical lab (NML) for 2 months in 2012, from which I learned some basic knowledges about fracture mechanics but it was still too far to be a scientist in this field. In 2014, I applied the PhD position provided by NML, and I was fortunately accepted as a PhD candidate. I am so appreciative for working with him in this long period. There were too many things learned from him no matter in research or in common life. He gave me adequate freedom and support so that I can independently carry out the researches on my PhD project. I benefited so much from his guidance and advices that I can come back to the track when I was lost. I cannot achieve the transformation from an engineer of material to a PhD of mechanics without his patience and encouragement.

I want to thank Dr. Anton Shterenlikht. He taught me so many things of CAFE method, spent his valuable time to help me solving the technical problem of CAFE code. The communications with him via emails greatly improved my acquaintances on the Linux OS and the application of CAFE method. Particularly, he hosted me when I visited the University of Bristol in UK in 2016. During that period, he always spent some time to discuss with me every day.

Faithful thanks are given to my co-supervisor Dr. Xiaobo Ren. My PhD project is intimately relevant to his work. So many helpful technical details from him always made me efficiently overcome the difficulties in numerical simulations, especially in the beginning of my PhD. His comments on the publication is very helpful. The same thanks are also given to Prof. Jianying He.

My thanks should go to my dear colleagues and friends, Dr. Jianyang Wu, Dr. Haiyang YU, Dr. Kai Zhao, Dr. Senbo Xiao, Dr. Shengwen Tu, Dr. Yuwang Xu et al. Many assistances were given by them on numerical simulation, code writing, utilizing of super-computer, scientific discussions and paper publications. Thanks also go to my colleagues in NML for their companionship, Dr. Zhiwei He, Dr. Mao Wang, Dr. Yi Gong, Dr. Xiao Wang, Dr. Hongliang Liu, Yizhi Zhuo, Li Sun, Feng Wang, Tong Li, Yuequn Fu, Siqi Liu, Bjørn Strøm, Verner Håkonsen, Sigrid Rønneberg, Merete Falck, Ingrid Snustad, Susanne Sandell, Sandra Sæther.

In the end, I must thank my parents, wife, daughter and sisters in China. I cannot intently do my PhD research without their solid supports.

List of Papers

The thesis is organized based on the following papers, which have been published or drafted by the candidate:

1. Yang Li, Xiaobo Ren, Jianying He and Zhiliang Zhang. Constraint effect on the brittle-to-ductile transition of single-crystal iron induced by dislocation mobility. *International Journal of Mechanical Sciences 149 (2018) 212–223.*
   Inspired by the theory of the shielding effect of dislocation dynamics on crack tip stress field and a continuum model developed in the literature to solve this problem in single-crystal materials. Finite element simulations has been performed. Proposed an approach to calculate the effective surface energy to assess the cleavage fracture in the transition region. Drafted the manuscript. All authors contributed to the discussion and revision.
2. Yang Li, Anton Shterenlikht, Xiaobo Ren, Jianying He and Zhiliang Zhang. CAFE based Multi-scale Modelling of Ductile-to-Brittle Transition of Steel with a Temperature Dependent Effective Surface Energy. *Materials Science and Engineering: A 755 (2019) 220-230.*
   Inspired by the CAFE method that can not only solve the numerical challenges, e.g., the competition between two different failure mechanisms in the transition region etc., but also incorporate the statistical nature of microstructure of materials. Developed the continuum model and a method to calculate the effective surface energy for the unstable cleavage fracture overcome the resistance of grain boundary in TMCR steel. Carried out all finite element simulations. Drafted the manuscript. All authors contributed to the discussion and revision.
3. Yang Li, Xiaobo Ren, Jianying He and Zhiliang Zhang. The effect of thermal residual stresses on the ductile-to-brittle transition of a bi-material specimen by using CAFE method. *Submitted to European Journal of Mechanics – A/Solids.*
   Inspired by the theory related to the inhomogeneities of materials, which can lead to an additional driving force on the crack with a shielding or anti-shielding effect. Designed two configurations of crack and interface with a mismatch of CTE. Employing the CAFE method, the influence of residual stresses on DBT has been studied. Conducted all finite element simulations and drafted the manuscript. All authors has contributed to the discussion and revision.

The PhD candidate has also held oral presentations in the following international conference/seminars:

1. Yang Li, Zhiliang Zhang, Anton Shterenlikht, Xiaobo Ren, Båod Nyhus. Predicting The Effect of Residual Stresses on Ductile to Brittle Transition of Steel by Using 3D Cellular Automata Finite Element Method. ECF21, Catania, Italy, Jun.22 2016. *Oral presentation.*

Contents

Chapter 1 Introduction

1.1 Motivation

It is expected that worldwide energy demand will increase slowly and become virtually flat after 2030, because of slower growth in productivity and global population, and continuous increases in energy efficiency. Although the mix and contribution of renewables will increase, driven by strong growth in solar and wind, the gas followed by oil will still be the two largest energy sources by the end of 2050, see Fig. 1.1 [1]. Consequently, continued investments on the exploring and developing of oil and gas will be needed over this time to maintain production at levels required to meet demand. As stated in Norwegian national technology strategy, OG21 [2], most of the "easily" recoverable hydrocarbon (HC) resources on the Norwegian continental shelf (NCS) have been produced. The exploring activity has to move into new areas with new challenges, e.g., arctic conditions. It has been assessed by the United States Geological Survey that about 30% of the world's undiscovered gas and 13% of the world's undiscovered oil may be found in the area north of the Arctic Circle [3]. It also can be estimated that the undiscovered oil and gas in NCS is 12% in the total undiscovered oil and gas in arctic region [4], see Fig. 1.2. Exploring and producing the resources in arctic region undoubtedly require further technology advancement. A very strong expanded industry consortium, built on the previously run KMB Arctic Materials project [5], shows a great industrial need on the topic. Therefore, a project SMACC (Fundamental Studies of MAterials' behavior for future Cold Climate applications), so-called Arctic Material II, see Fig. 1.3, had been launched by SINTEF in 2013 to establish a knowledge basis for robust material design and fabrication in future applications

in cold climate, which will be an essential contributor in the development of special arctic exploration technology [6].

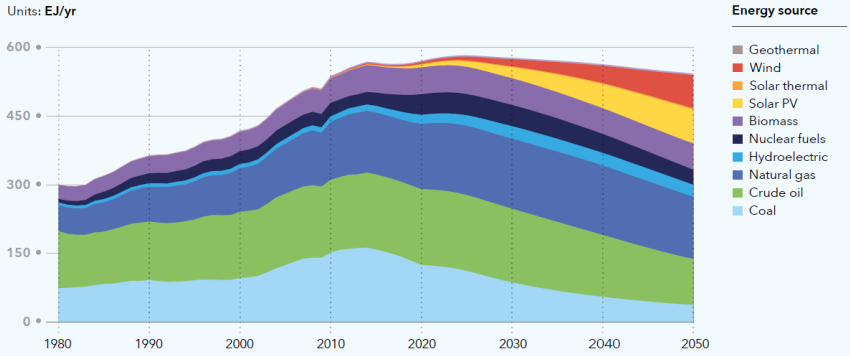

Figure 1.1 the primary energy supply by source in the world [1].

In arctic conditions, the main challenge for the application of materials and components is related to the brittle fracture possibly resulted by low temperature, which often lead to a catastrophic consequences in the engineering practice. The AM project has provided the to-date most systematic study of fracture behavior of steels in the temperature range of interest for arctic applications [7-10]. To prevent the materials or structures failed by brittle fracture, the most direct way is to explore the accurate ductile-to-brittle transition (DBT) temperature of the material, and then to ensure its DBT temperature lower than the service temperature. The transition of fracture mode from ductile to brittle is a crucial phenomenon of structural materials, e.g., body centered cubic (BCC) metals with strong interatomic forces which are normally brittle at low temperatures or high loading rates, become ductile at high temperatures or low loading rates. As such, the DBT turns to be a very important topic worthy of being studied for the materials potentially applied in arctic engineering, particularly the most widely used material, e.g., steel.

Welding process is widely utilized in fabrication because of simple procedure and minimum preparation of equipment, and furthermore the cost of welding is also economical if compared with other processes [11]. Residual stresses in engineering components are intrinsically induced by incompatible internal permanent strains due to inhomogeneous inelastic deformation, temperature gradients, or phase transformations during manufacturing and processing of the components. Residual stress produced in the welding process is a critical issue covering the whole life-cycle of welded structure. It is widely accepted that the presence of the welding residual stresses can have a significant effect on the subsequent failure

characteristics of engineering materials and components [12], for example, plastic collapse, fracture, creep, fatigue, stress corrosion, assessment of structural integrity etc. In service, the associated residual stresses may combine with applied stresses to cause unexpected failure or to shorten the component lifetime [13]. However, it has been demonstrated that the current procedures can significantly overestimate the residual stress effects in most cases [14]. In this regard, residual stresses associated with welding are an unavoidable topic and play an important role in the fracture of materials and structures applied in arctic environment.

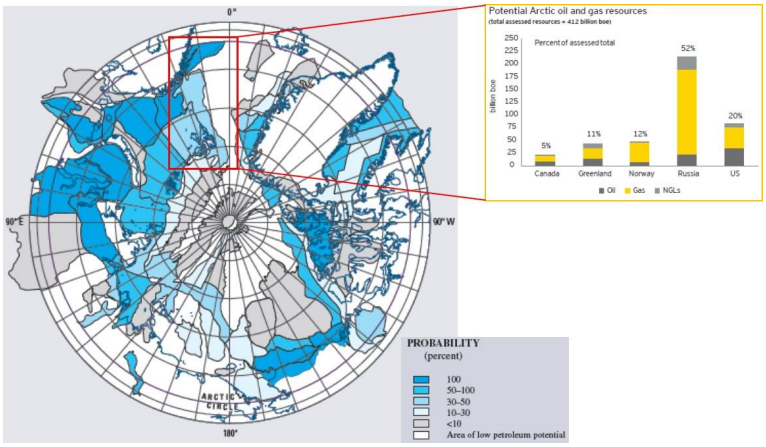

Figure 1.2 distribution of undiscovered oil and gas in arctic region and the fraction of Norway [4].

The topic of the DBT or residual stress is generally a conventional issue but quite important for the application of materials and components in arctic engineering. Although DBT or residual stress has been well-studied individually in the past decades, there are still some challenges or uncertainty need to be resolved. However, the coupling of both, namely the effect of residual stress on DBT, has rarely been studied in the literature. In this perspective, the study focused on the influence of residual stress on the DBT is not only a practical issue to arctic engineering but also a scientific topic in the fracture mechanics.

1.2 objectives and technical route

The present PhD thesis written as a part of SMAAC project, was motivated by the developing a framework on the modelling of the DBT of steel, and further applying this framework in the study of the effect of residual stress on the DBT. Particularly, in order to distinguish with the work in the literature, a certain of physically-based variable and solutions have to be addressed and explored. To this end, several critical tasks are brought into the focus in present PhD study:

- The mechanism of the DBT needs to be intrinsically understood, by which a physically-based variable is found so that the temperature dependent fracture toughness in fracture transition region can be captured.
- A framework of modelling of the DBT of a TMCR steel is to be established when numerical approaches is adopted.
- The effect of residual stresses on DBT of a weld TMCR steel, in which the possible configurations of the crack and interface formed by the mismatch of CTE are considered for the common welding practice and subsequent fracture toughness test.

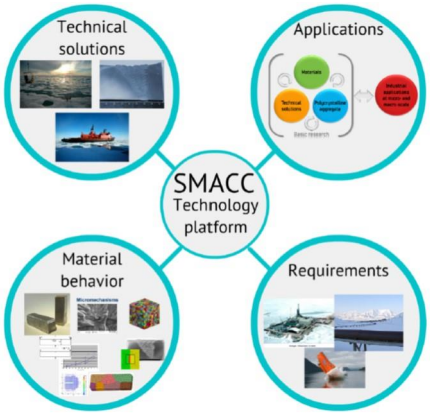

Figure 1.3 the schematic of the project of SMACC [6].

To achieve the objectives, a technical route has been designed to perform the PhD work, presented in Fig. 1.4, in which all the important steps in each task are also included. In task 1, following the theory of the shielding effect of dislocation dynamics on crack tip, a fundamental work of studying the BDT of single-crystal iron is conducted to reveal the mechanism of DBT by using a continuum approach, in which a method to estimate the effective surface energy, e.g., γ_{eff}, in the transition region is established. In task 2, a new continuum approach is developed to calculate the effective surface energy of unstable cleavage formation in a TMCR steel, e.g., γ_{pm}, based on the continuum model developed in task 1. In order to describe the essence of the competition between particle size and grain size-controlled propagation of unstable cleavage, a more robust variable, γ_{mm} e.g., the effective surface energy for unstable cleavage propagation, is proposed on the basis of γ_{pm}. Finally, a framework for the modelling of DBT is explored through implementing the γ_{mm} into the CAFE method. In task 3, the developed modelling framework of the DBT is applied to investigate the influence of residual stresses on DBT of the weld joint of TMCR steel. It is known that an additional driving force

on crack can be produced due to the inhomogeneity of material. The residual stress is essentially caused by the inhomogeneity of material at the interface in a weld joint, e.g., the mismatch of CTE. 2 configurations of crack and interface are designed corresponding to the common welding practice and subsequent fracture toughness test, e.g., Charpy tests on the repair weld and girth weld. The influence of residual stresses on the DBT of a weld joint is studied with these 2 configurations.

It should be noted that the continuum approach and the variable γ_{pm} in task 2 are very similar to the continuum model and effective surface energy γ_{eff} in task 1. To explain this, the hidden logic between task 1 and task 2 has to be introduced. The necessity of exploring a physically-based variable, e.g., effective surface energy of unstable cleavage formation, e.g., γ_{pm}, to capture the temperature dependence fracture toughness in the transition region is actually motivated by the modelling of the DBT of steel with CAFE method. However, it is too difficult to directly obtain this variable with a continuum model. To circumvent the complexity induced by grain boundary, pre-existing dislocations and particles, we have to start from a simpler body centered cubic (BCC) material, e.g., single-crystal iron. In addition, the theory of the shielding effect of dislocation dynamics on crack tip is rigorously only applicable to single crystal material. On the basis of the continuum model for single crystal material, the new continuum approach can be developed to calculate the effective surface energy of steel.

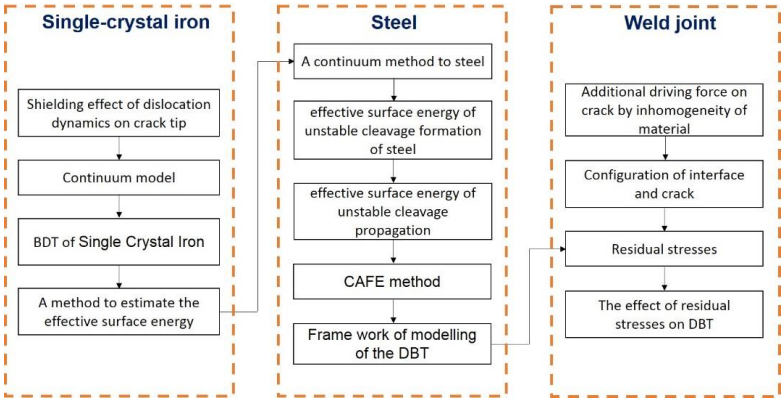

Figure 1.4 technical route of the work in PhD thesis

1.3 Thesis outline

The thesis consists of two main parts, namely a general introduction and a collection of 3 peer-reviewed journal papers. The introduction of PhD thesis is divided into four chapters. The

motivation, project background and research objectives are presented in C**hapter 1**. Then, the literatures relevant to this PhD work are reviewed in **Chapter 2**. **In Chapter 3**, the theories, continuum model and micromechanical approach, numerical procedures adopted in this work are introduced, the designed configurations for residual stress generation and the method for the constraint on crack tip due to residual stress and are presented as well. The main findings of this PhD study are summarized in **Chapter 4**. Finally, recommendations of further work are provided in **Chapter5**.

Chapter 2 Literature Review

Fracture of materials and components has been studied for almost one hundred years. To assess the integrity of structures with flaws, methodologies with a single parameter, such as G [15, 16] and K [17, 18] based on linear elastic fracture mechanics (LEFM), J [19] and $CTOD$ [20] based on elastic-plastic fracture mechanics (EPFM), have been developed to deal with problem under small-scale yielding (SSY). Further, two-parameter approaches have been proposed to characterize constraint effect on crack tip by geometries J–T [21, 22], J–Q [23-25] , J–A2 [26], mismatch J-M [27], residual stress J-R [28] and pre-strain J-P [29], through extending the HRR solution with higher-order terms. These approaches, so-called 'global approach', are extremely useful and definitely necessary, but also they have some limitations [30]: (i) these approaches have dramatic dependence of geometry and are not the intrinsic properties of material, (ii) the mechanism of failure of material are not adequately disclosed, e.g., ductile damage and cleavage. In this chapter, a review on the research relevant to the PhD work in the literature is presented, especially regarding the micro-mechanistically based approaches applied for the numerical simulation.

2.1 Ductile fracture

Polycrystalline metal alloys, e.g., carbon steel and aluminum alloy, may fail in a ductile, most often transgranular manner, involving extensive plasticity and rough fracture surfaces. The ductile fracture can be usually physically-described as a three stages process [31]. Voids nucleate at material defects, e.g., inclusions and second-phase particles, by either interface decohesion or particle cracking. Growth of voids around the particles due to the plastic strain

and stress triaxiality. Coalescence of growing voids with adjacent voids forms a microcrack finally leads to a macroscopic failure. This classic description of ductile damage process mostly prevails at high stress triaxiality, in which the coalescence of the enlarged coarser voids initiated from large inclusions occurs by a mechanism of internal necking of voids. For example, in a notched round tensile bar failed by the void coalescence, the fracture path is normally flat or zigzagged. However, ductile failure often occurs due to the plastic instability of the specimen. Accordingly, the fracture surface exhibits total or partial slanting, or tensile bars in plane strain and thin sheets present a cup-cone fracture in the shear lips, which is normally referred as shear failure. Shear failure is associated with the formation of shear bands [32], particularly, in the absence of a shear component in the remote loading. The schematic illustration of these two mechanisms of ductile failure is presented in Fig. 2.1.

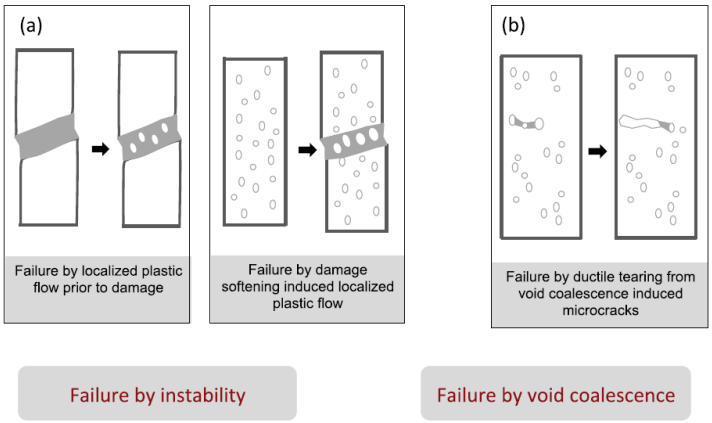

Figure 2.1 The two generic modes of ductile failure [33]: (a) by plastic instability; and (b) by void coalescence.

2.1.1 Micromechanics of ductile damage

Void nucleation. The void nucleates at the second phase particles commonly by means of particle decohesion and particle cracking. It is observed by means of X-ray tomography [34], nucleation predominately occurs by particle decohesion in a soft matrix, e.g., pure Al, see Fig. 2.2 (a). On the contrary, in a hard matrix, e.g., structural Al alloy, particle cracking is typically favored, see Fig. 2.2 (b). Other parameters except for the matrix hardness also play a role in particle induced void nucleation [33], e.g., matrix yield stress, matrix hardening exponent, particle stiffness, stress triaxiality and load orientation etc. Under shear dominated loading, void nucleation occurs by decohesion at a hard particle of a alumina [35], however in the end void distortion takes place since that the lack of hydrostatic tension does not provide a driving force for growth.

Since second phase particles are often considered to be purely elastic and brittle, the condition of void nucleation is usually similar to the criterion of brittle fracture in terms of the Griffith theory, e.g., the energy release rate must exceed or equal the surface energy required to create a new surface. As such, cracking occurs when local stresses at particle-matrix interface are higher than a material dependent critical stress, e.g., σ_c, which leads to a critical nucleation strain expressed as a function of the particle radius, the particle volume fraction and macroscopic mean stress [36, 37]. Beremin research group applied Argon et al. [37] criterion to experimental data for a C-Mn steel has proposed an analytical method to predict the void nucleation,

$$\sigma_c = \sigma_1 + \beta\kappa\left(\sigma_{eq} - \sigma_0\right) \qquad (2-1)$$

where σ_1 is the macroscopic maximal principal stress, σ_{eq} is the macroscopic von Mises stress and σ_0 the yield stress, κ is a geometrical factor depending on the inclusion shape and β is a numerical factor which accounts for local matrix hardening. Some FE simulations have been performed to study the particle cracking and interface decohesion by using cohesive zone models (CZM) [38-40].

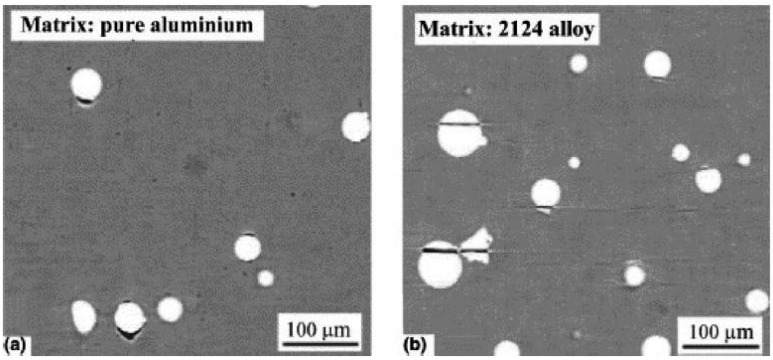

Figure 2.2 Mechanisms of void nucleation in simple tension of model Al metal matrix composites [34]: (a) Particle-matrix decohesion in a soft matrix, (b) Particle cracking in a hard matrix.

Void growth. The growth of artificially inserted voids has been observed in situ by means of tomography by Weck et al. [41], in which the void enlargement occurs in copper subjected to simple tension. Since the stress concentrates on the void, the voids elongate at a relatively larger rate along the tensile direction, and also grow laterally to an extent commensurate with the increase of triaxiality induced by necking. With the increase of load, the kinetics of void growth dramatically changes due to plastic flow localization in the elongated ligaments. In contrast to above cases where large voids are artificially embedded in the material, engineering alloys also have populations of second phase particles as the potential void nucleation sites,

where nucleation simultaneously occurs at multiple separate scales except for the large voids growth. This brings a certain of challenges for modeling with the conventional continuum framework, e.g., analytical model proposed by Rice and Tracy [42]. In particular, the nucleation at fine precipitates can affect the plastic flow behavior (strength and hardening). In most cases the critical voids enlarge while the fine particles remain intact e.g., carbides in steels, see Fig. 2.3.

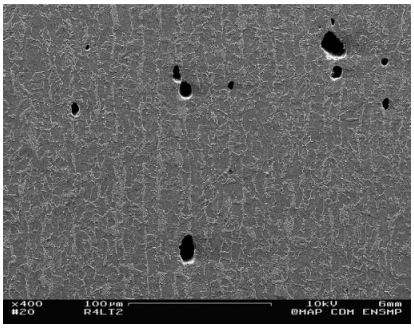

Figure 2.3 Void growth in low carbon steel [33]. Voids nucleate at large inclusions while carbides remain intact.

The first micromechanical models to describe the void growth were developed for an isolated cylindrical [43] or spherical void [42] in a rigid plastic matrix, which are related to the stress triaxiality and plastic strain. It has been found by Rice and Tracy [42] that for a spherical void in a variety of stress states, the void growth rate could be approximated by an analytical relationship

$$\frac{\dot{R}}{R} = \alpha exp\left(\frac{3}{2}\frac{\sigma_m}{\sigma_0}\right)\dot{\varepsilon}_{eq} \qquad (2-2)$$

where R is the radius of the void, $\dot{R}$ is the growth rate of void, α is a numerical factor, σ_m is mean stress, $\dot{\varepsilon}_{eq}$ is the equivalent plastic strain rate. The Rice and Tracy model does not consider the interaction between voids and the effect of void growth on material behavior, e.g., softening. To solve this problem, Gurson [44] proposed a model for a finite sphere containing a spherical void in a rigid perfectly plastic matrix, in which a variable f, e.g., void volume fraction, is used to describe the damage. Later, Tvergaard [45, 46] modified the Gurson model by analyzing the plastic flow in a porous medium by assuming that the material behaves as a continuum, so-called GT model. This modification to conventional plasticity theory has the effect of introducing a strain-softening term. In contrast to the Rice and Tracy model, GT model contains a failure criterion. Ductile fracture is assumed to occur as the result of a plastic instability that produces a band of localized deformation. Such an instability occurs more

readily in a GT material since the strain softening induced by hydrostatic stress [47]. A plastic yield function taking into account the porosity can be described by

$$\frac{\sigma_{eq}^2}{\bar{\sigma}^2} + 2q_1 f cosh\left(\frac{3q_2}{2}\frac{\sigma_m}{\sigma_0}\right) - (1 + q_3 f^2) = 0 \qquad (2-3)$$

where $\bar{\sigma}$ is the flow stress for the matrix material, q_1, q_2 and q_3 are constant. Further, Foleskog et al. [48] have addressed that q_1, q_2 and q_3 are relevant to the strain hardening and yield stress of matrix material when studying the void growth by using unit cell method. The void growth rate is obtained by following form

$$\dot{f} = (1-f)\dot{\varepsilon}_{kk}^p \qquad (2-4)$$

where $\dot{\varepsilon}_{kk}^p$ is the trace of the rate of plastic strain tensor. These models introduced above only deal with the spherical void in the matrix material. Lately, Gologanu et al. [49] proposed a model incorporating the effect of void shape on ductile damage with a shape factor *S*. Further, on the basis of GT model a model coupling the void shape and plastic anisotropy was proposed by Benzaga et al. [50] and Monchiet et al. [51].

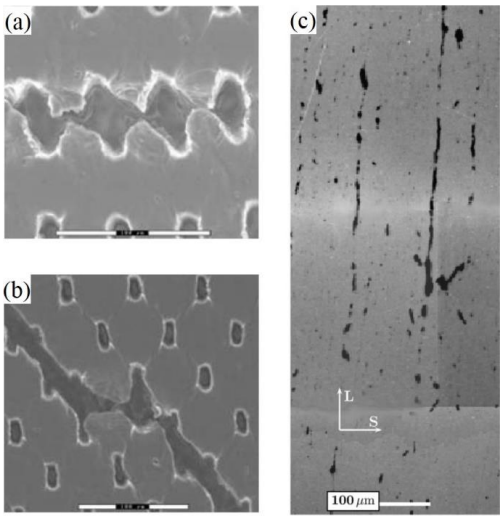

Figure 2.4 Modes of void coalescence: (a) internal necking [52], (b) internal sheering [52], (c) 'necklace' formation [33].

Void coalescence. The coalescence of voids is a stage where a stable diffuse plastic deformation prompting the voids growth transits to a localized mode of plastic deformation within the ligament separating two voids or a row of voids. Void coalescence may generally be categorized into 3 modes [33]: (i) internal necking, where the ligament between the two voids shrinks with a typical necking process [52], see Fig. 2.4 (a); (ii) internal shearing of the intervoid ligament, see Fig. 2.4 (b), in which localized shear causes distant voids to coalesce

by void rotation from an initial orientation at 45 degree from the loading axis. The micrograph normally shows inside the shear localization band with the presence of secondary small voids, so-called void sheeting [31, 32]. This mode of coalescence is often found in high strength material with low or moderate strain hardening capacity. Due to the particle locking on voids at equators, internal necking is not possible despite of the close packing, and finally coalescence by localized shear might occur [33]; (iii) "necklace" coalescence [33], see Fig. 2.4 (c), where linking-up of the voids takes place in rows of closely spaced voids gathering within elongated clusters. This coalescence mode is less common in practice.

A model proposed by Thomason [53, 54] assumes that void coalescence occurs when the intervoid ligament reaches its plastic limit load. This model derives from an axisymmetric unit cell for a periodic array of ellipsoidal voids in an elastic-perfectly plastic matrix, see Fig. 2.5. The internal necking is assumed to take place in the plane normal to the principal tensile stress, e.g., σ_I. The Thomason's coalescence can be written:

$$\phi^T(\sigma, \chi, w) = \sigma_I - \sigma^T = 0 \qquad (2-5)$$

$$\sigma^T(\chi, w) \equiv \sigma_0(1-\chi^2)\left[\alpha^T\left(\frac{\chi^{-1}-1}{w}\right)^2 + \beta^T\sqrt{\chi^{-1}}\right] \qquad (2-6)$$

where σ_0 is the yield stress of matrix, σ^T is the critical net section stress between voids, α^T and β^T are constant equal to 0.1 and 1.2 respectively. Zhang et al. [55] firstly compared the prediction of coalescence of an initially spherical void against to the numerical results of cell model analysis by Koplik and Needleman [56]. The comparison showed that the Thomason model is surprisingly accurate in describing the coalescence. later, Pardoen and Hutchinson [57] extend this model through incorporating the effect of strain hardening by treating $\alpha^T(n)$ and $\beta^T(n)$ as functions of the strain hardening exponent n. Recently, the Thomason's model is revised by considering a circular cylindrical geometry of the void [58]. In addition, an extension of the condition (2-6) to the presence of a second population of voids has been proposed by Fabregue and Pardoen [59]. These models are basically applicable to the coalescence under predominate tensile load and predict no effect of shear on coalescence. However, Torki et al. [60] extends the theory to the void coalescence under combined tension and shear by explicitly considering the microscopic deformation field around the void in fully analytical form. Tvergaard and Needleman [61] have attempted to model void coalescence by artificially replacing f in Eq. (2-3) with an effective void volume fraction f^*in the following way:

$$f^* = \begin{cases} f & for\ f \le f_c \\ f_c - \dfrac{f_u^* - f_c}{f_F - f_c}(f - f_c) & for\ f > f_c \end{cases} \qquad (2-7)$$

where f_c is the void volume fraction at the onset of coalescence, f_c, f_u^* and f_F can be fitted through cell computation parameters. The effect of hydrostatic stress is amplified when $f > f_c$, which accelerates the onset of a plastic instability.

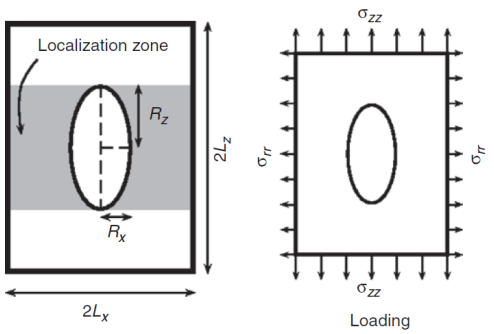

Figure 2.5 Geometry of Thomason coalescence model [30]. Here, $\chi = \frac{R_x}{L_x}$, $w = \frac{R_z}{R_x}$.

Additionally, quantitatively study on the void coalescence has been performed by finite element unit cell calculations [48, 56, 62], in which the material is often idealized by a periodic packing of simple unit cells containing spheroidal voids of volume fraction f_0, aspect ratio, and spacing parameter.

Ductile failure by instability. Ductility can also be limited by mechanical instability of the test piece or component. The key difference between failure by void coalescence and plastic instability is that damage by void nucleation, distortion and coalescence is essential in the former, however, damage may or may not be important in the latter depending on what drives the plastic instability. Failure by instability normally involves the formation of shear bands and failure along the most intense shear band, which is often induced by strain localization at a length scale greater than the mean spacing between voids [33]. The aspects triggering shear band have been widely studied in the literature by both analytical and computational methods, which have been summarized in the Ref. [33]. For precracked specimens, the failure mechanism in thin sheet of high strength Al alloy and steel presents a slant mode [63, 64], which develops soon after crack initiation with the occurrence of shear bands near the crack tip. In general, the following conditions is going to favor the slant fracture [33]: (i) a low strain hardening capacity; (ii) plastic anisotropy; (iii) void nucleation at second population of voids; (iv) decrease the thickness of specimen with a plane strain condition; (v) no side grooves.

Classical metal plasticity theory assumes that the flow stress is independent of the third deviatoric stress invariant (or Lode angle parameter). However, recent experiments on metals have shown that both the pressure effect and the effect of the third deviatoric stress invariant should be included in the constitutive description of the material [65]. Zhang et al. [66] and Gao and Kim [62] observed that ductile damage are strongly related to both the stress triaxiality and the degree of shear loading defined by the Lode parameter. The influence of lode parameter on the shear failure has been intensively studied [67-71]. Under the shear dominated load, an initially spherical void would be elongated, and rotate, eventually close into a penny shaped crack, unless localization in the ligament takes place before closure [33]. This could be illustrated in Fig. 2.6, where void drastically distorts by the void rotation in a shear field and results in a strain localization as a wide shear band. Recently, Xue [72] introduced a Lode-dependent shear damage parameter based upon the solution of McClintock et al. [73] for coalescence in a shear band. Nahshon and Hutchinson [74] extended the GT model to account for shear-induced softening by directly incorporating the third stress invariant into the void evolution model.

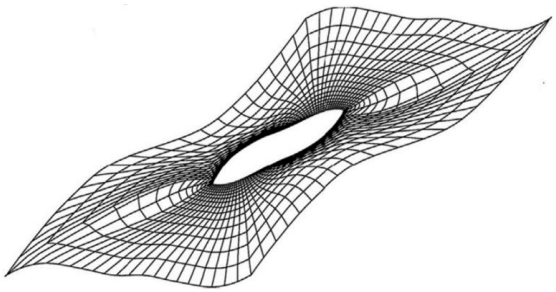

Figure 2.6 simulated void distortion in a shear field [69].

2.1.2 Predictive models for ductile fracture

GTN model. On the basis of GT model, see Eq. (2-3) and (2-4), Chu and Needleman [75] modified the void growth with the contribution of new void nucleation as

$$\dot{f} = (1-f)\dot{\varepsilon}_{kk}^{p} + \Lambda\dot{\varepsilon}_{eq}^{p} \qquad (2-8)$$

where the first term defines the growth rate of the preexisting voids, and the second term quantifies the contribution of new voids are nucleated with plastic strain, e.g., nucleation at small second-phase particles. The scaling coefficient Λ was given by

$$\Lambda = \frac{f_N}{S_N\sqrt{2\pi}} exp\left[-\frac{1}{2}\left(\frac{\varepsilon_{eq}^{p} - \varepsilon_N}{S_N}\right)^2\right] \qquad (2-9)$$

It assumes that the plastic strain range at nucleation of new voids follows a normal distribution with a mean value ε_N, a standard deviation S_N, and a volume fraction of void nucleating particles f_N. Later, Tvergaard and Needleman [61] have introduced a void coalescence criterion f_c, see Eq. (2-7), and replace the void volume fraction f with an effective void volume fraction f^* in Eq. (2-3) of GT model. Then, the micromechanical model, so-called Guron-Tvergaard-Needleman (GTN) model, are formed, which is widely used to predict the ductile fracture with a damage process of void nucleation, growth and coalescence.

However, in GTN model the void coalescence criterion f_c is an empirical variable selected beforehand or numerically fitted from tension tests. Moreover, there was no experimental and numerical evidence to support the stress state independence of f_c [76]. There actually are two modes of plastic deformation, e.g., diffuse plasticity described by GT model and localized plasticity during calescence represented by Thomason's model. This implies that the yield surface of voided material is given by the intersection of two surfaces correspondence to each deformation mechanism [30], see Fig. 2.7. Recall the Thomason model [53, 54] (Eq. (2-5) and (2-6)), it neglects the damage growth and overestimate the localized deformation. As such, Zhang [76] modified the GT model by coupling the Thomason model [53, 54] to deal with the void coalescence, so-called the complete Gurson model (CGM).

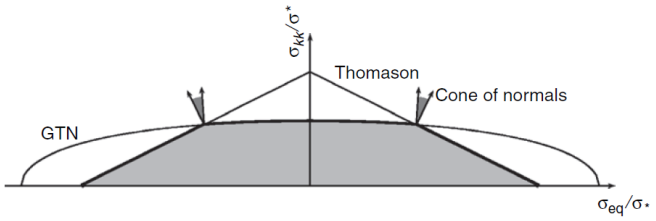

Figure 2.7 yield surface as the intersection of the GTN yield surface (thick line) and Thomason yield surface [30]. σ^* is the effective stress of matrix.

Rousselier model. Based on the thermodynamics framework proposed in Lemaitre and Chaboche [77], Rousselier [78, 79] has developed a model, in which the damage originated from second phase particles under external load is described with a damage variable. The yield surface is expressed as

$$\frac{\sigma_{eq}}{\rho} + B(\beta)Dexp\left(\frac{\sigma_m}{\rho\sigma_1}\right) - H(\varepsilon_{eq}) = 0 \qquad (2-10)$$

where $H(\varepsilon_{eq})$ is the hardening property of material; σ_1 and D are material constants that need to be tuned; σ_{eq}, σ_m and ε_{eq} are equivalent stress, mean stress and equivalent strain; β is a

scalar damage variable; ρ is relative density obtained by dividing the density of the damaged material by that of the undamaged material, which can be described by

$$\rho = \frac{1}{1 - f_0 + f_0 exp\beta} \qquad (2-11)$$

$B(\beta)$ is the function of damage variable β, which can be written as

$$B(\beta) = \frac{\sigma_1 f_0 exp\beta}{1 - f_0 + f_0 exp\beta} \qquad (2-12)$$

where f_0 is initial void volume fraction. β is related to plastic deformation and damage which can be described as

$$\dot{\beta} = \dot{\lambda} D exp\left(\frac{\sigma_m}{\rho\sigma_1}\right) \qquad (2-13)$$

Where $\dot{\lambda}$ is the increment of the plastic multiplier. The von Mises yield surface and the yield surface modified by the Rousselier Eq. (2-10) is presented in Fig. 2.8. Samal [80] has developed a nonlocal damage law for the Rousselier model, so-called non-local Rousselier model, trying to solve the mesh dependence problem in numerical simulation, where the damage growth law is defined in terms of the local void volume fraction but keeping a local definition for strain.

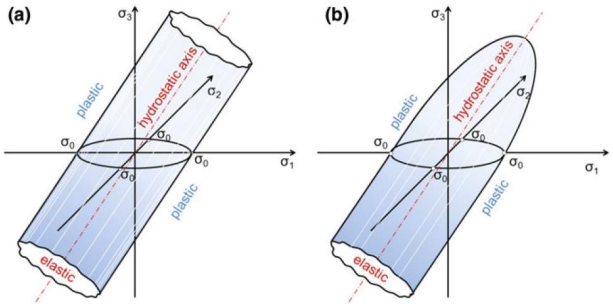

Figure 2.8 Yield surface [81]: (a) von Mises, (a) Rousselier.

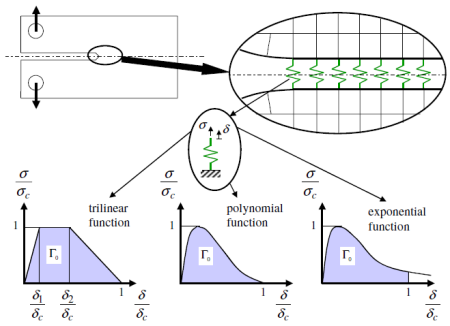

Figure 2.9 Cohesive zone model approach with three typical traction-separation laws used in the literature [33].

CZM. The cohesive zone model (CZM) is a phenomenological approach to treat fracture as a gradual phenomenon in which the separation takes place across an extended crack tip or cohesive zone, and is resisted by cohesive tractions. Cohesive zone elements do not denote any physical material, but describe the cohesive forces of material elements under external load, e.g., tensile. CZM has been developed firstly for the brittle fracture and also widely adopted to simulate the fracture in ductile materials [82-85] through a traction-separation law (TSL), see Fig. 2.9. In these TSLs, the failure in cohesive elements is all determined by the critical parameters, such as the work of separation, e.g., cohesive energy Γ_0, cohesive stress σ_c and critical separation length δ_c, in which the critical separation length δ_c can be calculated from the former two parameters in terms of the TSL.

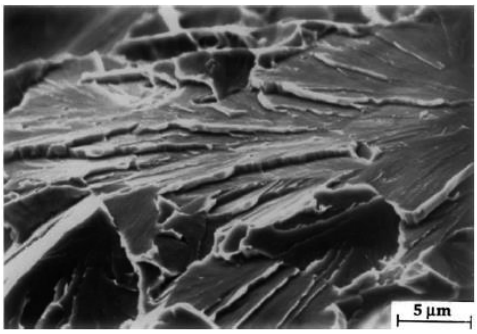

Figure 2.10 River patterns in an A 508 Class 3 steel [47].

2.2 Brittle fracture

A brittle fracture is an unstable failure process, where rapid crack propagation occurs with low energy releasing and without significant plastic deformation. Brittle fracture in polycrystalline metals can be generally categorized into two types: transgranular fracture e.g., cleavage, and intergranular fracture. The crack of cleavage fracture always propagates along a particular crystallographic plane with the lowest packing density, where fewer bonds is to be broken and the spacing between planes is greater, e.g., $\{100\}$ plane of body centered cubic (BCC) metals. The propagating crack changes direction when it crosses a grain boundary, sub-grain boundary or twin boundaries, which leads to various cleavage facet with different orientation. However, on a macroscopic scale, the nominal orientation of the cleavage crack is always perpendicular to the maximum principal stress, e.g., mode I fracture. The cleavage fracture normally shows a 'river patterns' on its fracture surface, see Fig. 2.10. The intergranular fracture is usually caused by the aspects, such as, the segregation of impurities or precipitation of brittle particles at the grain boundary, intergranular corrosion, grain boundary cavitation and cracking at high

temperature etc. In this section, it is emphasized on the cleavage fracture since it is more commonly observed on the structural materials.

2.2.1 Mechanism of cleavage

Theoretically, the normal stress, σ_c, needed to fracture a crystal, e.g., a single-crystal iron at 0 K, by cleavage, can easily be determined provided that the bonding energy, U, between the atoms located across the cleavage plane is known. For single-crystal iron The σ_c can be calculated as [33]

$$\sigma_c = (E\gamma_s/b)^{0.5} \qquad (2-14)$$

where $E = 200\ GPa,\ b$ burger's vector equals 0.3 nm, surface energy $\gamma_s = 1 J/m^2$. Then, the σ_c is estimated to be $E/10$. This theoretical value of σ_c is much higher than the experimental values found for classical metallic samples. The reasons for the large difference between the observed and the calculated values for σ_c ascribes to the local stress concentration due to the inherent defects in the polycrystalline materials, e.g., micro-cracks or second phase particles. In this case, the fracture stress is given by the Griffith theory σ_c^G under the condition of plane stress [47]:

$$\sigma_c^G = (E\gamma_s/\pi a)^{0.5} \qquad (2-15)$$

where a is the size of defect.

It has been observed that in ferritic steel cleavage is formed with three elementary steps: (i) particle cracking induced by dislocation piled up, so-called cleavage nucleation; (ii) microcrack propagation across the interface between particle and matrix; (iii) crack propagation across the grain boundary. The first event is governed by a critical stress described in Eq. (2-1), which is normally applies when the particle size is larger than 0.1-1.0μm [33]. Otherwise, a dislocation-based theory should be used [36]. The mechanisms of the latter two steps of cleavage fracture can be described in terms of local values of the fracture toughness [33], $K_{Ia}^{c/f}$(carbide/ferrite) and $K_{Ia}^{f/f}$(ferrite/ferrite), or $\gamma_{c/f}$ and $\gamma_{f/f}$in terms of surface energy, that must be satisfied for the crack propagation across the first barrier (particle/matrix) and the second barrier (grain boundary), as schematically shown in Fig. 2.11. Accordingly, the critical values of the particle and grain size in this figure, C* and D* are simply related to the local value of the maximum principal stress, σ_I, in terms of the Griffith theory [47].

$$C^* = \left(\frac{\delta K_{Ia}^{c/f}}{\sigma_I}\right)^2 \ and\ D^* = \left(\frac{\delta K_{Ia}^{f/f}}{\sigma_I}\right)^2 \qquad (2-16)$$

where δ is a numerical factor related to the shape of the microcrack and close to 1. Once the crack arrests at the interface of particle and matrix, the broken particle could be the source of void initiation as mentioned in section 2.1.1. Crack arresting at boundaries with large misorientation has been found in ferritic steel [86-88], and crack arresting at boundaries with a large twist angle has been also reported [89-91]. It is reported that the local values of the calculated fracture toughness $K_{Ia}^{c/f}$ and $K_{Ia}^{f/f}$ are much lower than the macroscopic fracture toughness, K_{IC} [33]. One of the reasons for this is related to possible dynamic effects, not accounted for in cleavage propagation. As such, a similar theory about the cleavage fracture has been proposed by Lin et al. [92], in which the dynamic strain energy release rate (effective fracture energy), G_{cf} and G_{ff} for crack propagation across the interface and grain boundary to capture the dynamic response on the cleavage fracture, as a schematically shown in Fig. 2.12. Accordingly the fracture stress for crack propagating across the interface and grain boundary can be calculated by

$$\sigma_{cf} = \sqrt{\frac{\pi E G_{cf}}{(1-\nu^2)C}} \; and \; \sigma_{ff} = \sqrt{\frac{\pi E G_{ff}}{(1-\nu^2)D}} \qquad (2-17)$$

where C and D are particle and grain size corresponding to the C* and D* in Eq. 2-16. The dynamic behaviour of cleavage crack nucleation has been studied by Kroon and Faleskog [93] via the unit cell dynamic FEM calculation. It indicates that the microscopic stress for cleavage initiation within a dynamic process could be overestimated in terms of the Griffith criterion, see Fig. 2.13. Actually Eq. 2-15 and Eq. 2-16 are essentially identical since both G_{cf} and G_{ff} are unlikely to obtained from experimental work. In practice, G_{cf} and G_{ff} are substituted by $\gamma_{c/f}$ and $\gamma_{f/f}$, so-called effective surface energy in two critical steps of cleavage fracture, to estimate the fracture stress. If cleavage fracture is local stress dominated, then it implies that the unstable cleavage propagation depends on the competition of these two criteria, see Eq. (2-16) and (2-17). At very low temperature, cleavage can be controlled by the microcrack propagating across the interface, while at increasing temperature cleavage is controlled by the propagation of microcracks across the grain boundaries. This competition and the role of grain boundaries on the cleavage have been discussed in detail in paper 2 [94]. Few experimental results have been published in the literature to validate these models. However, these models have been adopted to estimate the effective surface energy for crack of cleavage fracture to overcome the barrier of grain boundaries, e.g., $\gamma_{f/f}$, based on the competition between two criteria [94-96]. The results shown that $\gamma_{f/f}$ is much larger than $\gamma_{c/f}$ and is strongly temperature dependent, in which a constant value of $\gamma_{c/f} = 7J/m^2$ tested by Bowen et al. [97]

at 77*K* is widely used. However, the effective surface energy for cleavage initiation from a particle is essentially temperature dependent as well, which has been studied by authors by using a dislocation dynamics based approach [94, 98]. Moreover, a more complex criteria of cleavage fracture have been proposed by Chen et al. [99, 100] based on their experimental work, which are related to the critical plastic strain at crack tip to let particle cracking, critical stress triaxiality to prevent crack blunting and the principal tensile stress to make crack propagation.

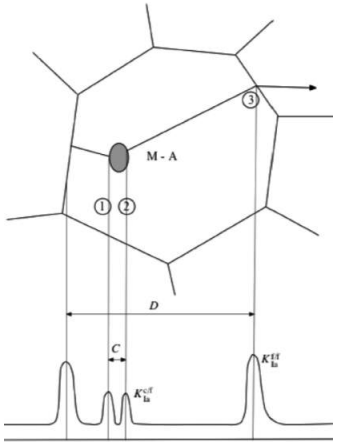

Figure 2.11 Initiation of a cleavage microcrack from a carbide, e.g., M-A [33]. The crack may eventually be arrested at the interface carbide-ferrite; then propagates through the matrix and is arrested at the grain boundary.

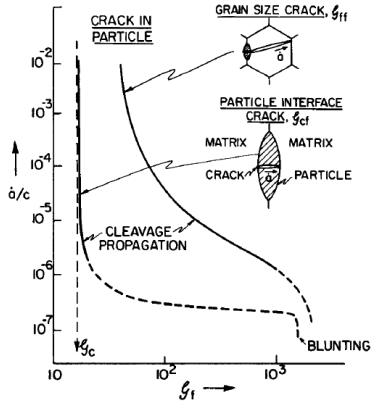

Figure 2.12 Schematic representation of the variation in the dynamic strain energy release rate with crack velocity $\dot{a}$ for the propagation of a cleavage crack extension of either a microcrack in the particle interface or a grain-size microcrack [92].

2.2.2 Weakest-link model

A simple model proposed by Ritchie, Knott and Rice [101], so called RKR model, assumes that cleavage failure occurs when the maximum principle stress ahead of the crack tip exceeds

the fracture stress σ_f over a characteristic distance. In order to describe the statistical nature of micro-cracks in the stress field, micromechanical models following the weakest-link philosophy [102] have been reformulated based on RKR model by Beremin [103], Wallin [104, 105], and Evans [106], which provide a promising local approach to understand cleavage fracture. One of the most widely used approaches is Beremin model [103].

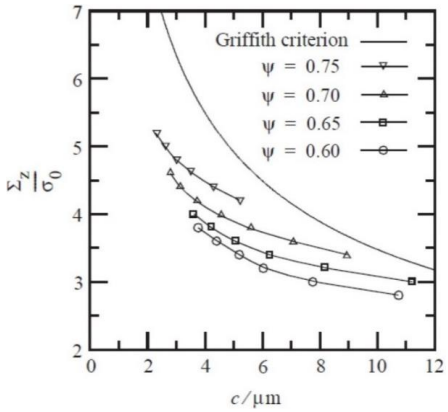

Figure 2.13 Global stress level vs. critical carbide size for four levels of triaxiality [93]. Here, Σ_Z is macroscopic stress for cleavage initation, σ_0 is yield stress of matrix, c is particle size, ψ is stress triaxiality in the unit cell model.

It is assumed that the probability of finding a microcrack of critical length is a function of the volume of material involved. Moreover, fracture will take place at the longest microcrack. Therefore the knowledge of the microcrack distribution is required only for the longest cracks. Further, it is assume that the stressed volume can be divided into smaller volumes V_0, so-called reference volume, and V_0 must include a certain number of grains so that hat the probability of finding a microcrack of reasonable length will not be vanishingly small. In each volume V_0, the probability of finding a microcrack of length between C and $C + dC$ accords with a power law, which can be taken as

$$p(C)dC = \gamma C^{-\beta} dC \qquad (2-18)$$

where γ and β are material constants, then in a given volume V_0 where stress level is σ, the probability of failure is

$$P(\sigma) = \int_{C^*}^{\infty} p(C)dc \qquad (2-19)$$

where C^* is given by Griffith theory for a through thickness defect, i.e.,

$$C^* = 2E\gamma_s/(1-\nu^2)\sigma^2 \qquad (2-20)$$

Thus, $P(\sigma)$ can be written as

$$P(\sigma) = \left(\frac{\sigma}{\sigma_u}\right)^m \quad (2-21)$$

where $m = 2\beta - 2$ and σ_u is a material constant independent with the temperature if assumed γ_s does not change with temperature.

In a volume V, which is uniformly loaded and contains a number of statistically independent elements like V_0, according to the weakest link theory the cumulative probability to failure can thus be expressed as,

$$P_R = 1 - exp\left[-\left(\frac{\sigma_w}{\sigma_u}\right)^m\right] \quad (2-22)$$

$$\sigma_w = \left[\frac{1}{V_0}\int_V \sigma_1^m\right]^{1/m} \quad (2-23)$$

Where σ_w is Weibull stress, σ_1 is the maximum principal stress in the volume. In a pre-cracked specimen with a pre-crack or notch, the volume *V* always denotes the interest region in the fracture process zone. More detailed derivation has been presented in the Ref. [103]. An exponential law of $p(C)$ has also been reported and accordingly another expression of P_R has been derived as well [107, 108]. A threshold stress σ_{th} has also been introduced into Eq. 2-21 by some studies [109-113], in which a modified form of Eq. (2-22) is given by

$$P_R = 1 - exp\left[-\left(\frac{\sigma_w - \sigma_{w_{min}}}{\sigma_u - \sigma_{u_{min}}}\right)^m\right] \quad (2-24)$$

where $\sigma_{w_{min}}$ represents the minimum value of σ_w at which cleavage fracture becomes possible. A number of studies have reported that m is close to 20 when no threshold is introduced [103, 114]. Lower values for *m* have found when a threshold is introduced [113, 115, 116].

It is noted that the Beremin theory does not assign a completely clear meaning to the defects distributions given by Eq. (2-18), since it only consider the defect originated form particles, e.g., carbides, and not consider the role of grain boundary on cleavage fracture. It should be realized that the nature of the defects introduced in Eq. (2-18) may change with test temperature. As we already discussed in section 2.2.2, at low temperature cleavage fracture is always dominated by the crack penetration into interface of particle and matrix depending on the particle size. However, at high temperature and in the DBT regime the critical defects are grain-sized microcracks. The distribution laws for these two types of defects are expected to be different. This variation in the nature of the defects with temperature or with loading and constraint may induce variations in the values of the parameter σ_u (and eventually m) in Eq. (2-21). Several attempts to develop such expressions have been made in the literature. One of the most advanced attempts based on a physical description of cleavage fracture was made by

Chen [99, 117]. However this author has not been able to derive an explicit expression as simple as Eq. (2-18) to determine the probability of failure.

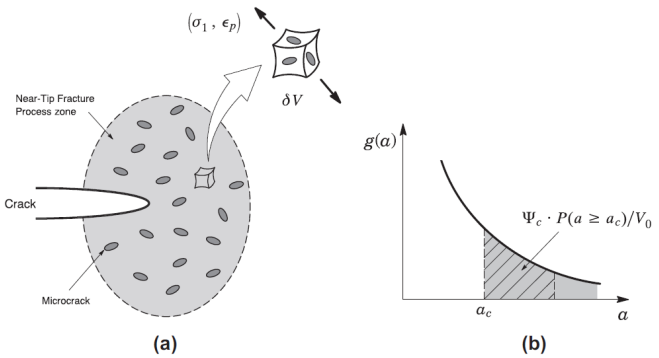

Figure 2.14 schematically illustration of the modified Beremin model with a term related to plastic strain [118]: (a) Near-tip fracture process zone ahead a macroscopic crack containing randomly distributed flaws. (b) Schematic of power-law type microcrack size distribution.

The probabilistic approach, e.g., Beremin model, strongly relies upon the assumption that Griffith-like microcracks form immediately at the onset of yielding and thus the associated statistical distribution of microcrack size remains unchanged with increased loading and deformation. It has been observed that plastic strain has a strong effect on cleavage fracture in ferritic steels at varying temperatures by Kaechele and Tetelman [119] and Gurland [120], particularly on the density of Griffith like microcracks, which can directly connect to the material fracture behaviour at the microscale. Since all cleavage fracture models based on the weakest link philosophy involve a local Griffith instability of the most favourably microcrack, it becomes clear that increased plastic strains correlate directly with increased likelihood of cleavage failure. To incorporate the effect of plastic strain on cleavage fracture, Ruggieri et al. [118] has modified the original Beremin model by introducing a term related to the plastic strain, e.g., $\Psi_c(\varepsilon_p)$, see Fig. 2.14, then Eq.(2-22) can be expressed as

$$P_R = 1 - exp\left[-\frac{1}{V_0}\int_V \Psi_c(\varepsilon_p)\left(\frac{\sigma_1}{\sigma_u}\right)^m dV\right] \qquad (2-25)$$

accordingly Eq.(2-23) can be expressed as

$$\tilde{\sigma}_w = \left[\frac{1}{V_0}\int_V \Psi_c(\varepsilon_p)\sigma_1^m\right]^{1/m} \qquad (2-26)$$

where, four cases of interest for defining the function $\Psi_c(\varepsilon_p)$ are considered, which have a direct bearing on the connection between the Weibull stress and macroscale fracture toughness: (i) exponential dependence of eligible microcracks on ε_p; (ii) limiting distribution of fracture

stress using particle distribution; (iii) the modified Beremin model incorporating plastic strain and (iv) the influence of plastic strain on microcrack density.

Bordet et al. [121-123] and Bernauer et al. [124] have also modified the Beremin model by incorporating the effect of plastic strain in cleavage fracture. The difference between the concepts of Ruggieri [118] is that they just considered the fact that the number of microcracks nucleated from carbides increases with plastic strain.

2.3 Ductile-to-brittle transition (DBT)

The transition of fracture mode from ductile to brittle is a crucial phenomenon of structural materials, e.g. body centered cubic (BCC) metals with strong interatomic forces which are normally brittle at low temperatures or high loading rates, become ductile at high temperatures or low loading rates. Although the general concern in engineering practice is ductile-to-brittle transition, the mechanism can be fundamentally revealed by studying the reverse process in which an intrinsically brittle material fractures in a ductile manner [125]. It has been indicated that brittle-to-ductile transition (BDT) always involves a thermally-activated process of dislocations emission followed by their motion and multiplication near the crack tip [125]. To circumvent the complexity of problem, e.g. pre-existing dislocations, grain boundary or impurity in the material which affect dislocation activity near crack tip, single crystalline metals has been always selected for the study of BDT. In this section, the essence of BDT will be firstly introduced, then the DBT in polycrystalline materials will be introduced next.

2.3.1 BDT in single crystal metals

Materials normally present two kinds of brittle-to-ductile transition nature [126], gradual and sharp, e.g. BCC metals, intermetallics, MgO etc., which exhibit increasing fracture stress over a long temperature range with the order of 100K or more, while in some cases, e.g. for Si and Al2O3 single crystals whose transition is very sharp occurring over a temperature range of lower than 10K. In past decades, single crystalline metals, e.g. Si [127-131], Tungsten [132-134], iron [135-137], etc. have been widely experimentally studied for the fundamental mechanisms of BDT. Many models have been developed to investigate the BDT behavior, and most of them address the intimate connection between the dislocation activity near the crack tip and fracture toughness. These models can be generally classified into two groups, e.g. dislocation nucleation controlled [138-141] and dislocation motion controlled [128, 130, 142, 143].

Models in the first category suggest that the competition between dislocation emission and atomic decohesion at crack tip is the controlling factor in the ductile versus brittle behavior of a material. Rice and Thomason [138] has firstly proposed a theoretical criterion to distinguish which materials are intrinsically ductile or brittle in terms of the spontaneous emission of dislocations from an atomically sharp cleavage. Through analyzing dislocation nucleation from crack tip based on the Peierls concept, Rice et al. [139] has suggested that the ratio of γ_s/γ_{us} could be used to evaluate brittle vs. ductile response in metals through the competition between dislocation nucleation and Griffith cleavage at a crack tip, see Fig. 2.15. The criterion for crack tip blunting by dislocation nucleation under the load of mode I can be expressed as

$$\frac{\gamma_{us}}{\gamma_s} = 4\frac{1+(1-\nu)\tan\phi}{(1+\cos\theta)\sin^2\theta} \qquad (2-27)$$

where, γ_s is surface energy, γ_{us} is unstable stacking energy, θ is the inclination angle between crack plane and dislocation slip plane, ϕ is the angle between the dislocation slip direction and the normal direction of crack tip.

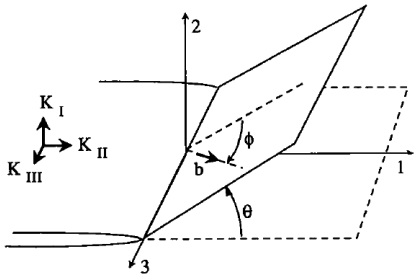

Figure 2.15 Schematic illustration of the configuration of the crack of cleavage fracture and dislocation in the K field.

Further study carried by Rice et al. [144] has extended his previous work to the nucleation of dislocation from stressed crack tip in which the energy required to thermally activate a stable and incipient dislocation has been taken into account. Xu et al. [140] have investigated the nucleation of dislocation at the sharp crack under mixed loading mode and establish a relation between the critical BDT temperature and the activation energy of dislocation nucleation at crack tip. These dislocation nucleation dominated BDT models can intrinsically distinguish the materials to be brittle or ductile, but fail to predict the temperature and loading rate dependence of the BDT behavior.

It has been found that the toughness of the material against crack propagation depends on the shielding of dislocations on the crack from the external stress [145]. A local K-field of the crack tip can be expressed with the shielding contribution of the dislocations [146]

$$K_I^t = K_I^a - K_D \qquad (2-28)$$

Where, K_I^t is the stress intensity factor at crack tip; K_I^a is the applied stress intensity factor; K_D is the shielding effect of dislocations [145, 146], for mode I and II fracture and in 2D plane strain, which can be expressed as

$$K_D = \sum_i \frac{\mu b g(\theta)}{(1-\nu)\sqrt{2\pi\xi_i}} \qquad (2-29)$$

where $g(\theta)$ is a function depending on θ; θ is inclination angle of dislocation slip plane to the crack plane; μ and ν are shear modulus and Poisson's ratio respectively; b the modulus of Burger's vector; ξ_i is position of the ith dislocation. It has to be mentioned that the blunting effect of dislocation on crack tip is neglected since that the analysis by Thomason et al. [145, 146] addresses only sharp cracks. According to the formulation for the forces on the defect, e.g. dislocations, derived by Thomason et al. [145, 146], the shear stress on a dislocation with a position $\xi = \xi_i$ in the presence of a crack and embedded in a cloud of other dislocations can be expressed as:

$$\tau_{\xi_i} = \frac{K}{\sqrt{2\pi\xi_i}} g'(\theta) - \alpha\frac{\mu b}{\xi_i} + \frac{\mu b}{2\pi}\sum_{ij}\sqrt{\frac{\xi_j}{\xi_i}}\frac{1}{\xi_i - \xi_j} \qquad (2-30)$$

where K is stress intensity factor of external loading; ξ_i or ξ_j is position of the ith or jth dislocation; $g'(\theta)$ is the coefficient related to θ; α is image stress parameter. The first term is the direct shear stress by the crack on the dislocation in a *K* dominated elastic field, the second term is the image stress that is always attractive toward the crack and the third term is the stress caused by interactions between dislocations.

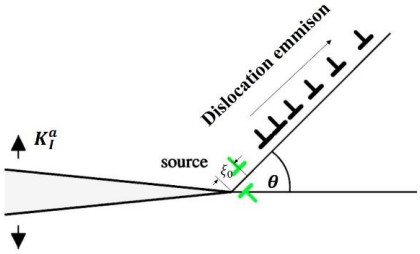

Figure 2.16 schematic illustration of crack of cleavage fracture under load of mode I in dislocation clouds induced by dislocation motion. K_I^a is applied stress intensity factor, ξ_0 is the distance of dislocation source away from the crack tip, θ is the inclination angle between crack plane and dislocation slip plane.

The dynamics of dislocation emission and motion in the crack tip stress field is the essence of the formation of dislocation clouds that result in the shielding effect on crack tip[143], see the schematic illustration in Fig. 2.16. The dislocation velocity v can be described as function of resolved shear stress τ and temperature Θ by an empirical Arrhenius type law

$$v = v_0 exp\left(-\frac{Q}{k_B \Theta}\right)\left(\frac{\tau}{\tau_0}\right)^m \qquad (2-31)$$

where Q is the activation energy for dislocation velocity; k_B is the Boltzmann constant; m is temperature dependent stress exponent; v_0 is material specific reference dislocation velocity; τ_0 is normalization shear stress; Θ is the absolute temperature in Kelvin. For a given material, the value of m can be measured through the relationship of dislocation velocity and applied stress (e.g. Fig. 3.11 [147]). The activation energy Q, for dislocation motion can be obtained from the relationship of loading rate and temperature [135, 136]. At a specific temperature, Eq. (2-31) can be written as $v = v_0'\left(\frac{\tau}{\tau_0}\right)^m$. If write $v = \frac{d\xi}{dt} = \dot{K}\frac{d\xi}{dK}$, then the resolved shear stress on the dislocation can be expressed as [126]:

$$\tau = \tau_0 \left(\frac{\dot{K}}{v_0'}\right)^{1/m}\left(\frac{d\xi_i}{dK}\right)^{1/m} \qquad (2-32)$$

where $\dot{K}$ is the loading rate of applied stress intensity factor, v_0' is a constant. Substituting τ in (2-32) for τ_{ξ_i} in (2-30), then

$$\tau_0 \left(\frac{\dot{K}}{v_0'}\right)^{1/m}\left(\frac{d\xi_i}{dK}\right)^{1/m} = \frac{K}{\sqrt{2\pi\xi_i}} g'(\varphi) - \alpha\frac{\mu b}{\xi_i} + \frac{\mu b}{2\pi}\sum_{ij}\left(\frac{\xi_j}{\xi_i}\right)^{\frac{1}{2}}\frac{1}{\xi_i - \xi_j} \qquad (2-33)$$

For a constant loading rate $\dot{K}$, the position of the dislocations ξ_i is a function of K. The initial condition for this function is that a dislocation emission occurs when $\tau_{\xi_0} = \tau_f$, τ_{ξ_0} is the resolved shear stress for dislocation nucleation with a distance ξ_0 from the crack tip, τ_f is the lattice friction stress. At each time step, under a given $\dot{K}$ and temperature incorporated in the term of v_0', the positions ξ_i of the dislocations can be determined with the applied K. Accordingly, the shielding effect of dislocation on crack tip K_D and the local stress intensity factor at crack tip can be solved when the position of dislocations is determined. Here, it is assumed that emission of a dislocation occurs once that crack tip stress on a dislocation at a critical distance, e.g. ξ_0, exceeds τ_f, and also that dislocations emission from a source at or near the crack plane have to move a certain distance before they can shield the crack [143]. Gradual and sharp BDT transition of single-crystal solids has been successfully predicted with detailed configurations of dislocation near the crack tip [126, 128, 130, 143, 148] based on dislocation mobility models. Fig. 2.17 shows the predicted BDT results of single-crystal Si by Xin and Hisa [148]. Further, a continuum model on the basis of dislocation mobility proposed by Nitzsche et al. [149] has been adopted to simulate the BDT of single-crystal Si [149] and single-crystal Tungsten by Hartmaier et al. [133]. The BDT of single-crystal iron has also been

studied by authors [98] by using this continuum model based on the experimental results by Tanaka et al. [135].

2.3.2 DBT in polycrystalline materials

Ductile-to-brittle transition (DBT) is normally found in the BCC materials, e.g., steel, due to temperature decreasing and loading rate elevation. Ductile fracture usually occurs at higher temperature, e.g. the upper-shelf. Unstable cleavage fracture initiated by second-phase particle cracking due to dislocation pile-up commonly occurs at lower temperature, e.g., the lower-shelf. In the DBT transition regime, the competition between ductile tearing and cleavage fracture controls the macroscopic fracture behavior of steel. Ductile crack growth can enable the structure withstanding a significant amount of stable ductile crack propagation without substantial loss of load-bearing capacity. On the other hand, unstable cleavage fracture leads to catastrophic failure, and the initiation of cleavage is limiting the load-bearing capacity of the structure.

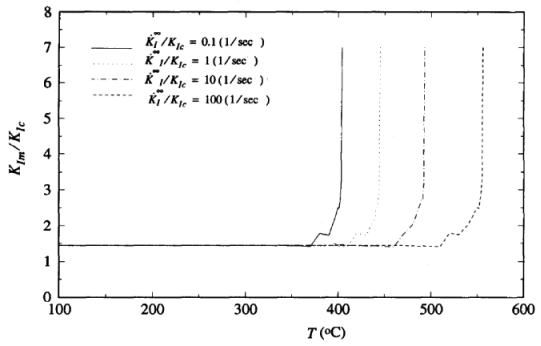

Figure 2.17 Simulation results of BDT of single-crystal Si, as a function of temperature T [148]. Here, K_{Im} is fracture toughness, K_{IC} is critical stress intensity factor of Si, $\dot{K}_I^{\infty}$ is loading rate.

An apparent reason for the existence of the transition of fracture mode lies in the fact that the stress–strain curve increases with decreasing temperature, which leads to an increase of the normal stress ahead of the crack tip with decreasing temperature. This results in the increase of the possibility of the occurrence of cleavage when the maximum normal stress ahead of the propagating crack requires the attainment of the cleavage stress. However, this simple explanation can hardly reflect the change in failure mechanism from ductile to cleavage fracture. A combination of additional causes exists. Possible causes for this change are [150]:

- Ductile crack growth leads to a higher stress at crack tip than the stress ahead of a static crack, which has been reported by Xia et al. [151].

- The volume of material sampled during ductile crack propagation increases with crack extension, e.g., the plastic zone ahead of the crack increases with the crack extension. According to the weakest link theory, this results in an increasing probability of cleavage fracture.
- The number of cleavage initiation sites may decrease due to the elimination of eligible particles for brittle fracture, which is induced by the formation of voids from inclusions or second phase particles. However the voids formed from nucleation sites may also produce stress concentrations, as illustrated in Fig. 2.18 where cleavage fracture is initiated from ductile voids.

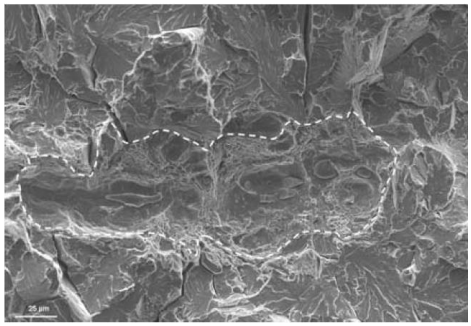

Figure 2.18 Cleavage fracture observed in a notched specimen of A 508 steel tested at $-150℃$ [150]. Cleavage is initiated from ductile dimples containing MnS inclusions.

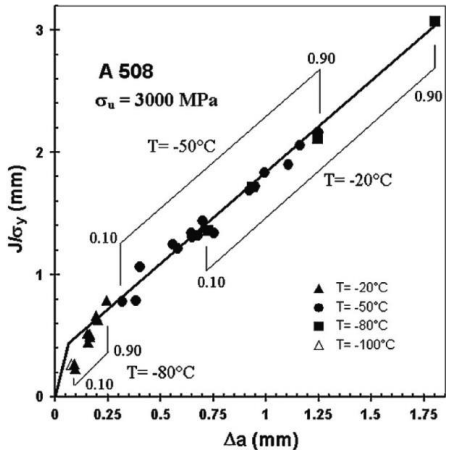

Figure 2.19 The evaluation of the probabilities to initiate cleavage fracture of 10% and 90% after some ductile crack growth at different temperatures based on the experimental J–R curve of pressure vessel steel (A 508) [150].

There is one simple approach to predict cleavage fracture after some ductile crack extension on the basis of the experimental J–R curve or $J/\sigma_0 - R$ curve to account for the temperature dependence. The probability to the failure for various stationary crack lengths can be calculated

by using the Beremin theory [103]. This simple approach is easy to apply using a post processing routine, which has been adopted for the theoretical failure prediction in A 508 RPV steel [152], see Fig. 2.19. However, this simplified approach involves strong limitations since it does not account for the changes in the stress field ahead of a propagating crack, and does not account for a possible change in the nature of cleavage initiating sites during crack propagation [150].

Xia and shih [151, 153, 154] have numerically simulated the ductile fracture by using GTN model and pointed out that the maximum tensile stress, e.g., σ_{22}, ahead of a growing crack increases with crack extension. This elevation of the tensile stress ahead of the propagating crack tip can thus increase the probability of cleavage fracture. However, the stress elevation during crack growth is less pronounced in specimen geometry in which the constraint effect is less dependent on crack length, such as tensile bars with one single edge crack, as shown by Xia and Cheng [109]. The effect of a growing crack on stress profiles has also been further studied by Dodds et al. [155] and Tanguy et al. [156]. These studies suggest that the DBT behavior is strongly dependent on the specimen geometry. In addition, the softening effect brought by the ductile damage law on the reduction of local stress, i.e., GTN model, and its influence on the calculation of the Weibull stress have been quantified by Busso et al. [157].

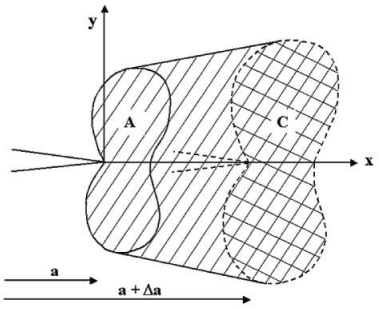

Figure 2.20 Schematic illustration of the change of plastic zones ahead of a propagating crack [150].

It has been mentioned that the volume of material sampled for cleavage initiation during ductile crack propagation increases with crack extension, see Fig. 2.20. The plastic zone ahead of the crack as shown in zone A, experienced severe stress and strain fields without triggering cleavage fracture, will increase to a zone C as a result of the ductile crack extension, where elevated stresses involve the creation of new cleavage initiation sites. In this zone both the stress elevation as discussed above and the increasing probability to contain more microdefects, which were not sampled during the earlier crack extension, can favor the cleavage initiation. When calculate the probability to failure, the volume of material hatched in Fig. 2-20 must be

considered [105, 158, 159]. Thus, Wallin [105, 159] has proposed a simplified expression for the ductile crack growth correction which can be used without knowing the J−R curve:

$$\sqrt[4]{ln\left(\frac{1}{1-P_R}\right)} = \frac{K_i}{K_0}\left(1+\frac{2\Delta a\sigma_c^2}{K_i^2\beta}\right) \qquad (2-34)$$

where K_i is the initial value of the stress intensity factor at ductile crack initiation, K_0 is a normalizing value for the stress intensity factor, σ_c is the cleavage stress, $\beta \cong x/(K_i/\sigma_c)^2$ defines the cleavage fracture process zone size. However, this prediction can be usually achieved in a numerical way.

Modelling of the DBT of steel has aroused great interest in the past decades. Ductile damage models (e.g., GTN, Rousselier) combined with RKR criterion model [101] or local approach (e.g. Beremen model) have been widely applied to model the DBT of steel under quasi-static load [160, 161] or dynamic loading [162-167]. Cohesive zone method (CZM) has also been used to model the DBT independently (the so-called unified cohesive zone approach [168]) or together with a Non-local Gurson model [169], in which cleavage occurs when the maximum principle stress exceeds the cohesive strength. Although ductile fracture model combined with RKR model or local approach has been widely applied to predict the DBT of steel, it is basically a post-processing solution to evaluate the occurrence of cleavage after stress field ahead of crack tip obtained from the constitutive equation of ductile model. The competition between two failure mechanisms (characterized by the two different failure criteria, e.g., f_c for ductile damage and fracture stress σ_f or Weibull stress σ_w for cleavage fracture), and the interaction between two failure modes in the transition region are not involved indeed. Furthermore, the fracture in the transition region occurs on two independent scales of microstructure size, ductile fracture related to the spacing of the dominant voids initiated from particles, while the brittle fracture related to the grain or cleavage facet size. It is difficult to handle two fracture modes with only one mesh size using the finite element method. Although attempts have been conducted to overcome this problem by using non-local approaches [160, 161, 169], it is still a challenge to represent the competition between two failure mechanisms and the interaction between two failure modes in the transition region. However, one approach coupled cellular automata (CA) and finite element (FE), so-called CAFE method, provides a practical solution to solve these two challenges simultaneously [170]. In addition, the statistical feature of microstructure of material can also be represented in this method, e.g. initial void distribution, grain size distribution, misorientation of grain boundaries etc., such that the scatter of toughness

in the transition region can be captured. The principle and implementation of CAFE method have been thoroughly described in the ref. [170-175].

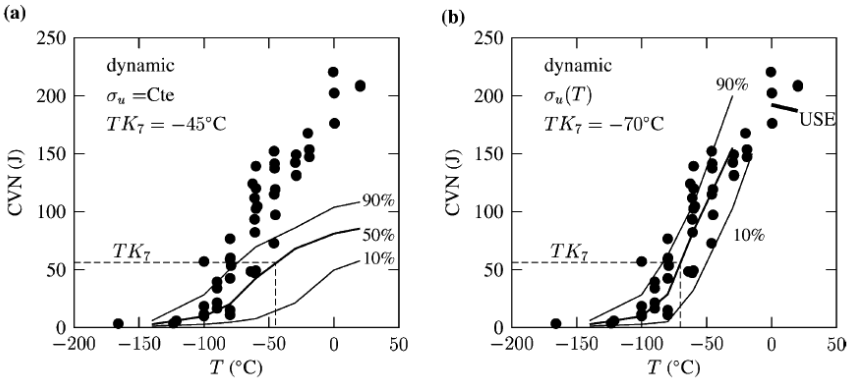

Figure 2.21 Prediction of DBT of Charpy test on a A508 steel [167]: (a) with a constant σ_u, (b) with a temperature-dependent σ_u.

As reported by Rossoll et al. [165], Tanguy et al. [167] and Shterenlikht et al. [170], only temperature-dependent flow stress is not enough to predict the transition behavior of materials. Many efforts have been made to describe temperature dependence of fracture toughness in the DBT transition region. A global approach, the so-called Master curve method has been adopted in ASTM E1921 [176], in which the variation of fracture toughness with temperature in DBT region can be described with a reference temperature T_0. A temperature-dependent σ_u has been utilized by Tanguy et al. [167] for the simulation of the DBT Charpy impact test on a A508 steel when using Rousselier model [78] combined with Beremin model [103]. The numerical simulation results agree well with the experimental results, see Fig. 2.21. The temperature dependent σ_u of Beremin model [103] has been greatly studied in the past years on the fracture in transition region by Petti et al. [115], Wasiluk et al. [177], Cao et al. [178] and Qian et al. [179]. Gao et al. [180] has found that σ_u increased with temperature reflecting the combined effects of temperature on material flow properties and toughness. Moattari et al. [181] accurately predicted the fracture toughness in DBT transition region by introducing a temperature-dependent σ_u described with a summation of athermal and thermally activated stress contribution. Moreover, a temperature dependent misorientation of grain boundary proposed by Shterenlikht et al. [170] has been implemented into the CAFE method to model the DBT of Charpy test of TMCR steel. It has to be noticed that either the temperature dependent σ_u or misorientation proposed in the literature is just a phenomenological parameter for DBT modelling. Therefore, exploring a physically-based variable to disclose the nature of temperature dependent fracture toughness in the transition region is not only significant but

also necessary. In our work of paper 2, a second temperature dependent variable, e.g., effective surface energy, to characterize the temperature dependent fracture toughness in the transition region of a TMCR steel, has been explored. The DBT of Charpy test has been successfully predicted comparing to experimental results by using CAFE method implemented with such a temperature dependent surface energy [94].

2.4 Residual stress

Residual stresses are those stresses which retained within a body when no external forces are acting [12], and are stationary and at equilibrium with their surroundings [182]. Residual stresses are caused by incompatible internal permanent strains induced by inelastic deformation, temperature gradients, or phase transformations during manufacturing and processing of the components. For example, residual stresses generated in the welding process, a common practice of the assembly of components in the industry, are always at a remarkable level, whose effect would exist in the whole life-cycle of the structure. Thus, the role of residual stresses on failure of materials or structures becomes an important issue, for instance, for plastic collapse, fracture, fatigue, creep, stress corrosion, assessment of structural integrity etc. Before the assessment of the influence of residual stresses on failure of structure, a quantitative measurement on the residual stresses is necessary. During the past years many different methods for the measurement of residual stresses in different types of components have been developed. They can be classified as either mechanical method or non-destructive method [183]. The mechanical methods rely on the measurement of deformations due to the release of residual stresses upon removal of material from the specimen, such as sectioning, contour, hole-drilling, ring-core and deep-hole etc. Non-destructive methods are techniques usually measuring some parameter related to the stress, which include X-ray or neutron diffraction, ultrasonic methods and magnetic methods. In this section, it is emphasized on the effect of residual stresses on the fracture behavior of materials or structures. After that, the residual stresses involving with the material inhomogeneity, e.g., mismatch of thermal expansion, will be introduced shortly.

2.4.1 The influence of residual stresses on fracture

Numerical approach is an effective method and usually applied to study the influence of residual stress on fracture. To study and understand the effect of residual stresses on fracture behavior, it is necessary to introduce well characterized and reproducible residual stresses firstly. There are generally three approaches to introduce the residual stresses into the

numerical model: (i) reconstructing the residual stresses field measured from a component in the numerical model by using SIGINI subroutine implemented in Abaqus [184, 185]; (ii) eigenstrain approach [13, 185-187], where eigenstrain (ε^*) is a non-uniform inelastic strain which causes elastic strains and hence stresses. If the residual stresses are known throughout the whole component, then ε^* can be determined from the relation directly, e.g., $\varepsilon^* = -C_{ijkl}^{-1}\sigma_{kl}^{res}$, where C is the elastic constants tensor and $\sigma^{res}$are the measured residual stresses. The eigenstrain method is schematically shown in Fig. 2.22; (iii) numerically reproducing the residual stresses generated in the laboratory fracture specimens, e.g., the local out-of-plane compression (LOPC) on a CT specimen by Mohmoudi et al. [188] and Coules et al.[189] , in-plane compression on a SEN(B) specimen by Mirzaee-Sisan et al. [190], and bending and unloading of the specimen by Yazdani Nezhad and O'Dowd [191] etc.

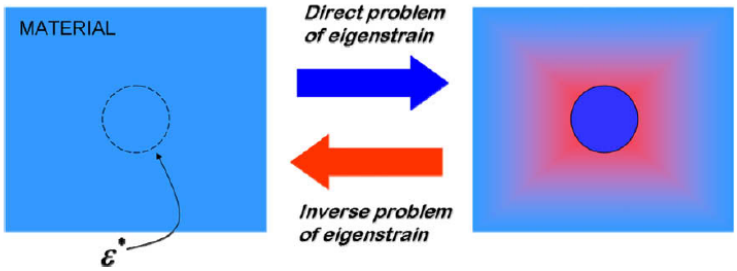

Figure 2.22 illustration of the concept of eigenstrain method [13].

Several aspects regarding the influence of residual stresses on fracture have been investigated, e.g., effect of residual stress on crack driving force [192-194], crack tip constraint [28, 195, 196], ductile fracture [188, 189, 196-200], brittle fracture [190, 196, 201-203], hydrogen embrittlement [204, 205] etc. Panontin and Hill [196] have predicted the brittle and ductile fracture initiation by micromechanical models and showed that the effect of residual stress on the ductile fracture initiation toughness is negligible. Sherry et al. [200] have demonstrated that a high strength low toughness aluminum alloy AL2024-T351 showed a marked reduction in initiation and tearing toughness for specimens containing a mechanically induced residual stress field. Mahmoudi et al. [188] have reported that the ductile tearing resistance of A12024 alloys decreases when tensile residual stresses are presented. Coules et al.[189] have also found that the crack resistance curve of aluminum alloy 7475-T7351 obviously decreases when the residual stresses are introduced, see Fig. 2.23. However, the experiments performed by Mirzaee-Sisan et al. [198] on the AISI Type 361H stainless steel indicates a negligible impact on ductile tearing toughness at load ratio L_r close to 1, i.e. close to the plastic collapse of the specimen. To date, the fundamental understanding of the effect of the residual stresses on

ductile fracture resistance remains a challenge. The cleavage fracture toughness exhibits sensitivity to the local stress and deformation fields due to its highly localized character of the failure mechanism [206]. Understanding how residual stresses influence the cleavage fracture behavior becomes more and more important when high strength steels are increasingly utilized in structural engineering. Experimental work undertaken by Mirzaee-Sisan et al. [190] has indicated an apparent reduction in mean cleavage fracture toughness of an A553-B ferritic steel of 50% from conventional fracture toughness data. Panontin and Hill [196] have adopted the RKR model [101] to predict the effect of residual stresses on brittle fracture initiation and found that the constraint generated by the residual stress decreases the initiation toughness of brittle fracture.

The transition of fracture from ductile to brittle, so-called DBT, is a crucial phenomenon of structural materials, e.g., steel, which has been aroused great concerns in engineering practice. However, few work has been performed to study the effect of residual stresses on the DBT so far. Satoh et al. [207] showed that the hot straining embrittlement of material as well as residual stresses due to welding elevates brittle fracture initiation temperature in comparison with the base metal. The residual stresses on DBT of a welded TMCR steel has been numerically studied by using CAFE method by the author in paper 3, in which the transition curve can be dramatically changed by the residual stress.

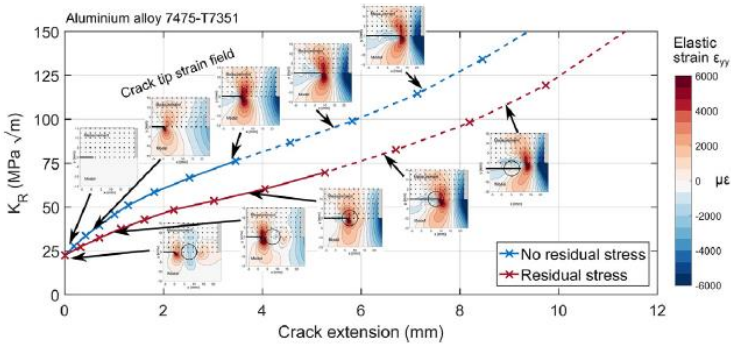

Figure 2.23 the influence of residual stresses on the crack resistance curve [189].

2.4.2 Inhomogeneity of materials

In a 2D body containing a crack and sharp interface (perpendicular to the crack propagation), when the material properties exhibit a jump at the interface, the configuration forces at the interface could induce a contribution to the crack driving force [208], see Fig. 2.24. This contribution, namely additional driving force, induced by the material heterogeneity can be described with a material inhomogeneity term [209, 210], e.g., C_{inh}. Then, the effective crack-

driving force at crack tip, represented by the J-integral around the crack tip, J_{tip}, is depicted by the sum of the far-field J-integral, J_{far}, and the material inhomogeneity term [209, 210]:

$$J_{tip} = J_{far} + C_{inh} \tag{2-35}$$

$$C_{inh} = -e \cdot \int_{\Sigma} \left([[\phi]] I - [[F^T]] \cdot \langle S \rangle \right) n dl \tag{2-36}$$

where ϕ is the strain energy density, I is the identity tensor, F^T is the transpose of the deformation gradient, S is the 1st Piola–Kirchhoff stress, the vector n is the unit normal to the interface Σ, e is the unit vector in the direction of crack growth. In this regard, a shielding/anti-shielding effect can be brought onto the crack, which depends on the magnitude of C_{inh}, in a negative or positive manner.

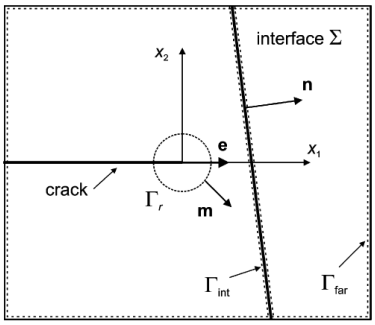

Figure 2.24 A two-dimensional bimaterial body containing a crack and a sharp interface [208].

The effect of material inhomogeneities has been explored for linear-elastic and elastic-plastic bimaterial with sharp and graded interfaces [209-211]. The mismatch in elastic modulus, yield stress and strain hardening exponent at the interface have been investigated [209-212]. Residual stresses are inherently found in materials or structures with a mismatch of CTE when cooling from an elevated temperature, for example welded joints, composite, structure with coatings etc. Like the mismatch of material properties, e.g., elastic modulus, yield stress, strain hardening, the variation of CTE is also an origin of the heterogeneity of graded materials or layered structures. The pronounced anti-shielding effect or shielding effect resulted by residual stresses on crack in the bimaterial with mismatch of CTE has also been investigated [213-215]. Inspired by these studies on the effect of material inhomogeneity on crack, the influence of residual stresses on DBT of welded TMCR steel is investigated in paper 3 based on two configurations of crack pertaining to the interface of bimaterial with the mismatch of CTE.

2.5 The effective surface energy

The Griffith criterion, $G_c = 2\gamma_s$, has been broadly applied to study brittle fracture, where G_c is the critical strain energy release rate and γ_s is the surface energy. To account for the work of plastic deformation in the vicinity of crack tip in the advance of brittle fracture, Irwin [216] and Orowan [217] independently modified the Griffith theory, accordingly the modified Griffith criterion of cleavage can be written as $G_c = 2(\gamma_s + \gamma_p)$, in which a material's resistance to crack extension is determined by the sum of γ_s and the plastic work γ_p (both per unit crack surface area). However, how to quantitatively estimate plastic work γ_p during fracture of material is a challenge. McMahon and Vitek [218] and Jokl et al. [219] derived an exponential dependence of γ_p on γ_s so that a relatively small change in γ_s may lead to a large change in γ_p. Wallin et al. [104] proposed a simple equation to calculate plastic work related to temperature and the Peierls-Nabarro force. Since the modified Griffith theory can also be written as $G_c = 2\gamma_{eff}$ (γ_{eff} is the effective surface energy), the estimation of the γ_{eff} can be an alternative solution for evaluation of plastic work during fracture. In terms of modified Griffith theory, the measured the fracture stress of specimen tested at various temperature has been converted to the effective surface energy by Linaza et al. [95] and San Martin et al. [96]. However, the measured γ_{eff} is apparently geometry dependent and cannot be generally applied in practice. An explicit function for the estimation of effective surface energy of LiF single-crystal was derived by Burns et al. [220] based on the dynamic fracture in a double cantilever specimen, which depends on the temperature, geometry, crack speed, dislocation density at crack tip etc. However, since it cannot explicitly predict the dislocation multiplication in the process of cleavage fracture, real-time measurement on dislocation density at propagating crack tip is necessary when using such law. Consequently, it is still a challenge to theoretically estimate the effective surface energy to assess the cleavage fracture.

Charpter 3 Modelling approaches

3.1 Continuum model for the studying of BDT of single-crystal iron

A dislocation mobility based theory for the prediction of BDT of single-crystal metals has been presented in the section 2.3.1. Many studies on BDT of single-crystal metals have been carried out through a numerical solution based on the similar theory presented in section 2.3.1 [128, 143, 148]. On the other hand, it can be inferred from section 2.3.1 that the shielding effect of dislocation dynamics on crack tip stress field is equivalent to that of rate-dependent plasticity in a finite region around the crack tip due to dislocation emission and motion. In this manner, the shielding effect of dislocation mobility on crack tip and the local stress intensity factor at crack tip can be resolved with a continuum method, which will be an alternative solution to replace the numerical solution.

To this end, a modified boundary layer (MBL) model is adopted, in which the crack-tip region consists of an elastic zone surrounding the crack tip and an elastic-viscoplastic material outside of the elastic zone. The applied K with a constant loading rate $\dot{K}$ is implemented in this model through the nodal displacement on the outer boundary layer. The model used here was developed by Nitzsche et al. [149] to investigate the sharp BDT of single-crystal silicon, which was also adopted by Hartmaier et al. [133] to study the BDT of single-crystal Tunston. The configuration of this model is inspired by the concept proposed by Suo et al. [221], which states the fracture process can be divided into two elements in the transition region, atomic decohesion and background dislocation motion. The crack tip elastic zone is a dislocation free zone at a length scale (comparable to dislocation spacing) so that atomic decohesion dominates the fracture process. In order to describe the dislocation motion, two assumptions are made:

the material is assumed to be isotropic even though single-crystals are usually anisotropic. The rate-dependent plastic deformation is only a result of dislocation motion.

To describe the plasticity generated by dislocation motion, according to Orowan law, the shear strain rate, $\dot{\gamma}^p$, can be written

$$\dot{\gamma}^p = \beta \rho_D b v \qquad (3-1)$$

where β is a proportionality constant; ρ_D is the dislocation density. The resolved shear stress τ in Eq. (2-31) and plastic shear strain rate $\dot{\gamma}^p$ in Eq. (3-1) can be replaced by the von Mises equivalent stress σ_{Mis} and the equivalent plastic strain rate $\dot{\varepsilon}^p$ since the isotropic material has no preferred slip plane. Therefore, insert the dislocation velocity according to Eq. (2-31) into Eq. (3-1), the viscoplastic response of the material can then be described as

$$\dot{\varepsilon} = \dot{\varepsilon}_0 \exp\left(-\frac{Q}{k_B \Theta}\right)\left(\frac{\sigma_{Mis}}{\sigma_0}\right)^m \qquad (3-2)$$

where $\dot{\varepsilon}$ is equivalent plastic strain rate; $\dot{\varepsilon}_0$ is a reference strain rate, which incorporates the v_0, β, ρ_D and b, e.g. $\dot{\varepsilon}_0 = v_0 \beta \rho_D b$; σ_0 is a normalization stress.

Since the shielding effect of dislocation mobility is localized in a finite region around crack tip, only the elastic zone and viscoplasctic zone near crack tip have been incorporated in this continuum model. For a semi-infinite crack the long range stress field in this model is still dominated at infinity by the K-field, because viscoplastic zone is restricted to a finite distances from the crack, i.e., small scale yielding approximation. Consistency simulation results have been achieved from the investigation of BDT of single-crystal Tungsten by such a continuum elastic-vicoplastic model and discrete dislocation dynamics method by Hartmaier et al.[133]. Although such a continuum model has a certain of limitation that is the dislocation motion in various slip systems is not considered since the isotropic material is assumed, it still can be used to qualitatively study how BDT is affected by the parameters, for instance, temperature, loading rate and constraint effect etc.

Only upper-half of the model is illustrated in Fig. 3.1 due to symmetry. The radius of model (R) is 20 times larger than the crack tip elastic zone size r_{el}, which is assumed to be a circle around the crack tip with a radius of 1μm. A crack with an initial radius of $1.15 \times 10^{-4} R$ is located in the center of model. Abaqus 6.14 is employed, and 4-node and plane strain elements (CPE4) are used in all simulation. The meshes are refined in the elastic region where the size of smallest elements is 10 nm. Following the work of Williams, the first two terms in the expansion of linear elastic crack-tip stress field can be written as [222]

$$\sigma_{ij} = \frac{K_I}{\sqrt{2\pi r}} f_{ij}(\theta) + T \delta_{1i} \delta_{1j} \qquad (3-3)$$

where $f_{ij}(\theta)$ are dimensionless functions of θ, T is regarded as a stress parallel to the crack flanks. Larsson and Carlsson [223] have demonstrated that the second term in the series has a significant effect on the shape and size of the plastic zone which develops at the crack tip. Therefore, T-stress has been widely used to describe the crack tip stress field in real flawed structures. A linear elastic K_I field is applied to the outer boundary of the model with nodal displacements controlled by the elastic asymptotic stress field of a crack

$$u(r,\theta) = K_I \frac{(1+\nu)}{E}\sqrt{\frac{r}{2\pi}}\, cos\left(\frac{\theta}{2}\right)(3-4\nu-cos\theta) + T\frac{1-\nu^2}{E} r cos\theta \qquad (3-4a)$$

$$v(r,\theta) = K_I \frac{(1+\nu)}{E}\sqrt{\frac{r}{2\pi}}\, sin\left(\frac{\theta}{2}\right)(3-4\nu-cos\theta) - T\frac{\nu(1+\nu)}{E} r sin\theta \qquad (3-4b)$$

where K_I is applied mode I stress intensity factor; E is Young's modulus, r and θ are polar coordinates centered at the crack tip. In the present study, only a stationary crack is investigated. For a sharp crack tip, cleavage fracture is assumed to occur when the crack tip stress intensity factor reaches the critical value of material, i.e. $K_{\mathrm{I}}^t = K_{\mathrm{I}C}$. According to the Griffith criterion, $K_{\mathrm{I}C}$ depends only on the material's surface energy γ_s. The crack tip stress intensity factor is calculated from the J-integral through,

$$K_I^t = \sqrt{EJ/(1-\nu^2)} \qquad (3-5)$$

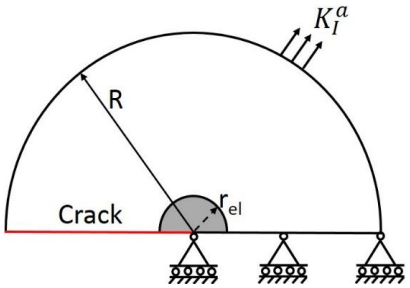

Figure 3.1 MBL model to describe BDT dominated by dislocation motion with a rate-dependent plasticity. The viscoplastic zone is white, the elastic zone dark gray [98].

3.2 The estimation of effective surface energy

Due to the shielding effect of plastic deformation on the crack tip stress field, the local stress intensity factor K_I^t at crack tip is always lower than the applied stress intensity factor K_I^a, particularly at higher temperature. The applied stress intensity factor K_{I}^a at the moment of failure, e.g. $K_{\mathrm{I}}^t = K_{\mathrm{I}C}$ is regarded as the fracture toughness of material. Since the modified Griffith theory can be expressed as $G_c = 2\gamma_{eff}$, where $\gamma_{eff} = \gamma_s + \gamma_p$, then the effective surface energy used for the description of cleavage fracture can be calculated by

$$\gamma_{eff} = \frac{(1-\nu^2)}{2E} K^2 \qquad (3-6)$$

where K is the applied stress intensity factor, e.g., K_I^a, see Fig. 3.1 in section 3.1. Therefore, once the fracture toughness K_I^a at the occurrence of cleavage is obtained in section 3-1, the effective surface energy γ_{eff} can be estimated by the Eq. (3-6).

It has to be noticed that the Eq. (3-6) to calculate the effective surface energy is only applicable for the single-crystal metals, e.g., iron. It is known that DBT normally occurs in body centered cubic (BCC) metals, e.g., single-crystal iron, Fe alloys and steel, due to the thermal-activated dislocation emission and motion [125]. The difference between single-crystal iron and steel is the presence of impurities (e.g., particles), grain boundary and preexisting dislocations in the latter, which affect the dislocation behavior, for instance, nucleation, motion, multiplication etc. If their effect on the fracture of the latter can be described by the change of dislocation density near crack tip comparing with that of former, see Eq. (3-1), the model developed for single-crystal iron is possible to be applied to the steel according to the theory of the shielding effect of dislocation mobility on crack tip. To do this, several assumptions have to be made. Firstly, a micro-crack is assumed to be initiated within a grain boundary particle, e.g., carbide or inclusion, at a position x_c ahead of the notch/crack tip where the local tensile stress equals to the maximum principal stress, see Fig. 3.2(a). Then, the nucleated micro-crack will penetrate the interface between particle and matrix once that local tensile stress at the interface exceeds the fracture stress. Secondly, we postulate that the penetration of the micro-crack into the interface leads to the final unstable cleavage fracture, namely the crack resistance of grain boundary is not taken into account. Further, it is assumed that the crack penetration from particle into matrix is dominated by a local K-field.

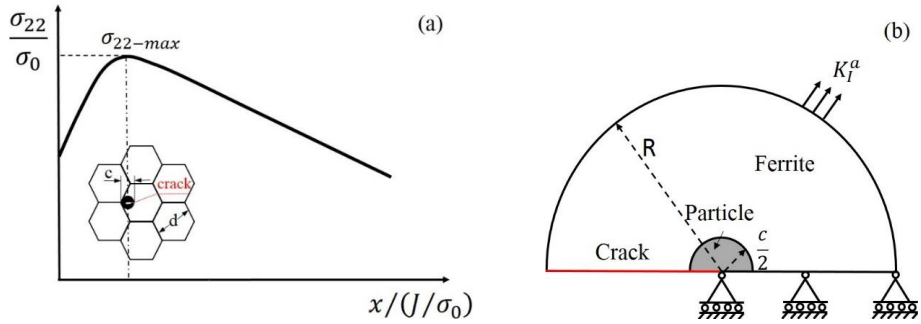

Figure 3.2 the continuum model [94]: (a) the schematic illustration of the micro-crack initiation and propagation across the interface and grain boundary, c is the particle diameter, and d is grain size; (b) MBL model to calculate the effective surface energy for cleavage extension across the interface between particle and matrix. c is particle size.

The elastic zone (dislocation free zone) in the continuum model for single-crystal material [98] is replaced with an elastic particle, and the viscoplasitic material outside the elastic region is defined as the ferrite, e.g., a time-dependent plastic matrix. Thus, a new continuum model can be adopted to estimate the fracture toughness of steel in the transition region, see Fig. 3.2 (b), where only the upper-half of model is presented due to symmetry. Similar with the single-crystal iron, the fracture toughness K_I^a in the transition region of steel can be predicted with the continuum method introduced in section 3.1 and the model illustrated in Fig. 3.2. Accordingly, the effective surface energy for the cleavage of steel can be calculated in terms of the Eq. (3-6).

3.3 Identification of parameters for the continuum approach

For the prediction of BDT and the estimation of effective surface energy of either single-crystal iron or steel, the parameters utilized in the continuum approach have to be identified based on the experimental results in the literature.

3.3.1 single-crystal iron

Through experiments on single-crystal metals, a relation between loading rate $\dot{K}$ and Θ_c has been found [130]

$$ln\dot{K} = -E_a/k_B\Theta_c + const. \qquad (3-7)$$

where E_a is the activation energy for the BDT, which has been found to be equal to the activation energy Q for dislocation velocity. For the BDT of single-crystal metals, there is always a critical transition temperature Θ_c, at or beyond which failure mode becomes ductile fracture. This means that crack tip stress intensity factor, e.g., K_I^t, will never exceed K_{IC} when temperature is higher than the critical temperature Θ_c. The BDT occurs at this circumstance and the temperature is called critical BDT temperature, and the method to determine the Θ_c has been introduced in the paper 1.

Tanaka et al. [135] have performed 4-point bend tests to measure the BDT temperature of single-crystal iron, in which different outer-fiber strain rates have been applied in their tests. The outer-fiber strain rate can be calculated by [224]

$$\dot{\varepsilon}_f = \frac{4B}{S_1^2}\dot{\delta} \qquad (3-8)$$

where $\dot{\varepsilon}_f$ is the outer-fiber strain rate and $\dot{\delta}$ is the cross head speed, B is the thickness of specimen and S_1 is the outer span of specimen. For a 4-point bend test, the applied stress intensity factor can be calculated by using the following equation [225],

$$K_I = \frac{3F(S_1 - S_2)}{2BW^2}\sqrt{a}Y \qquad (3-9)$$

where $Y = \frac{1.1215\sqrt{\pi}}{(1-a/W)^{3/2}}\left[\frac{5}{8} - \frac{5}{12}\frac{a}{W} + \frac{1}{8}\left(\frac{a}{W}\right)^2 + 5\left(\frac{a}{W}\right)^2\left(1 - \frac{a}{W}\right)^6 + \frac{3}{8}\exp\left(-6.1342\frac{a}{W-a}\right)\right]$, F is loading force, S_2 is inner span, W is width of specimen and a is notch depth. Three-dimensional modelling of the four-point bend tests of single-crystal iron have been carried out in present work, in which the cross head speed applied for modelling is converted from outer-fiber strain rates utilized by Tanaka et al. [135] according to Eq. (3-8) and only a stationary crack is studied. The Young's modulus E and poison's ratio ν of iron are 206GPa and 0.29 respectively [135]. Then, the rates of stress intensity factor applied on the four-point bend specimen can be calculated by Eq. (3-9). The outer-fiber strain rates and corresponding applied rates of stress intensity factor are listed in table 3.1. To obtain the BDT temperatures for each loading rate in Table 3-1, several groups of parameters have been tried. By doing this, one group of parameters is chosen, which are $r_{el} = 1\mu m, \dot{\varepsilon}_0 = 13044s^{-1}$, $m = 3.5$, $\sigma_0 = 1$MPa and $Q = 0.33ev$. The computed BDT temperatures under different loading rates has been compared with experimental results by Tanaka et al. [135] in Fig. 3.3. It is shown that the computational results of single-crystal iron agree well with experimental results, which indicates that this group of parameters employed is reliable. Therefore, the verified parameters will be adopted in the prediction of BDT and the estimation of the γ_{eff} of single-crystal iron.

Table 3.1 The calculated applied rates of stress intensity factor from the outer-fiber strain rates of the four point bend tests for single-crystal iron [135].

$\dot{\varepsilon}, s^{-1}$	$\dot{K}_I^a$, MPam0.5s^{-1}
4.46e-5	0.2579
4.46e-4	2.579
4.46e-3	25.79

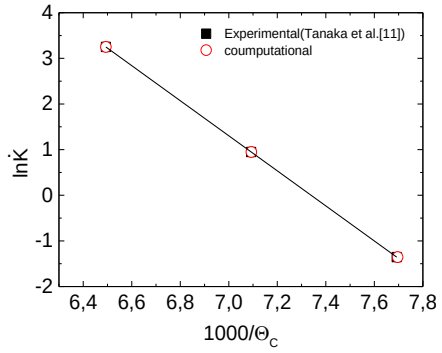

Figure 3.3 comparison of computed and experimental critical BDT temperature of single-crystal iron [98]. The parameters in the model are $r_{el} = 1\mu m, \dot{\varepsilon}_0 = 13044s^{-1}$, $m = 3.5$, $\sigma_0 = 1$MPa, $Q = 0.33$ev.

3.3.2 TMCR steel

It is found that the variation of activation energy of BDT among single-crystal iron, poly-crystal iron and Fe-alloys is relatively minor [226, 227], e.g., in the range of 0.2-0.5. This implies that the minor difference between parameters calibrated from the activation energies of BDT of different steels can be expected. In addition, there are still some resemblances between low carbon steel studied by Tanaka et al. [227] and the TMCR steel investigated in the present work, e.g., the ferritic type of microstructure and controlled-rolling process of production. Since the absence of the test results of activation energy of BDT of the TMCR steel, the activation energy of a low carbon steel experimentally obtained by Tanaka et al. [227] is utilized to approximately identify the parameters for the calculation of the effective surface energy of the TMCR steel. In order to explore a solution to estimate the effective surface energy in transition region, the gap between two materials, e.g., low carbon steel and the TMCR steel can be ignored.

The critical transition temperature, e.g., Θ_c, of low-carbon steel has been measured by Tanka et al. [227] via 4-point bend test, in which specimens have the identical geometry with these used for measuring the Θ_c of the single-crystal iron. Because of this, the procedure of the identification of parameters used in the continuum method for the low carbon steel is similar with that for single-crystal iron introduced in section 3.3.1. The Young's modulus E and poison's ratio ν of steel are 206 GPa and 0.29 respectively. The outer-fiber strain rates and calculated loading rate, e.g., the applied rates of stress intensity factor, are listed in table 3.2.

Table 3.2 The outer-fiber strain rates of the four point bend tests on fully annealed low carbon steel [225] and the calculated applied rates of stress intensity factor.

$\dot{\varepsilon}, s^{-1}$	$\dot{K}_I^a$, MPam0.5s^{-1}
4.46e-5	0.2579
4.46e-4	2.579
4.46e-3	25.79

The critical DBT temperature under a specific loading rate can be predicted by using the continuum approach introduced in section 3.1. Different particle size of the model is also studied. To obtain the critical DBT temperatures under the loading rates listed in table 3.2, for each particle size, several groups of parameters have been tried following the method introduced in section 3.3.1. By doing this, groups of parameters are optimized for each elastic zone size, which are listed in the Table 3.3. The computed BDT transition temperatures under different loading rates are compared with experimental results by Tanaka et al. [227] in Fig. 3.4. It is shown that the computational results of low carbon steel agree well with experimental

results, which indicates that the group of parameters for each elastic zone size is reliable. Meanwhile, the influence of the elastic zone size on the fracture toughness in the transition region is also studied under the loading rate 10 MPam0.5s^{-1}. The applied stress intensity factor K_I^a normalized with the critical stress intensity factor K_{IC} vs. temperature are plotted in the Fig. 3.5 for each elastic zone size. Here, $K_{IC} = 1.77MPam^{0.5}$ is calculated from the widely used effective surface energy for cleavage of steel, e.g., $7J/m^2$, tested by Bowen et al. [97] according to Griffith theory. The identified Parameters for different elastic zone sizes (listed in the Table 3.3) are employed to achieve an identical DBT temperature, e.g., Θ_c. It is shown in Fig. 3.5 that the minor difference among the fracture toughness is presented in the whole temperature range. Recall the Eq. (2-31), (3-1) and (3-2), when activation energy Q is determined, either the shielding effect of dislocation dynamics on the crack or corresponding DBT behavior can be predicted with parameters, such as Θ, $\dot{\varepsilon}_0$ and m for the different elastic zone size. At a specific Θ and under the same stress level, the similar DBT behavior can be always can be always achieved with the combination of $\dot{\varepsilon}_0$ and m no matter how large particle size. It can be concluded that the predicted DBT of low carbon steel by using the continuum model is elastic zone size independent. In the following simulations, the parameters verified for particle size, c=2 μm will be adopted.

Table 3.3 Parameters for different elastic zone size.

c/2(μm)	$\dot{\varepsilon}_0(s^{-1})$	$Q(ev)$	m	σ_0
0.25	29934.39	0.236	1.45	1.0
0.50	11307.01	0.236	1.70	1.0
1.0	3898.48	0.236	2.00	1.0
2.0	1717.67	0.236	2.30	1.0

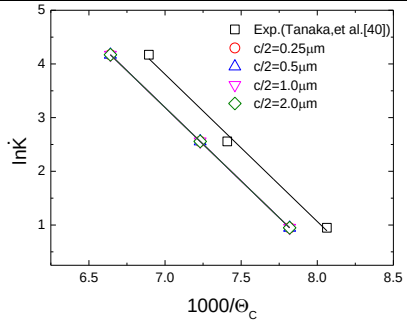

Figure 3.4 comparison of computed and experimental critical DBT temperature of low-carbon steel [94].

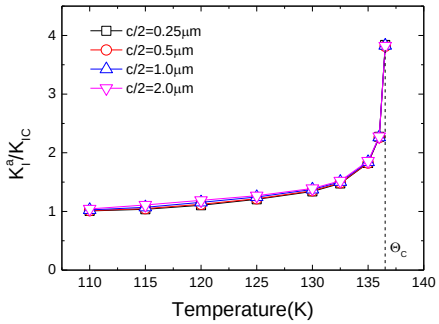

Figure 3.5 the DBT curve of steel predicted by the continuum model with different elastic zone size [94]. The loading rate is 10 $MPam^{0.5}s^{-1}$.

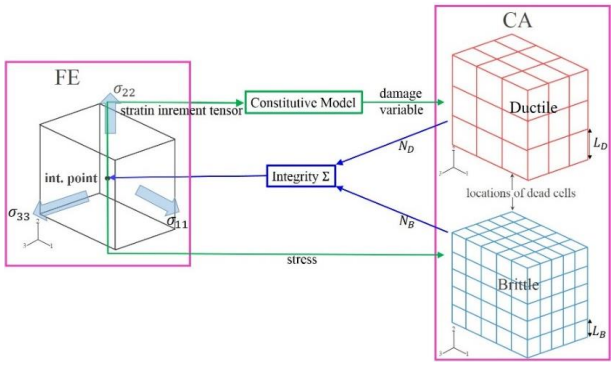

Figure 3.6 the illustration of the mechanism of CAFE method in which ductile damage and cleavage fracture have been coupled through two different CA arrays. Here, N_D and N_B are the number of 'dead' cell of ductile CA arrays and brittle CA arrays respectively; Σ is integration indicator; L_D and L_B are the size of cells in brittle and ductile CA arrays.

3.4 CAFE method for the prediction of DBT

The motivation of the CAFE method is to combine the structural and microstructural interactions by finite element method [170-172]. The method is divided into two phases: one is finite elements to capture the stresses or strains at the structural level, the other is to catch the mechanical essentials of the microstructural behavior and its development in a set of CA arrays. Fig. 3.6 shows the implementation of the above strategy to deal with the fracture in the transition region where both ductile and brittle micro-mechanisms work simultaneously [170]. In each material integration point, the microstructure is represented by two CA arrays, where the brittle array represents the cleavage behavior while the ductile array processes ductile damage. Structural information, for example, stress/strain and damage variable, processed in FE level inputs to CA levels, and, the microstructural evolution and the failure are integrated and send back to the FEs. To realize the CAFE method in finite element simulation, the explicit

dynamic process has been chosen to develop a VUMAT by Shterenlikht et al. [170-172] so that crack can propagate along a natural failure path through element removal approach.

The Rousselier ductile damage model [78] is adopted to describe the constitutive response at the integration point. The details of Rousselier model have been introduced in section 2.1.2. In ductile CA arrays, cell size L_D is used to characterize the unit cell size of ductile damage of material with a single void, which normally relates to the spacing of inclusions or large carbides in steel. According to modified Griffith theory, the critical fracture stress for cleavage can be calculated by

$$\sigma_F = \sqrt{\frac{\pi E \gamma_{eff}}{(1-\nu^2)d}} \qquad (3-10)$$

where γ_{eff} is effective surface energy for the cleavage fracture; E and ν are Young's modulus and Poisson's ratio respectively; d is grain size. In present work, a temperature dependent effective surface energy for cleavage will be applied in the CAFE method to calculate critical fracture stress of cleavage. A fraction of brittle cells, η, in each brittle CA array, is adopted to represent grains with adjacent grain boundary carbides, where micro-crack has already nucleated. In brittle CA arrays, the cleavage facet size (d_{CFS}) is applied as the size of cells in brittle CA arrays, e.g. L_B, which can be measured through fractographic analysis on the fracture surface of specimen [170]. Since the misorientation between grains is naturally the barrier of cleavage crack propagation crossing the grain boundary [228], a random orientation is assigned to each cell in brittle CA arrays, and a misorientation threshold, e.g., θ_{th}, is assumed so that crack can propagate from one cell to the other.

The property of CA depends on the state of cells. The state of each cell in next time increment is determined by its state and the states of neighboring cells at the previous time increment. Once that the cell is failed due to fracture propagation, the state of cell will be changed from 'alive', e.g., initial state, to 'dead'. Then, the closing neighborhood of 'dead' cell will be stress-concentrated since the 'dead' cell lost its load-bearing capacity. A framework [172, 175] has described in detail how to locate such a closing neighborhood around the 'dead' cell. The local concentration factors are utilized to solve this problem, which are C_D for ductile CA array and C_B for brittle CA array. Thus, at the next time increment, the states of concentrated cells (either ductile or brittle) are determined by the results of comparison between the product of damage variable and concentration factors and failure criteria mentioned above. An integrity indicator, Σ, is used to count the 'dead' cells of both ductile and brittle CA arrays by which the potential

fracture at every current time increment is evaluated. The Σ whose initial value is 1.0, decreases continuously with the accumulation of damage until N_D or N_B reaches its maximum value N_{D-max} or N_{B-max}. At this moment, the Σ turns to be zero, which means material inside the integration point is failed and the integration point does not have loading-bearing capacity any more. The FE will then be removed from the mesh when the zero Σ is transferred to FE. The Σ can be calculated by

$$\Sigma = 1 - \max\left(\frac{N_D}{N_{D-max}}, \frac{N_B}{N_{B-max}}\right) \qquad (3-11)$$

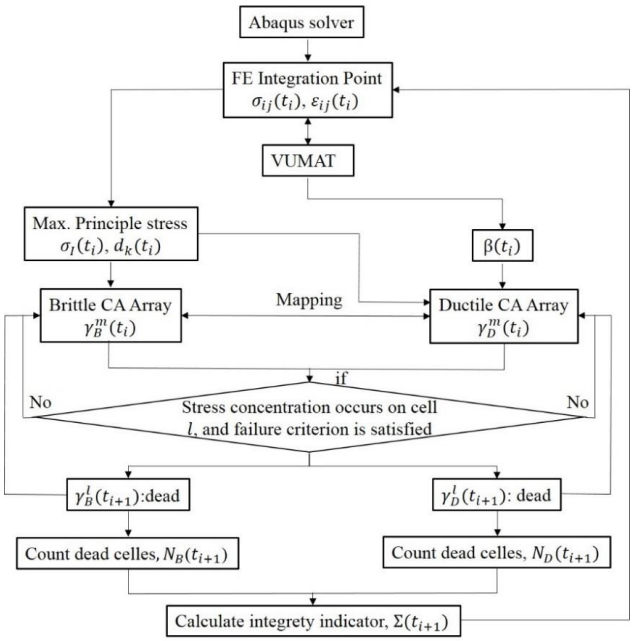

Figure 3.7 flow chart of the CAFE method [94]. Here, $\sigma_{ij}(t_i)$ and $\varepsilon_{ij}(t_i)$ are stress and strain tensors at time t_i provided by Abaqus solver; and $\beta(t_i)$ is damage variable of cells given by constitutive model to ductile CA array at time t_i; $\sigma_I(t_i)$ is the maximum principle stress of each element calculated from $\sigma_{ij}(t_i)$; $d_k(t_i)$ is the direction cosines of $\sigma_I(t_i)$; $\gamma_D^m(t_i)$ or $\gamma_B^m(t_i)$ is state of cell m in ductile or brittle CA arrays t_i; $\gamma_D^l(t_{i+1})$ or $\gamma_B^l(t_{i+1})$ is state of cell l where stress concentration occurs and failure criterion is satisfied in ductile or brittle cell arrays at time t_{i+1}; $N_D(t_{i+1})$ or $N_B(t_{i+1})$ is numbers of dead cells in ductile or brittle CA arrays at time t_{i+1}; $\Sigma(t_{i+1})$ is the integrity indicator at time at time t_{i+1}.

The calculation process of the CAFE method is presented in Fig. 3.7. It has to be mentioned that in order to reduce the calculation time, the damage variable $\beta(t_i)$ is given to the ductile CA array instead of the strain increment tensor $\Delta\varepsilon_{ij}(t_i)$, and accordingly only the solution dependent variable Σ is returned to the FE from CA array. Both ductile and brittle CA arrays are used only for the simulation of fracture propagation at each CA scale, while, the constitutive

response is calculated at FE level. In addition, for the easy achievement of convergence, in ductile CA array a normal distribution of damage value β_F rather than that of f_0 is adopted. At each increment of deformation, the model compares the present damage variable β with the failure value β_F until the material failed. Since two CA arrays occupy the same physical space, the evaluation of the cells shall be synchronized in both CA arrays. Thus, a mapping rule has been introduced in the CAFE method to reflect dead cells in ductile CA array into the corresponding brittle CA array, and vice versa [171]. After stress concentration occurred on the cell m in either CA arrays, it becomes dead when failure criteria are satisfied. A more detailed description about the CAFE method can be found in literature [171].

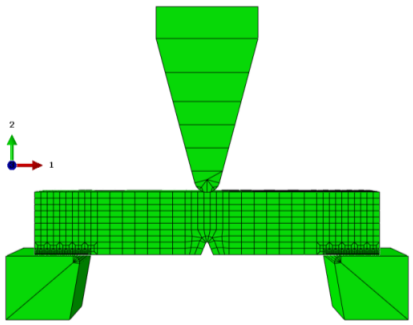

Figure 3.8 Finite element model of the Charpy test [94].

3.5 Simulation of Charpy impact test

An explicit dynamic process is adopted to model the DBT of Charpy test by using an explicit code with CAFE strategy implemented, which has been introduced in section 3.4. The geometry of Charpy V-notch specimen is 55mm×10mm×10mm according to the standard ASTM E23 16b [229], the notch radius and notch depth are 0.25mm and 2.0mm respectively. The striker and anvils size and geometry are also those of the standard ASTM E23 16b [229]. The finite element model of Charpy test is shown in Fig. 3.8, in which the full Charpy specimen is meshed with 8 nodes and reduced integration elements (C3D8R). Cells are assembled only to those elements in a small region in the center of specimen with a mesh size around 1mm, so-called damage zone, where damages in a real Charpy specimen is expected. The striker and two anvils are modelled as elastic body, and are meshed with C3D8R and C3D6 type of elements. The total number of elements in this model is 8250, in which damage zone composes of 700 elements. The contact between the Charpy specimen and striker and anvils is modeled with a friction coefficient 0.15. The initial velocity of striker is 5.5 m/s. It is noted that to improve the accuracy of computation, the mesh size in the damage zone of the numerical model

to study the influence of residual stress on the DBT of Charpy tests is reduced to 0.5mm. Accordingly, the number elements in damage zone and total number of elements in the model are 3560 and 20300 respectively.

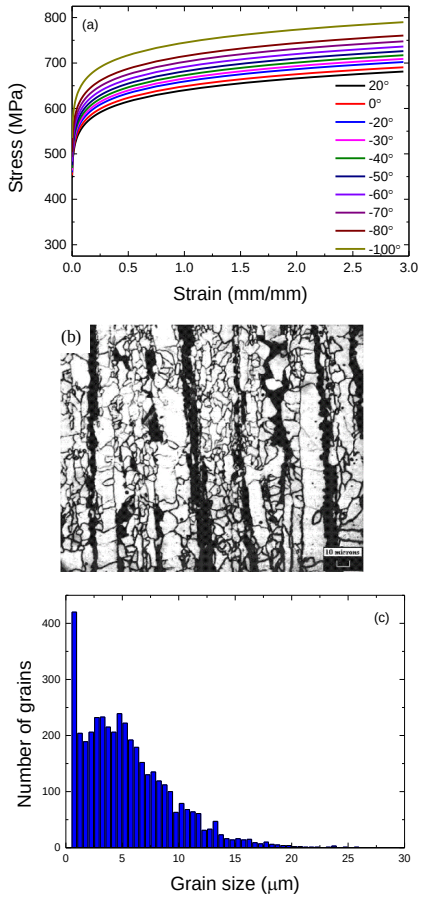

Figure 3.9 The properties and microstructure of TMCR steel: (a) flow stress and strain curve at different test temperatures[171], (b) the microstructure of TMCR steel [170] and (c) the histogram of grain size distribution [170].

The initial void volume fraction f_0 is assumed to be 0.0001. The statistical feature of damage failure value β_F conforms to a normal distribution, in which the mean value β_{F-mean} is 8.0 and the standard deviation β_{F-std} is 1.2. The material constant D and σ_1 are 1.65 and 400MPa respectively. These values of ductile damage variables used in the present work have been calibrated with experimental results of pure ductile fracture, for example the upper shelf energy (USE) of Charpy test. The flow property of the TMCR steel at different temperature is presented in Fig. 3.9 (a). The microstructure of this TMCR steel is presented in the Fig. 3.9 (b), which consists mainly of ferrite and some banded pearlites. Based on the measurement of grain size of this TMCR steel, the histogram of grain size distribution is obtained as shown in the

Fig. 3.9 (c), which presents a bimodal distribution. Since these tiny grains will never fracture as they have very high fracture strength, the modelling results are not affected by omitting this small volume of tiny grains. Hence, an equivalent unimodal three-parameter Weibull distribution is applied to characterize the grain size distribution of this material, in which the scale, shape and location parameter are 1.223, 5.392 and 0.516 respectively. The effective surface energy of TMCR steel estimated by using the continuum approach, which has been introduced in the section 3.3.2 is applied to calculate the cleavage fracture stress in terms of the Eq. 3-10. The fraction of brittle CA cells that cleavage is nucleated, η, is assumed to be 0.01. The misorientation threshold θ_{th} is assumed to be 40°. The effective surface energy for the fracture stress of cleavage will be calculated in the section 5.

3.6 Generation of residual stresses

When cooled down from a high temperature, residual stress can be generated in the materials or components where the mismatch of CTE exists. Recall the section 2.4.2, the mismatch of CTE is essentially a kind of material inhomogeneity, like the mismatch of hardening, yield stress, Young's modulus etc., which will produce an additional crack driving force according to the studies in the literature [209-212]. In principle, the interface, where material is inhomogeneous, is inclined to the crack extension with any angle, see Fig. 2.24. This implies that the variable configuration of crack and interface formed by the mismatch of CTE in the component could produce different residual stresses in the component. In the same time, these different residual stresses could also provide variable crack driving force. In present work, two extreme configurations, e.g., the interface perpendicular to crack extension (the mostly studied in the literature [213-215]), and the interface in parallel to the crack propagation, are designed for the common welding practice and subsequent fracture toughness tests, see the illustration in Fig. 3.10. In both configurations, the inhomogeneity of material is formed with a mismatch of CTE, namely ΔCTE denoted by $(\alpha_1 - \alpha_2)$, where α_1 and α_2 are also the CTE in two different regions in the configurations. It is assumed that the thermal expansion in different region is isotropic. In practice, the configuration 1 can be found in a full-thickness testing specimen with a pre-crack, cutting from a repair weld [230] or a clad pipe fabricated via explosive welding process [231], where the crack vertically propagates across the interface. The configuration 2 corresponds to a full-thickness testing specimen with a pre-crack extracted from a girth weld or butt weld in a pipeline [232], in which the pre-crack introduced in the weld meal extends in parallel to the interface formed by the weld metal and base metal. Here, the

difference is sharp crack in a CT type specimen applied in literatures [213-215] substituted with a blunt notch in a Chapry specimen in present work. Additionally, the inhomogeneity of material due to the mismatch of strength in base metal and weld metal is not considered here. Residual stresses in both configurations are generated by using the so-called eigenstrain method [13, 233] in a rapid cooling process. The thermal strain, namely, eigenstrain, induced by temperature change are given by

$$\varepsilon_{ij}^{*} = \alpha \Delta T \delta_{ij} \qquad (3-12)$$

where α is the CTE, ΔT is the temperature change and δ_{ij} is the unity tensor. Residual stresses are introduced by applying a unit temperature decrease into regions with different CTE within the specimen.

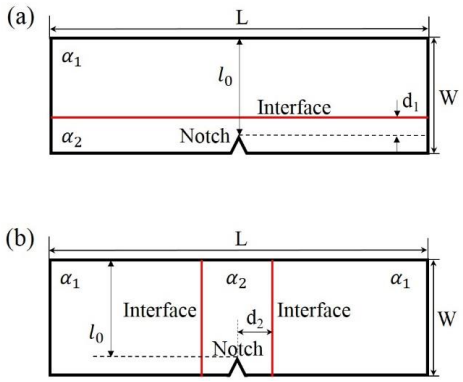

Figure 3.10 2D Configurations with crack and interface due to inhomogeneity of thermal expansion in the Charpy specimen: (a) interface perpendicular to the crack propagation; (b) interface parallel to the crack extension. Here, d_1 and d_2 are the distance of interface from notch root; l_0 is the ligament of Charpy specimen; L is the length of specimen; W is the width of specimen.

3.7 Constraint induced by the residual stress

O'Dowd and Shih [23, 234] has proposed a J-Q theory to describe the stress field near crack tip, which can be expressed by

$$\sigma_{ij} = \sigma_{ij}^{HRR} + Q\sigma_0 \left(\frac{r}{J/\sigma_0}\right)^{q} \tilde{\sigma}_{ij}(\theta, n) \qquad (3-13)$$

where

$$\sigma_{ij}^{HRR} = \left(\frac{J}{\alpha \varepsilon_0 \sigma_0 I_n r}\right)^{1/(n+1)} \sigma_0 \tilde{\sigma}_{ij}(\theta, n) \qquad (3-14)$$

σ_{ij}^{HRR} is the J-controlled HRR stress field proposed by Huthinson [235] and Rice and Rosengren [236]; r and θ are polar coordinates centered at the crack tip; n is the strain

hardening exponent; ε_0 is the yield strain; α is a material constant; σ_0 is the yield stress; $\tilde{\sigma}_{ij}$ is the dimensionless function of θ and n; Q is a hydrostatic stress parameter to quantify the crack-tip constraint caused by geometry or loading mode. A parameter, e.g., M, has been proposed by Zhang et al. [27, 237] to depict the constraint on the crack tip induced by the strength mismatch in the bi-material system of a weld component. The J-Q-M formulation has been developed to characterized the near-tip stress field in the presence of both geometry and material mismatch constraints [238], which also indicates that the constraint caused by geometry and mismatch are independent of each other. Following the similar philosophy, Liu et al. [195] and Ren et al. [28] have proposed an approach to describe the near-tip stress field in presence of residual stress, which can be expressed by

$$\sigma_{ij}^{RS} = \sigma_{ij}^{NoRS} + \sigma_0 R(r, \theta, n, J, \sigma_0 \ldots)\delta_{ij} \qquad (3-15)$$

where σ_{ij}^{NoRS} is near-tip stress field without the residual stress, which can be described by the Eq. (3-13) and (3-14); R is the constraint induced by the residual stress, which is relevant to r, θ, n, J and σ_0 etc. Thus, the R_{ij} can be estimated by

$$R_{ij} = \frac{\sigma_{ij}^{RS} - \sigma_{ij}^{NoRS}}{\sigma_0} \qquad (3-16)$$

In present work, the constraint R_{ij} on the notch root induced by the residual stresses are calculated according to the Eq. (3-16). And the features and evolution of constraint on the notch root due to different residual stresses generated in both configurations (introduced in section 3.6) has also been studied, which has been described in the paper 3 in detail.

Chapter 4. Main Results and Conclusions

As mentioned in the section 1.2, the main logical chain of present PhD thesis is: (i) firstly studying the reverse process of DBT, e.g., the BDT of single-crystal iron, to reveal its inherent mechanism and explore a physically-based variable to capture the temperature dependent fracture toughness of material in the transition regime; (ii) then, building a framework for the modelling of DBT of steel, achieved by implementing the numerical approach, e.g., CAFE method, with the physically-based variable obtained previously; (ii) investigating the influence of residual stress on the DBT of the welded components with the application of the framework of the modelling of DBT. Therefore, the main results and conclusions obtained in these three key topics will be introduced in this section.

4.1 The BDT of single-crystal iron

It has been mentioned in the section 2.3.1 that thermal activated dislocation nucleation and emission at crack tip can induce a shielding effect on the crack tip, which is the reason for the transition of brittle fracture to ductile fracture of single-crystal metals. Then, a continuum model, introduced in the section 3.1, has been employed to model the BDT behavior of single-crystal iron based on dislocation mobility controlled BDT theory. Since the constraint at crack tip usually exerts a significant influence on the fracture, the effect of *T*-stress on the BDT has also been studied, see also the section 3.1. Following the method and procedure introduced in the section 3.3.1, a group of parameters for the investigation of BDT has been identified and verified based on the experimental results by Tanaka et al. [135]. The effective surface energies for the assessment of cleavage fracture in transition region has been calculated in terms of the

method introduced in the section 3.2. The results obtained from the parametric study on BDT, e.g., the elastic zone size, temperature and exponent *m*, presents similar results in the literature, which proves that the continuum model is applicable for studying the BDT of single-crystal iron. The main finding of the present study can be concluded in the followings:

- The BDT behavior under different loading rates has been studied. It can be observed that lower loading rate can produce a smoother BDT curve and a lower critical BDT temperature, however loading rate has no effect on the fracture toughness at the critical BDT temperature.
- It is found that the change of the stress distribution ahead of crack tip due to the *T*-stress dictates the fracture toughness of single-crystal iron in the BDT transition region.
- Lower constraint leads to a higher fracture toughness in the transition region, a smoother transition curve and a lower critical BDT temperature, and also a higher fracture toughness at the critical BDT temperature.

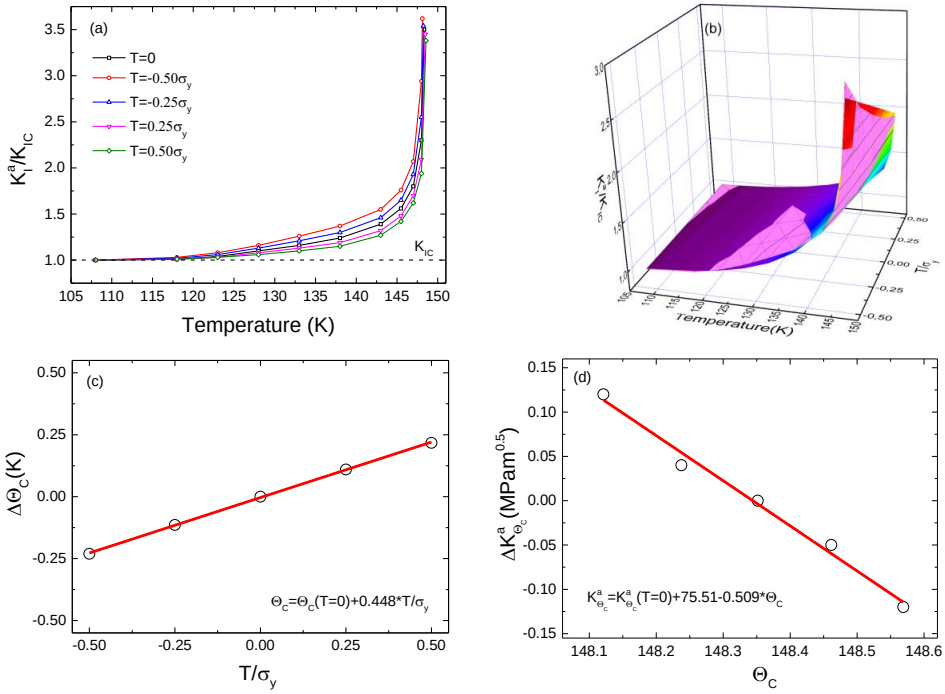

Figure 4.1 the constraint effect on BDT of single-crystal iron: (a) BDT curves at different T-stress, (b) comparison between predicted results and calculated results by Eq. 4-1(a), (c) critical transition temperature vs. T-stress, (d) fracture toughness vs. critical transition temperature.

- As shown in Fig. 4.1, A correlation between the fracture toughness and *T*-stress has been found: below critical BDT temperature, the fracture toughness is related to the

temperature dependent fracture toughness of a reference material without T-stress and the contribution of T-stress that relies on the temperature; at critical BDT temperature, the fracture toughness can be estimated with a linear function of T-stress, fracture toughness and critical BDT temperature of a reference material without T-stress. Therefore, a complete BDT curve can be predicted by the Eq. (4-1) created in present study once the amount of constraint and the BDT curve of a reference material without T-stress has been obtained.

$$K_I^a = \begin{cases} K_I^a(T=0) * \left[c_0 + g(\Theta) * \left(T/\sigma_y\right)\right], & \Theta < \Theta_C \\ K_I^a(T=0) + c_1 * \Theta_C(T=0) + c_2 * \left(T/\sigma_y\right) + c_3, & \Theta = \Theta_C \end{cases} \quad (4-1)$$

where c_0, c_1, c_2, and c_3 are constant can be obtained by fitting the predicted BDT curve with different T-stress.

- A solution to estimate the temperature-dependent effective surface energy law in the brittle-to-ductile transition has been explored in present work, which will benefit for the assessment cleavage fracture in the transition region.

4.2 Modelling of the DBT of a TMCR steel

As mentioned in the section 2.3.2, it is still a challenge to represent the competition between two failure mechanisms and the interaction between two failure modes in the transition region. To mitigate such a computational challenge in modelling of DBT, the CAFE method developed by Shterenlikht et al [170-172], introduced in the section 3.4, has been applied to predict the DBT of a TMCR steel, in which the statistical nature of microstructure has been incorporated at the same time. In order to realistically capture the temperature dependent fracture toughness in the transition region, a physically-based variable has to be searched, which is also one of the motivations of this work. Based on the work in paper 1, a continuum approach has been developed to estimate the effective surface energy for unstable cleavage formation, e.g., γ_{pm}, for the TMCR steel, which has been introduced in the section 3.2. Following the method and procedure introduced in the section 3.3.2, a group of parameters for the estimation the γ_{pm} has been identified and verified based on the experimental results by Tanaka et al. [227]. Further, to describe the essence of the competition between particle size and grain size controlled propagation of unstable cleavage, a more robust variable, effective surface energy for overcoming the barrier of grain boundary, e.g., γ_{mm}, was proposed. Finally, a framework for the modelling of DBT is explored through implementing the γ_{mm} into the CAFE method, in

which the numerical simulation of Charpy impact tests has been introduced in the section 3.5. Some important findings obtained in present work can be concluded as followings:

- It is proved that a second temperature dependent variable has to be found to reproduce the DBT curve, in addition to the temperature dependent flow properties. In present work, a continuum approach has been developed to establish the second temperature dependent variable, e.g., γ_{pm}. The calculated γ_{pm} of the TMCR steel is shown in Fig. 4.2(a).
- It is observed that the role of grain boundary on the unstable cleavage propagation cannot be ignored. Through analyzing the competition between the particle size and grain size dominated unstable cleavage propagation, a method to quantify the lower limit of γ_{mm} has been built, which is related to the γ_{pm} and a size ratio of grain size and critical particle size.

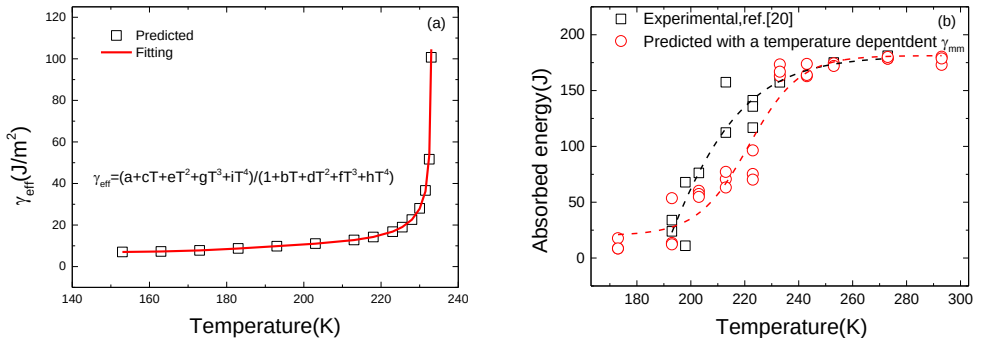

Figure 4.2 Prediction of the DBT of a TMCR steel: (a) Temperature dependent effective surface energy for the unstable cleavage formation, e.g., γ_{pm}; different T-stress, (b) the predicted DBT by using CAFE method implemented with γ_{mm}.

- Due to the fact that cleavage facet (unit) size or effective grain size, e.g., $d_{CF(U)S}$, is more appropriate for characterizing the cleavage fracture unit, the ratio of grain size to critical particle size has been replaced by $d_{CF(U)S}/c_{crit.}$. As such, an equation for the estimation of γ_{pm} has been built

$$\gamma_{mm} = \gamma_{pm} \cdot \left(d_{CF(U)S}/c_{crit.}\right) \qquad (4-2)$$

where $d_{CF(U)S}/c_{crit.}$ is a function of temperature. In the present work, a linear correlation of $d_{CF(U)S}/c_{crit.}$ and temperature is proposed based on the work by Lee et al. [107], which can be expressed as

$$\frac{d_{CF(U)S}}{c_{crit.}} = -0.025(\Theta - 273) + 4.0 \qquad (4-3)$$

- It is found that numerical simulation by using the CAFE method implemented with γ_{mm} is able to produce a full transition curve, especially with scattered absorbed energies in the transition region represented, see Fig. 4.2(b).

4.3 The effect of thermal residual stress on DBT

Inspired by studies on the effect of material inhomogeneity on fracture by Simha et al. [209-211] and the work by Rakin et al. [215], two configurations of the interface pertaining to the position of the notch root are designed with the mismach of CTE, which has been introduced in section 3.6. Residual stresses are generated with variable mismatch of CTE, e.g., ΔCTE, in both configurations of Charpy specimen by using the eigenstrain method. With the residual stress initially generated in the specimen, the influence of residual stress on DBT of welded TMCR steel has been studied by adopting CAFE method implemented with temperature dependent surface energy obtained in paper 2. The numerical simulation of Charpy impact tests has been introduced in section 3.5. To reveal the mechanism of residual stress on DBT, constraints in the vicinity of notch root induced by residual stresses have been estimated in both configurations. Some important findings obtained can be concluded as followings:

- Although the distribution of generated residual stresses presents a different feature in two configurations, it is observed that tensile residual stress is generated in the region where a higher CTE is employed in both configurations, and vice versa.
- The initial constraint caused by the residual stress in configuration 1is higher than that in configuration 2 when the same ΔCTE is adopted. However, with the increase of external load, the constraint in the vicinity of notch root induced by residual stress in configuration 1 vanishes much earlier than that in configuration 2.
- It is observed that in both configurations the absorbed energy of specimen decreases with the increase of residual stresses (e.g., corresponding to the decrease of ΔCTE). As a consequence, the DBT curves of two configurations generally shift to the higher temperature in the whole temperature range. The mechanism for the role of residual stress on the fracture toughness is that the constraint induced by the residual stresses on notch root can facilitate the fracture.
- It is found that the influence of residual stresses on the absorbed energies in both configurations shows a declining trend with the decrease of temperature. Therefore, a dramatic change on DBT due to the residual stress in both configurations can be observed at high temperature, e.g., the upper-shelf of transition curves.

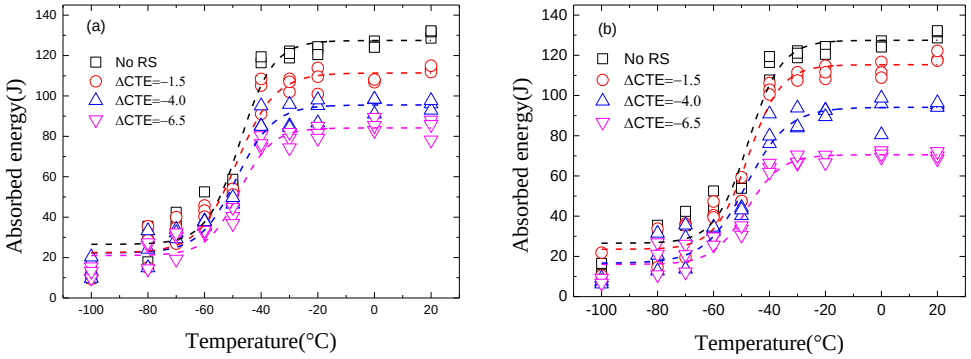

Figure 4.3 the influence of residual stress on DBT of a welded TMCR steel: (a) configuration 1, (b) configuration 2.

Chapter 5. Recommendations for Further Studies

This PhD thesis is written around a major topic DBT. Although some aspects pertaining to it have been involved, e.g., the fundamental mechanism, the framework of the numerical modelling, and the application to the component under residual stresses, there are still several aspects need to be further studied and some relevantly interesting issues to be explored in future studies.

5.1 Interaction between cleavage and crack tip plasticity

The essence of BDT is the consequence of the competition between cleavage fracture and the crack tip plasticity induced by the existence of dislocations. Although the elastic-viscoplastic continuum model based on dislocation dynamics used in present thesis can provide an applicable approach for dealing with such a competition on a continuum scale, however it has several limitations, for instance, anisotropy induced by the dislocation slip on multi-system, negligence of the dislocation nucleation, absence of dislocation multiplication etc. therefore, the following aspects would be interesting for the future work:

- To predict the BDT of single-crystal metals with dislocation slipping in multi-systems by using a numerical solution based on the dislocation dynamics [148].
- To predict the BDT of single-crystal metals by using Discrete Dislocation Dynamics approach [133], in which both screw dislocation and non-screw dislocation are involved, and a temperature dependent exponent m describing the dislocation motion is considered.

- To model the interaction between crack tip plasticity and brittle fracture by using a Multi-scale modeling framework, which combines 2D dislocation dynamics and cohesive zone model [239, 240], and to study the grain size effect on the fracture toughness in a polycrystalline metal [241] by using this frame work.
- To study the dislocation density evolution and interactions in crystalline materials by using Dislocation dynamics simulation [242, 243].

5.2 Modelling of DBT

The DBT of material under a dynamic load is simulated, e.g., Charpy test. And a framework for the DBT modelling has been built by implementing the CAFE method with a physically-based variable, e.g., the temperature dependent effective surface energy. However, some aspects pertaining to the numerical simulation and the framework still need to be further studied:

- The adiabatic heating effect and viscoplastic response of material with the elevation of loading rate should be considered [164, 167].
- The cleavage nucleation in the CAFE method should be studied and incorporated [174], and the real distribution of orientation of grains should be considered instead of a random distribution in the CAFE method.
- To calibrate or verify the parameters for the effective surface energy, the activation energy for the BDT, e.g., E_a, see section 3.3, should be measured on the targeted material through experiments [135, 227].
- To experimentally obtain the correlation between critical particle size and temperature of the targeted materials.
- The DBT of steel under a quasi-static load need to be studied, e.g., C(T) tests, SEN(B) tests etc., accordingly, a framework for this case needs to be explored and an implicit code of CAFE method needs to be developed.
- The DBT of large-scale structure under tensile load, e.g., curved wide plate tensile (CPT) tests [207].

5.3 The effect of residual stresses on fracture

The effect of residual stresses on DBT of welded TMCR steel has been studied by applying the framework for the modelling of DBT explored previously. The residual stresses are generated by using eigenstrain method in two designed configurations where interface formed by the

mismatch of thermal expansion of material is perpendicular or parallel to the crack extension. Some aspects will be interested in the future work:

- Since residual stresses can be easily changed by the large plastic deformation near the crack/notch tip due to the dynamic external load, it would be interesting to study the influence of residual stresses on the DBT or fracture of material/components under the condition of small scale yielding [189], e.g., C(T) tests, SEN(B) tests etc.
- Since the additional crack driving force, e.g., C_{inh}, has not calculated in present study, a direct answer for the mechanisms of the role of residual stresses on DBT or fracture cannot achieved in the perspective of the contribution of C_{inh} to fracture. Then, in a 2D case with a running crack, the estimation of C_{inh} induced by the mismatch of thermal expansion in the same configurations will facilitate the understanding the mechanism of residual stress on the fracture or DBT [213, 215].

Bibliography

[1] Oil and Gas Forecast to 2050, Energy transition outlook 2017, DNV.GL, 2017.
[2] OIL AND GAS FOR THE 21ST CENTURY, OG21, 2012.
[3] D.L. Gautier, K.J. Bird, R.R. Charpentier, A. Grantz, D.W. Houseknecht, T.R. Klett, T.E. Moore, J.K. Pitman, C.J. Schenk, J.H. Schuenemeyer, K. Sørensen, M.E. Tennyson, Z.C. Valin, C.J. Wandrey, Assessment of Undiscovered Oil and Gas in the Arctic, Science 324(5931) (2009) 1175-1179.
[4] D.L. Gautier, T.E. Moore, Introduction to the 2008 Circum-Arctic Resource Appraisal (CARA) professional paper, in: T.E. Moore, D.L. Gautier (Eds.) Professional Paper, Reston, VA, 2017, p. 20.
[5] The KMB project "Arctic Materials - Materials technology for safe and cost-effective exploration and operation under arctic conditions", Research Council of Norway, Contract Number 187389/S30 2008-2012.
[6] Project description-SMACC: Fundamental Studies of MAterials' behaviour for future Cold Climate applications, 2013.
[7] E. Østby, C. Thaulow, O.M. Akselsen, Quantitative Relation Between Acoustic Emission Signal Amplitude and Arrested Cleavage Microcrack Size, International Journal of Fracture (2012) 1-8.
[8] O.M. Akselsen, E. Østby, B. Nyhus, "Low temperature fracture toughness of X80 girth welds, ISOPE, Rhodes, Greece, 2012.
[9] O.M. Akselsen, E. Østby, C. Thaulow, Low temperature toughness in SA welding of 420 MPa steel, ISOPE, Hawaii, USA, 2011.
[10] P. Mohseni, J. Solberg, M. Karlsen, O. Akselsen, E. Østby, Investigation of mechanism of cleavage fracture initiation in intercritically coarse grained heat affected zone of HSLA steel, Materials Science and Technology 28(9-10) (2012) 9-10.
[11] A.M. Tahir, N.A.M. Lair, F.J. Wei, Investigation on mechanical properties of welded material under different types of welding filler (shielded metal arc welding), AIP Conference Proceedings 1958(1) (2018) 020003.
[12] P.J. Withers, Residual stress and its role in failure, Reports on Progress in Physics 70(12) (2007) 2211.
[13] T.-S. Jun, A.M. Korsunsky, Evaluation of residual stresses and strains using the Eigenstrain Reconstruction Method, International Journal of Solids and Structures 47(13) (2010) 1678-1686.
[14] X. Ren, A review on effect of residual stress on fracture, 2015.
[15] A.A. Griffith, G.I. Taylor, VI. The phenomena of rupture and flow in solids, Philosophical Transactions of the Royal Society of London. Series A, Containing Papers of a Mathematical or Physical Character 221(582-593) (1921) 163-198.
[16] G.R. Irwin, ONSET OF FAST CRACK PROPAGATION IN HIGH STRENGTH STEEL AND ALUMINUM ALLOYS, ; Naval Research Lab., Washington, D.C., 1956, p. Medium: X; Size: Pages: 17.
[17] H.M. Westergaard, Bearing Pressure and Cracks, Jouranl of Applied Mechanics 6 (1939) 49-53.
[18] G.R. Irwin, Analysis of Stresses and Strains Near the End of a Crack Traversing a Plate, J. Appl. Mech. (1957).
[19] J.R. Rice, A Path Independent Integral and the Approximate Analysis of Strain Concentration by Notches and Cracks, Journal of Applied Mechanics 35(2) (1968) 379-386.
[20] A.A. Wells, Unstable crack propagation in metals:cleavage and fast fracture, Proceedings of the Crack Propagation Symposium, Granfield, Uk, 1961.
[21] C. Betegón, J.W. Hancock, Two-Parameter Characterization of Elastic-Plastic Crack-Tip Fields, Journal of Applied Mechanics 58(1) (1991) 104-110.

[22] M.H. ZL Zhang, C Thaulow, The effect of T stress on the near tip stress field of an elastic-plastic interface crack, ICF 9, Sydney, Australia, 1997.
[23] N.P. O'Dowd, C.F. Shih, Family of crack-tip fields characterized by a triaxiality parameter—I. Structure of fields, Journal of the Mechanics and Physics of Solids 39(8) (1991) 989-1015.
[24] J. Xu, Z.L. Zhang, E. Østby, B. Nyhus, D.B. Sun, Effects of crack depth and specimen size on ductile crack growth of SENT and SENB specimens for fracture mechanics evaluation of pipeline steels, International Journal of Pressure Vessels and Piping 86(12) (2009) 787-797.
[25] C. Thaulow, E. Østby, B. Nyhus, Z.L. Zhang, B. Skallerud, Constraint correction of high strength steel: Selection of test specimens and application of direct calculations, Engineering Fracture Mechanics 71(16) (2004) 2417-2433.
[26] Y.J. Chao, S. Yang, M.A. Sutton, On the fracture of solids characterized by one or two parameters: Theory and practice, Journal of the Mechanics and Physics of Solids 42(4) (1994) 629-647.
[27] Z.L. Zhang, M. Hauge, C. Thaulow, Two-parameter characterization of the near-tip stress fields for a bi-material elastic-plastic interface crack, International Journal of Fracture 79(1) (1996) 65-83.
[28] X.B. Ren, Z.L. Zhang, B. Nyhus, Effect of residual stresses on the crack-tip constraint in a modified boundary layer model, International Journal of Solids and Structures 46(13) (2009) 2629-2641.
[29] P.A. Eikrem, Z.L. Zhang, B. Nyhus, Effect of plastic prestrain on the crack tip constraint of pipeline steels, International Journal of Pressure Vessels and Piping 84(12) (2007) 708-715.
[30] J. Besson, Continuum Models of Ductile Fracture: A Review, International Journal of Damage Mechanics 19(1) (2009) 3-52.
[31] W.M. Garrison, N.R. Moody, Ductile fracture, Journal of Physics and Chemistry of Solids 48(11) (1987) 1035-1074.
[32] L. Anand, W.A. Spitzig, Initiation of localized shear bands in plane strain, Journal of the Mechanics and Physics of Solids 28(2) (1980) 113-128.
[33] A. Pineau, A.A. Benzerga, T. Pardoen, Failure of metals I: Brittle and ductile fracture, Acta Materialia 107 (2016) 424-483.
[34] L. Babout, Y. Brechet, E. Maire, R. Fougères, On the competition between particle fracture and particle decohesion in metal matrix composites, Acta Materialia 52(15) (2004) 4517-4525.
[35] M. Achouri, G. Germain, P. Dal Santo, D. Saidane, Experimental characterization and numerical modeling of micromechanical damage under different stress states, Materials & Design 50 (2013) 207-222.
[36] S.H. Goods, L.M. Brown, Overview No. 1: The nucleation of cavities by plastic deformation, Acta Metallurgica 27(1) (1979) 1-15.
[37] A.S. Argon, J. Im, R. Safoglu, Cavity formation from inclusions in ductile fracture, Metallurgical Transactions A 6(4) (1975) 825.
[38] A. Needleman, A Continuum Model for Void Nucleation by Inclusion Debonding, Journal of Applied Mechanics 54(3) (1987) 525-531.
[39] A. Needleman, An analysis of tensile decohesion along an interface, Journal of the Mechanics and Physics of Solids 38(3) (1990) 289-324.
[40] J. Segurado, J. Llorca, A new three-dimensional interface finite element to simulate fracture in composites, International Journal of Solids and Structures 41(11) (2004) 2977-2993.
[41] A. Weck, D.S. Wilkinson, E. Maire, H. Toda, Visualization by X-ray tomography of void growth and coalescence leading to fracture in model materials, Acta Materialia 56(12) (2008) 2919-2928.
[42] J.R. Rice, D.M. Tracey, On the ductile enlargement of voids in triaxial stress fields∗, Journal of the Mechanics and Physics of Solids 17(3) (1969) 201-217.
[43] F.A. McClintock, A Criterion for Ductile Fracture by the Growth of Holes, Journal of Applied Mechanics 35(2) (1968) 363-371.

[44] A.L. Gurson, Continuum theory of ductile rupture by void nucleation and growth: Part 1Yield criteria and flow rules for a porous ductile media, 1977.
[45] V. Tvergaard, On localization in ductile materials containing spherical voids, International Journal of Fracture 18(4) (1982) 237-252.
[46] V. Tvergaard, Material Failure by Void Growth to Coalescence, in: J.W. Hutchinson, T.Y. Wu (Eds.), Advances in Applied Mechanics, Elsevier1989, pp. 83-151.
[47] T.L. Anderson, Fracture Mechanics: Fundamentals and Applications, Fourth Edition, CRC Press2017.
[48] J. Faleskog, X. Gao, C.F. Shih, Cell model for nonlinear fracture analysis – I. Micromechanics calibration, International Journal of Fracture 89(4) (1998) 355-373.
[49] M. Gologanu, J.-B. Leblond, J. Devaux, Approximate models for ductile metals containing non-spherical voids—Case of axisymmetric prolate ellipsoidal cavities, Journal of the Mechanics and Physics of Solids 41(11) (1993) 1723-1754.
[50] A.A. Benzerga, J. Besson, Plastic potentials for anisotropic porous solids, European Journal of Mechanics - A/Solids 20(3) (2001) 397-434.
[51] V. Monchiet, O. Cazacu, E. Charkaluk, D. Kondo, Macroscopic yield criteria for plastic anisotropic materials containing spheroidal voids, International Journal of Plasticity 24(7) (2008) 1158-1189.
[52] A. Weck, D.S. Wilkinson, Experimental investigation of void coalescence in metallic sheets containing laser drilled holes, Acta Materialia 56(8) (2008) 1774-1784.
[53] P.F. Thomason, A three-dimensional model for ductile fracture by the growth and coalescence of microvoids, Acta Metallurgica 33(6) (1985) 1087-1095.
[54] P.F. Thomason, Three-dimensional models for the plastic limit-loads at incipient failure of the intervoid matrix in ductile porous solids, Acta Metallurgica 33(6) (1985) 1079-1085.
[55] Z.L. Zhang, E. Niemi, A new failure criterion for the Gurson-Tvergaard dilational constitutive model, International Journal of Fracture 70(4) (1994) 321-334.
[56] J. Koplik, A. Needleman, Void growth and coalescence in porous plastic solids, International Journal of Solids and Structures 24(8) (1988) 835-853.
[57] T. Pardoen, J.W. Hutchinson, An extended model for void growth and coalescence, Journal of the Mechanics and Physics of Solids 48(12) (2000) 2467-2512.
[58] A.A. Benzerga, J.-B. Leblond, Effective Yield Criterion Accounting for Microvoid Coalescence, Journal of Applied Mechanics 81(3) (2013) 031009-031009-7.
[59] D. Fabrègue, T. Pardoen, A constitutive model for elastoplastic solids containing primary and secondary voids, Journal of the Mechanics and Physics of Solids 56(3) (2008) 719-741.
[60] M.E. Torki, A.A. Benzerga, J.B. Leblond, On Void Coalescence Under Combined Tension and Shear, Journal of Applied Mechanics 82(7) (2015) 071005-071005-15.
[61] V. Tvergaard, A. Needleman, Analysis of the cup-cone fracture in a round tensile bar, Acta Metallurgica 32(1) (1984) 157-169.
[62] X. Gao, J. Kim, Modeling of ductile fracture: Significance of void coalescence, International Journal of Solids and Structures 43(20) (2006) 6277-6293.
[63] A. Asserin–Lebert, J. Besson, A.F. Gourgues, Fracture of 6056 aluminum sheet materials: effect of specimen thickness and hardening behavior on strain localization and toughness, Materials Science and Engineering: A 395(1) (2005) 186-194.
[64] M.A. James, J.C. Newman, The effect of crack tunneling on crack growth: experiments and CTOA analyses, Engineering Fracture Mechanics 70(3) (2003) 457-468.
[65] Y. Bai, T. Wierzbicki, A new model of metal plasticity and fracture with pressure and Lode dependence, International Journal of Plasticity 24(6) (2008) 1071-1096.
[66] K.S. Zhang, J.B. Bai, D. François, Numerical analysis of the influence of the Lode parameter on void growth, International Journal of Solids and Structures 38(32) (2001) 5847-5856.

[67] I. Barsoum, J. Faleskog, Rupture mechanisms in combined tension and shear—Experiments, International Journal of Solids and Structures 44(6) (2007) 1768-1786.
[68] I. Barsoum, J. Faleskog, Rupture mechanisms in combined tension and shear—Micromechanics, International Journal of Solids and Structures 44(17) (2007) 5481-5498.
[69] V. Tvergaard, Bifurcation into a localized mode from non-uniform periodic deformations around a periodic pattern of voids, Journal of the Mechanics and Physics of Solids 69 (2014) 112-122.
[70] F. Scheyvaerts, P.R. Onck, C. Tekogˇlu, T. Pardoen, The growth and coalescence of ellipsoidal voids in plane strain under combined shear and tension, Journal of the Mechanics and Physics of Solids 59(2) (2011) 373-397.
[71] M. Dunand, D. Mohr, Effect of Lode parameter on plastic flow localization after proportional loading at low stress triaxialities, Journal of the Mechanics and Physics of Solids 66 (2014) 133-153.
[72] L. Xue, Constitutive modeling of void shearing effect in ductile fracture of porous materials, Engineering Fracture Mechanics 75(11) (2008) 3343-3366.
[73] F.A. McClintock, S.M. Kaplan, C.A. Berg, Ductile fracture by hole growth in shear bands, International Journal of Fracture Mechanics 2(4) (1966) 614-627.
[74] K. Nahshon, J.W. Hutchinson, Modification of the Gurson Model for shear failure, European Journal of Mechanics - A/Solids 27(1) (2008) 1-17.
[75] C.C. Chu, A. Needleman, Void Nucleation Effects in Biaxially Stretched Sheets, Journal of Engineering Materials and Technology 102(3) (1980) 249-256.
[76] Z.L. Zhang, C. Thaulow, J. Ødegård, A complete Gurson model approach for ductile fracture, Engineering Fracture Mechanics 67(2) (2000) 155-168.
[77] J. Lemaitre, J.-L. Chaboche, Mechanics of Solid Materials, Cambridge University Press, Cambridge, 1990.
[78] G. Rousselier, Ductile fracture models and their potential in local approach of fracture, Nuclear Engineering and Design 105(1) (1987) 97-111.
[79] G. Rousselier, Dissipation in porous metal plasticity and ductile fracture, Journal of the Mechanics and Physics of Solids 49(8) (2001) 1727-1746.
[80] M.K. Samal, M. Seidenfuss, E. Roos, A new mesh-independent Rousselier's damage model: Finite element implementation and experimental verification, International Journal of Mechanical Sciences 51(8) (2009) 619-630.
[81] H. Tu, The Rousselier Model, Numerical Simulation and Experimental Investigation of the Fracture Behaviour of an Electron Beam Welded Steel Joint, Springer International Publishing, Cham, 2018, pp. 53-73.
[82] V. Tvergaard, J.W. Hutchinson, Effect of strain-dependent cohesive zone model on predictions of crack growth resistance, International Journal of Solids and Structures 33(20) (1996) 3297-3308.
[83] T. Siegmund, W. Brocks, A numerical study on the correlation between the work of separation and the dissipation rate in ductile fracture, Engineering Fracture Mechanics 67(2) (2000) 139-154.
[84] Y.A. Roy, R.H. Dodds, Simulation of ductile crack growth in thin aluminum panels using 3-D surface cohesive elements, International Journal of Fracture 110(1) (2001) 21-45.
[85] I. Scheider, M. Schödel, W. Brocks, W. Schönfeld, Crack propagation analyses with CTOA and cohesive model: Comparison and experimental validation, Engineering Fracture Mechanics 73(2) (2006) 252-263.
[86] E. Bouyne, H.M. Flower, T.C. Lindley, A. Pineau, Use of EBSD technique to examine microstructure and cracking in a bainitic steel, Scripta Materialia 39(3) (1998) 295-300.
[87] H.M. Flower, T.C. Lindley, Electron backscattering diffraction study of acicular ferrite, bainite, and martensite steel microstructures, Materials Science and Technology 16(1) (2000) 26-40.

[88] A. Lambert-Perlade, T. Sturel, A.F. Gourgues, J. Besson, A. Pineau, Mechanisms and modeling of cleavage fracture in simulated heat-affected zone microstructures of a high-strength low alloy steel, Metall and Mat Trans A 35(3) (2004) 1039-1053.
[89] Y. Qiao, A.S. Argon, Cleavage crack-growth-resistance of grain boundaries in polycrystalline Fe–2%Si alloy: experiments and modeling, Mechanics of Materials 35(1) (2003) 129-154.
[90] Y. Qiao, A.S. Argon, Cleavage cracking resistance of high angle grain boundaries in Fe–3%Si alloy, Mechanics of Materials 35(3) (2003) 313-331.
[91] A. Pineau, Crossing grain boundaries in metals by slip bands, cleavage and fatigue cracks, Philosophical Transactions of the Royal Society A: Mathematical, Physical and Engineering Sciences 373(2038) (2015) 20140131.
[92] T. Lin, A.G. Evans, R.O. Ritchie, Stochastic modeling of the independent roles of particle size and grain size in transgranular cleavage fracture, Metall and Mat Trans A 18(4) (1987) 641-651.
[93] M. Kroon, J. Faleskog, Micromechanics of cleavage fracture initiation in ferritic steels by carbide cracking, Journal of the Mechanics and Physics of Solids 53(1) (2005) 171-196.
[94] Y. Li, A. Shterenlikht, X. Ren, J. He, Z. Zhang, CAFE based multi-scale modelling of ductile-to-brittle transition of steel with a temperature dependent effective surface energy, Materials Science and Engineering: A 755 (2019) 220-230.
[95] M.A. Linaza, J.M. Rodriguez-Ibabe, J.J. Urcola, DETERMINATION OF THE ENERGETIC PARAMETERS CONTROLLING CLEAVAGE FRACTURE INITIATION IN STEELS, Fatigue & Fracture of Engineering Materials & Structures 20(5) (1997) 619-632.
[96] J.I. San Martin, J.M. Rodriguez-Ibabe, Determination of energetic parameters controlling cleavage fracture in a Ti-V microalloyed ferrite-pearlite steel, Scripta Materialia 40(4) (1999) 459-464.
[97] P. Bowen, S.G. Druce, J.F. Knott, Effects of microstructure on cleavage fracture in pressure vessel steel, Acta Metallurgica 34(6) (1986) 1121-1131.
[98] Y. Li, X. Ren, J. He, Z. Zhang, Constraint effect on the brittle-to-ductile transition of single-crystal iron induced by dislocation mobility, International Journal of Mechanical Sciences 149 (2018) 212-223.
[99] J.H. Chen, G.Z. Wang, H.J. Wang, A statistical model for cleavage fracture of low alloy steel, Acta Materialia 44(10) (1996) 3979-3989.
[100] J.H. Chen, Q. Wang, G.Z. Wang, Z. Li, Fracture behavior at crack tip — a new framework for cleavage mechanism of steel, Acta Materialia 51(7) (2003) 1841-1855.
[101] R.O. Ritchie, J.F. Knott, J.R. Rice, On the relationship between critical tensile stress and fracture toughness in mild steel, Journal of the Mechanics and Physics of Solids 21(6) (1973) 395-410.
[102] W. Weibull, A Statistical Distribution Function of Wide Applicability, A Statistical Distribution Function of Wide Applicability (1951) 293-297.
[103] F.M. Beremin, A. Pineau, F. Mudry, J.-C. Devaux, Y. D'Escatha, P. Ledermann, A local criterion for cleavage fracture of a nuclear pressure vessel steel, Metallurgical Transactions A 14(11) (1983) 2277-2287.
[104] K. Wallin, T. Saario, K. Törrönen, Statistical model for carbide induced brittle fracture in steel, Metal Science 18(1) (1984) 13-16.
[105] K. Wallin, Fracture Toughness Transition Curve Shape for Ferritic Structural Steels, in: S.H. Teoh, K.H. Lee (Eds.), Fracture of Engineering Materials and Structures, Springer Netherlands, Dordrecht, 1991, pp. 83-88.
[106] T. Lin, A.G. Evans, R.O. Ritchie, A statistical model of brittle fracture by transgranular cleavage, Journal of the Mechanics and Physics of Solids 34(5) (1986) 477-497.
[107] S. Lee, S. Kim, B. Hwang, B.S. Lee, C.G. Lee, Effect of carbide distribution on the fracture toughness in the transition temperature region of an SA 508 steel, Acta Materialia 50(19) (2002) 4755-4762.

[108] B. Tanguy, J. Besson, A. Pineau, Comment on "Effect of carbide distribution on the fracture toughness in the transition temperature region of an SA 508 steel", Scripta Materialia 49(2) (2003) 191-197.
[109] L. Xia, L. Cheng, Transition from ductile tearing to cleavage fracture: A cell-model approach, International Journal of Fracture 87(3) (1997) 289-306.
[110] Gao, Faleskog, F. Shih, Analysis of ductile to cleavage transition in part-through cracks using a cell model incorporating statistics, Fatigue & Fracture of Engineering Materials & Structures 22(3) (1999) 239-250.
[111] X. Gao, J. Faleskog, C.F. Shih, Cell model for nonlinear fracture analysis – II. Fracture- process calibration and verification, International Journal of Fracture 89(4) (1998) 375-398.
[112] X. Gao, C. Ruggieri, R.H. Dodds, Calibration of Weibull stress parameters using fracture toughness data, International Journal of Fracture 92(2) (1998) 175-200.
[113] X. Gao, R.H. Dodds, Constraint effects on the ductile-to-brittle transition temperature of ferritic steels: a Weibull stress model, International Journal of Fracture 102(1) (2000) 43-69.
[114] F. Minami, M. Iida, W. Takahara, N. Konda, K. Arimochi, Fracture mechanics analysis of Charpy test results based on the weibull stress criterion, in: D. François, A. Pineau (Eds.), European Structural Integrity Society, Elsevier2002, pp. 411-418.
[115] J.P. Petti, R.H. Dodds, Calibration of the Weibull stress scale parameter, σu, using the Master Curve, Engineering Fracture Mechanics 72(1) (2005) 91-120.
[116] J.P. Petti, R.H. Dodds, Ductile tearing and discrete void effects on cleavage fracture under small-scale yielding conditions, International Journal of Solids and Structures 42(13) (2005) 3655-3676.
[117] J.H. Chen, Physical models for cleavage fracture at various temperatures—Bases for local approach to fracture of HSLA steel, Materials Science and Engineering: A 486(1–2) (2008) 369-375.
[118] C. Ruggieri, R.H. Dodds, A local approach to cleavage fracture modeling: An overview of progress and challenges for engineering applications, Engineering Fracture Mechanics 187 (2018) 381-403.
[119] L.E. Kaeghele, A.S. Tetelman, A statistical investigation of microcrack formation, Acta Metallurgica 17(4) (1969) 463-475.
[120] J. Gurland, Observations on the fracture of cementite particles in a spheroidized 1.05% c steel deformed at room temperature, Acta Metallurgica 20(5) (1972) 735-741.
[121] S.R. Bordet, A.D. Karstensen, D.M. Knowles, C.S. Wiesner, A new statistical local criterion for cleavage fracture in steel. Part I: model presentation, Engineering Fracture Mechanics 72(3) (2005) 435-452.
[122] S.R. Bordet, A.D. Karstensen, D.M. Knowles, C.S. Wiesner, A new statistical local criterion for cleavage fracture in steel. Part II: application to an offshore structural steel, Engineering Fracture Mechanics 72(3) (2005) 453-474.
[123] S.R. BORDET, B. TANGUY, J. BESSON, S. BUGAT, D. MOINEREAU, A. PINEAU, Cleavage fracture of RPV steel following warm pre-stressing: micromechanical analysis and interpretation through a new model, Fatigue & Fracture of Engineering Materials & Structures 29(9-10) (2006) 799-816.
[124] G. Bernauer, W. Brocks, W. Schmitt, Modifications of the Beremin model for cleavage fracture in the transition region of a ferritic steel, Engineering Fracture Mechanics 64(3) (1999) 305-325.
[125] A.S. Argon, Mechanics and Physics of Brittle to Ductile Transitions in Fracture, Journal of Engineering Materials and Technology 123(1) (2000) 1-11.
[126] P.B. Hirsch, S.G. Roberts, Modelling plastic zones and the brittle-ductile transition, Philosophical Transactions of the Royal Society of London. Series A: Mathematical, Physical and Engineering Sciences 355(1731) (1997) 1991-2002.

[127] M. Brede, P. Haasen, The brittle-to-ductile transition in doped silicon as a model substance, Acta Metallurgica 36(8) (1988) 2003-2018.
[128] M. Brede, The brittle-to-ductile transition in silicon, Acta Metallurgica et Materialia 41(1) (1993) 211-228.
[129] J.S.a.S.G. Roberts, The brittle–ductile transition in silicon. I. Experiments, Proceedings of the Royal Society of London. A. Mathematical and Physical Sciences 421(1860) (1989) 1-23.
[130] P.B. Hirsch, S.G. Roberts, The brittle-ductile transition in silicon, Philosophical Magazine A 64(1) (1991) 55-80.
[131] B.J. Gally, A.S. Argon, Brittle-to-ductile transitions in the fracture of silicon single crystals by dynamic crack arrest, Philosophical Magazine A 81(3) (2001) 699-740.
[132] P. Gumbsch, J. Riedle, A. Hartmaier, H.F. Fischmeister, Controlling Factors for the Brittle-to-Ductile Transition in Tungsten Single Crystals, Science 282(5392) (1998) 1293-1295.
[133] A. Hartmaier, P. Gumbsch, Thermal activation of crack-tip plasticity: The brittle or ductile response of a stationary crack loaded to failure, Physical Review B 71(2) (2005) 024108.
[134] A. Hartmaier, P. Gumbsch, The brittle-to-ductile transition and dislocation activity at crack tips, Journal of Computer-Aided Materials Design 6(2) (1999) 145-155.
[135] M. Tanaka, E. Tarleton, S.G. Roberts, The brittle–ductile transition in single-crystal iron, Acta Materialia 56(18) (2008) 5123-5129.
[136] M. Tanaka, A.J. Wilkinson, S.G. Roberts, Ductile–brittle transition of polycrystalline iron and iron–chromium alloys, Journal of Nuclear Materials 378(3) (2008) 305-311.
[137] A.P.L. Turner, T. Vreeland, The effect of stress and temperature on the velocity of dislocations in pure iron monocrystals, Acta Metallurgica 18(11) (1970) 1225-1235.
[138] J.R. Rice, R. Thomson, Ductile versus brittle behaviour of crystals, Philosophical Magazine 29(1) (1974) 73-97.
[139] J.R. Rice, Dislocation nucleation from a crack tip: An analysis based on the Peierls concept, Journal of the Mechanics and Physics of Solids 40(2) (1992) 239-271.
[140] G. Xu, A.S. Argon, M. Ortiz, Nucleation of dislocations from crack tips under mixed modes of loading: Implications for brittle against ductile behaviour of crystals, Philosophical Magazine A 72(2) (1995) 415-451.
[141] G.E. Beltz, D.M. Lipkin, L.L. Fischer, Role of Crack Blunting in Ductile Versus Brittle Response of Crystalline Materials, Physical Review Letters 82(22) (1999) 4468-4471.
[142] A.S. Argon, Brittle to ductile transition in cleavage fracture, Acta Metallurgica 35(1) (1987) 185-196.
[143] S.G.R.a.J.S. P. B. Hirsch, The brittle-ductile transition in silicon. II. Interpretation, Proceedings of the Royal Society of London. A. Mathematical and Physical Sciences 421(1860) (1989) 25-53.
[144] J.R. Rice, G.E. Beltz, The activation energy for dislocation nucleation at a crack, Journal of the Mechanics and Physics of Solids 42(2) (1994) 333-360.
[145] R.M. Thomson, J.E. Sinclair, Mechanics of cracks screened by dislocations, Acta Metallurgica 30(7) (1982) 1325-1334.
[146] I.H. Lin, R. Thomson, Cleavage, dislocation emission, and shielding for cracks under general loading, Acta Metallurgica 34(2) (1986) 187-206.
[147] D.J.B. D. Hull, introduction to dislocations, Fifth Edition, Elsevier Ltd, Oxford, 2011.
[148] Y.-B. Xin, K.J. Hsia, Simulation of the brittle-ductile transition in silicon single crystals using dislocation mechanics, Acta Materialia 45(4) (1997) 1747-1759.
[149] V.R. Nitzsche, K.J. Hsia, Modelling of dislocation mobility controlled brittle-to-ductile transition, Materials Science and Engineering: A 176(1) (1994) 155-164.
[150] A. Pineau, Modeling ductile to brittle fracture transition in steels—micromechanical and physical challenges, International Journal of Fracture 150(1) (2008) 129-156.

[151] L. Xia, C.F. Shih, Ductile crack growth—III. Transition to cleavage fracture incorporating statistics, Journal of the Mechanics and Physics of Solids 44(4) (1996) 603-639.
[152] E. Amar, A. Pineau, Application of a local approach to ductile-brittle transition in a low-alloyed steel, Nuclear Engineering and Design 105(1) (1987) 89-96.
[153] L. Xia, C.F. Shih, Ductile crack growth-I. A numerical study using computational cells with microstructurally-based length scales, Journal of the Mechanics and Physics of Solids 43(2) (1995) 233-259.
[154] L. Xia, C.F. Shih, Ductile crack growth—II. Void nucleation and geometry effects on macroscopic fracture behavior, Journal of the Mechanics and Physics of Solids 43(12) (1995) 1953-1981.
[155] R. Dodds, C. Ruggieri, K. Koppenhoefer, 3-D Constraint Effects on Models for Transferability of Cleavage Fracture Toughness, 3-D Constraint Effects on Models for Transferability of Cleavage Fracture Toughness1997.
[156] B. Tanguy, J. Besson, R. Piques, A. Pineau, Numerical modeling of Charpy V—notch tests, in: D. François, A. Pineau (Eds.), European Structural Integrity Society, Elsevier2002, pp. 461-468.
[157] E.P. Busso, Y. Lei, N.P. O'Dowd, G.A. Webster, Mechanistic Prediction of Fracture Processes in Ferritic Steel Welds Within the Transition Temperature Regime, Journal of Engineering Materials and Technology 120(4) (1998) 328-337.
[158] K. Wallin, The effect of ductile tearing on cleavage fracture probability in fracture toughness testing, Engineering Fracture Mechanics 32(4) (1989) 523-531.
[159] K. Wallin, Statistical Aspects of Constraint with Emphasis on Testing and Analysis of Laboratory Specimens in the Transition Region, Statistical Aspects of Constraint with Emphasis on Testing and Analysis of Laboratory Specimens in the Transition Region1993.
[160] M.K. Samal, M. Seidenfuss, E. Roos, B.K. Dutta, H.S. Kushwaha, Experimental and numerical investigation of ductile-to-brittle transition in a pressure vessel steel, Materials Science and Engineering: A 496(1) (2008) 25-35.
[161] M.K. Samal, J.K. Chakravartty, M. Seidenfuss, E. Roos, Evaluation of fracture toughness and its scatter in the DBTT region of different types of pressure vessel steels, Engineering Failure Analysis 18(1) (2011) 172-185.
[162] V. Tvergaard, A. Needleman, An analysis of the temperature and rate dependence of Charpy V-notch energies for a high nitrogen steel, International Journal of Fracture 37(3) (1988) 197-215.
[163] V. Tvergaard, A. Needleman, An analysis of the brittle-ductile transition in dynamic crack growth, International Journal of Fracture 59(1) (1993) 53-67.
[164] A. Needleman, V. Tvergaard, Numerical modeling of the ductile-brittle transition, International Journal of Fracture 101(1) (2000) 73.
[165] A. Rossoll, C. Berdin, C. Prioul, Determination of the Fracture Toughness of a Low Alloy Steel by the Instrumented Charpy Impact Test, International Journal of Fracture 115(3) (2002) 205-226.
[166] B. Tanguy, J. Besson, R. Piques, A. Pineau, Ductile to brittle transition of an A508 steel characterized by Charpy impact test: Part I: experimental results, Engineering Fracture Mechanics 72(1) (2005) 49-72.
[167] B. Tanguy, J. Besson, R. Piques, A. Pineau, Ductile to brittle transition of an A508 steel characterized by Charpy impact test: Part II: modeling of the Charpy transition curve, Engineering Fracture Mechanics 72(3) (2005) 413-434.
[168] P. Chakraborty, S.B. Biner, A unified cohesive zone approach to model the ductile to brittle transition of fracture toughness in reactor pressure vessel steels, Engineering Fracture Mechanics 131 (2014) 194-209.

[169] G. Hütter, T. Linse, S. Roth, U. Mühlich, M. Kuna, A modeling approach for the complete ductile–brittle transition region: cohesive zone in combination with a non-local Gurson-model, International Journal of Fracture 185(1) (2014) 129-153.
[170] A. Shterenlikht, I.C. Howard, The CAFE model of fracture—application to a TMCR steel, Fatigue & Fracture of Engineering Materials & Structures 29(9-10) (2006) 770-787.
[171] A. Shterenlikht, 3D CAFE modelling of transitional ductile-brittle fracture in steel, The University of Sheffield, UK, 2003.
[172] A. Shterenlikht, I.C. Howard, Cellular Automata Finite Element (CAFE) modelling of transitional ductile-brittle fracture in steel, The 15th European Conference of Fracture (ECF15), KTH, Stockholm, Sweden, 2004.
[173] S.J. Wu, C.L. Davis, A. Shterenlikht, I.C. Howard, Modeling the ductile-brittle transition behavior in thermomechanically controlled rolled steels, Metall and Mat Trans A 36(4) (2005) 989-997.
[174] S. Das, A. Shterenlikht, I.C. Howard, E.J. Palmiere, A general method for coupling microstructural response with structural performance, Proceedings of the Royal Society A: Mathematical, Physical and Engineering Science 462(2071) (2006) 2085-2096.
[175] A. Shterenlikht, L. Margetts, Three-dimensional cellular automata modelling of cleavage propagation across crystal boundaries in polycrystalline microstructures, Proceedings of the Royal Society of London A: Mathematical, Physical and Engineering Sciences 471(2177) (2015).
[176] Standard Test Method for Determination of Reference Temperature, T0, for Ferritic Steels in the Transition Range (ASTM E1921-18), American Society for Testing and Materials, 2018.
[177] B. Wasiluk, J.P. Petti, R.H. Dodds, Temperature dependence of Weibull stress parameters: Studies using the Euro-material, Engineering Fracture Mechanics 73(8) (2006) 1046-1069.
[178] Y. Cao, H. Hui, G. Wang, F.-Z. Xuan, Inferring the temperature dependence of Beremin cleavage model parameters from the Master Curve, Nuclear Engineering and Design 241(1) (2011) 39-45.
[179] G. Qian, V.F. González-Albuixech, M. Niffenegger, Calibration of Beremin model with the Master Curve, Engineering Fracture Mechanics 136 (2015) 15-25.
[180] X. Gao, G. Zhang, T.S. Srivatsan, A probabilistic model for prediction of cleavage fracture in the ductile-to-brittle transition region and the effect of temperature on model parameters, Materials Science and Engineering: A 415(1) (2006) 264-272.
[181] M. Moattari, I. Sattari-Far, I. Persechino, N. Bonora, Prediction of fracture toughness in ductile-to-brittle transition region using combined CDM and Beremin models, Materials Science and Engineering: A 657 (2016) 161-172.
[182] P.J. Withers, H.K.D.H. Bhadeshia, Residual stress. Part 1 – Measurement techniques, Materials Science and Technology 17(4) (2001) 355-365.
[183] N.S. Rossini, M. Dassisti, K.Y. Benyounis, A.G. Olabi, Methods of measuring residual stresses in components, Materials & Design 35 (2012) 572-588.
[184] C.D.M. Liljedahl, O. Zanellato, M.E. Fitzpatrick, J. Lin, L. Edwards, The effect of weld residual stresses and their re-distribution with crack growth during fatigue under constant amplitude loading, International Journal of Fatigue 32(4) (2010) 735-743.
[185] C.D.M. Liljedahl, M.L. Tan, O. Zanellato, S. Ganguly, M.E. Fitzpatrick, L. Edwards, Evolution of residual stresses with fatigue loading and subsequent crack growth in a welded aluminium alloy middle tension specimen, Engineering Fracture Mechanics 75(13) (2008) 3881-3894.
[186] E. Salvati, A.M. Korsunsky, A simplified FEM eigenstrain residual stress reconstruction for surface treatments in arbitrary 3D geometries, International Journal of Mechanical Sciences 138-139 (2018) 457-466.
[187] E. Salvati, A.J.G. Lunt, S. Ying, T. Sui, H.J. Zhang, C. Heason, G. Baxter, A.M. Korsunsky, Eigenstrain reconstruction of residual strains in an additively manufactured and shot peened nickel

superalloy compressor blade, Computer Methods in Applied Mechanics and Engineering 320 (2017) 335-351.
[188] A.H. Mahmoudi, C.E. Truman, D.J. Smith, Using local out-of-plane compression (LOPC) to study the effects of residual stress on apparent fracture toughness, Engineering Fracture Mechanics 75(6) (2008) 1516-1534.
[189] H.E. Coules, G.C.M. Horne, K. Abburi Venkata, T. Pirling, The effects of residual stress on elastic-plastic fracture propagation and stability, Materials & Design 143 (2018) 131-140.
[190] A. Mirzaee-Sisan, C.E. Truman, D.J. Smith, M.C. Smith, Interaction of residual stress with mechanical loading in a ferritic steel, Engineering Fracture Mechanics 74(17) (2007) 2864-2880.
[191] H. Yazdani Nezhad, N.P. O'Dowd, Study of creep relaxation under combined mechanical and residual stresses, Engineering Fracture Mechanics 93 (2012) 132-152.
[192] Y. Lei, N.P. O'Dowd, G.A. Webster, Fracture mechanics analysis of a crack in a residual stress field, International Journal of Fracture 106(3) (2000) 195-216.
[193] W.A. Meith, M.R. Hill, Domain-independent values of the J-integral for cracks in three-dimensional residual stress bearing bodies, Engineering Fracture Mechanics 69(12) (2002) 1301-1314.
[194] H.E. Coules, D.J. Smith, P.J. Orrock, K. Abburi Venkata, T. Pirling, A Combined Experimental and Modelling Approach to Elastic–Plastic Crack Driving Force Calculation in the Presence of Residual Stresses, Experimental Mechanics 56(8) (2016) 1313-1325.
[195] J. Liu, Z.L. Zhang, B. Nyhus, Residual stress induced crack tip constraint, Engineering Fracture Mechanics 75(14) (2008) 4151-4166.
[196] T.L. Panontin, M.R. Hill, The effect of residual stresses on brittle and ductile fracture initiation predicted by micromechanical models, International Journal of Fracture 82(4) (1996) 317-333.
[197] X.B. Ren, Z.L. Zhang, B. Nyhus, Effect of residual stresses on ductile crack growth resistance, Engineering Fracture Mechanics 77(8) (2010) 1325-1337.
[198] A. MIRZAEE-SISAN, C.E. TRUMAN, D.J. SMITH, M.C. SMITH, Interaction of residual stress with mechanical loading in an austenitic stainless steel, Fatigue & Fracture of Engineering Materials & Structures 31(3-4) (2008) 223-233.
[199] M. Nose, H. Amano, H. Okada, Y. Yusa, A. Maekawa, M. Kamaya, H. Kawai, Computational crack propagation analysis with consideration of weld residual stresses, Engineering Fracture Mechanics 182 (2017) 708-731.
[200] A.H. Sherry, M.A. Wilkes, J.K. Sharples, P.J. Budden, The Assessment of Residual Stress Effects on Ductile Tearing Using Continuum Damage Mechanics, Journal of Pressure Vessel Technology 130(4) (2008) 041212-041212-8.
[201] X.B. Ren, Z.L. Zhang, B. Nyhus, Effect of residual stress on cleavage fracture toughness by using cohesive zone model, Fatigue & Fracture of Engineering Materials & Structures 34(8) (2011) 592-603.
[202] H. Moshayedi, I. Sattari-Far, The effect of welding residual stresses on brittle fracture in an internal surface cracked pipe, International Journal of Pressure Vessels and Piping 126-127 (2015) 29-36.
[203] M. Hill, T. Panontin, Effect of Residual Stress on Brittle Fracture Testing, Effect of Residual Stress on Brittle Fracture Testing1999.
[204] M. Niwa, T. Shikama, A. Yonezu, Mechanism of hydrogen embrittlement cracking produced by residual stress from indentation impression, Materials Science and Engineering: A 624 (2015) 52-61.
[205] J. Toribio, V. Kharin, M. Lorenzo, D. Vergara, Role of drawing-induced residual stresses and strains in the hydrogen embrittlement susceptibility of prestressing steels, Corrosion Science 53(10) (2011) 3346-3355.
[206] X. Gao, R.H. Dodds Jr, An engineering approach to assess constraint effects on cleavage fracture toughness, Engineering Fracture Mechanics 68(3) (2001) 263-283.

[207] K. Satoh, M. Toyoda, Y. Kawaguchi, K. Arimochi, Influence of Hot Straining Embrittlement on Brittle Fracture in Welded Steel Plates, Transactions of the Japan Welding Society 8(1) (1977) 59-68.
[208] O. Kolednik, J. Predan, F.D. Fischer, Cracks in inhomogeneous materials: Comprehensive assessment using the configurational forces concept, Engineering Fracture Mechanics 77(14) (2010) 2698-2711.
[209] N.K. Simha, F.D. Fischer, O. Kolednik, C.R. Chen, Inhomogeneity effects on the crack driving force in elastic and elastic–plastic materials, Journal of the Mechanics and Physics of Solids 51(1) (2003) 209-240.
[210] N.K. Simha, F.D. Fischer, O. Kolednik, J. Predan, G.X. Shan, Crack Tip Shielding or Anti-shielding due to Smooth and Discontinuous Material Inhomogeneities, International Journal of Fracture 135(1) (2005) 73-93.
[211] N.K. Simha, F.D. Fischer, G.X. Shan, C.R. Chen, O. Kolednik, J-integral and crack driving force in elastic–plastic materials, Journal of the Mechanics and Physics of Solids 56(9) (2008) 2876-2895.
[212] O. Kolednik, J. Predan, G.X. Shan, N.K. Simha, F.D. Fischer, On the fracture behavior of inhomogeneous materials—A case study for elastically inhomogeneous bimaterials, International Journal of Solids and Structures 42(2) (2005) 605-620.
[213] C.R. Chen, J. Pascual, F.D. Fischer, O. Kolednik, R. Danzer, Prediction of the fracture toughness of a ceramic multilayer composite – Modeling and experiments, Acta Materialia 55(2) (2007) 409-421.
[214] F.D. Fischer, J. Predan, O. Kolednik, N.K. Simha, Application of material forces to fracture of inhomogeneous materials: illustrative examples, Archive of Applied Mechanics 77(2) (2007) 95-112.
[215] M. Rakin, O. Kolednik, B. Medjo, N.K. Simha, F.D. Fischer, A case study on the effect of thermal residual stresses on the crack-driving force in linear-elastic bimaterials, International Journal of Mechanical Sciences 51(7) (2009) 531-540.
[216] G.R. Irwin, Fracture dynamics, Fracture of metals, American Society for Metals, Cleveland, OH, 1948, pp. 147-166.
[217] E. Orown, Fracture and Strength of Solids, Reports on Progress in Physics 12 (1948) 185.
[218] C.J. McMahon, V. Vitek, The effects of segregated impurities on intergranular fracture energy, Acta Metallurgica 27(4) (1979) 507-513.
[219] M.L. Jokl, V. Vitek, C.J. McMahon, A microscopic theory of brittle fracture in deformable solids: A relation between ideal work to fracture and plastic work, Acta Metallurgica 28(11) (1980) 1479-1488.
[220] S.J. Burns, W.W. Webb, Fracture Surface Energies and Dislocation Processes during Dynamical Cleavage of LiF. I. Theory, Journal of Applied Physics 41(5) (1970) 2078-2085.
[221] Z. Suo, C.F. Shih, A.G. Varias, A theory for cleavage cracking in the presence of plastic flow, Acta Metallurgica et Materialia 41(5) (1993) 1551-1557.
[222] M.L. Williams, On the Stress Distribution at the Base of a Stationary Crack, Journal of Applied Mechanics 24(1) (1956) 109-114.
[223] S.G. Larsson†, A.J. Carlsson, Influence of non-singular stress terms and specimen geometry on small-scale yielding at crack tips in elastic-plastic materials, Journal of the Mechanics and Physics of Solids 21(4) (1973) 263-277.
[224] G.W. Hollenberg, G.R. Terwilliger, R.S. Gordon, Calculation of Stresses and Strains in Four-Point Bending Creep Tests, Journal of the American Ceramic Society 54(4) (1971) 196-199.
[225] T. Fett, Stress Intensity Factors – T-Stresses – Weight Functions, Supplement Volume, KIT Scientific Publishing, 2009.
[226] A. Giannattasio, M. Tanaka, T.D. Joseph, S.G. Roberts, An empirical correlation between temperature and activation energy for brittle-to-ductile transitions in single-phase materials, Physica Scripta 2007(T128) (2007) 87.

[227] M. Tanaka, K. Higashida, T. Shimokawa, T. Morikawa, Brittle-Ductile Transition in Low Carbon Steel Deformed by the Accumulative Roll Bonding Process, MATERIALS TRANSACTIONS 50(1) (2009) 56-63.
[228] M. Stec, J. Faleskog, Micromechanical modeling of grain boundary resistance to cleavage crack propagation in ferritic steels, International Journal of Fracture 160(2) (2009) 151.
[229] ASTM E23-18 Standard Test Methods for Notched Bar Impact Testing of Metallic Materials, 2018.
[230] A. Aloraier, A. Al-Mazrouee, J.W.H. Price, T. Shehata, Weld repair practices without post weld heat treatment for ferritic alloys and their consequences on residual stresses: A review, International Journal of Pressure Vessels and Piping 87(4) (2010) 127-133.
[231] E. Zamani, G.H. Liaghat, Explosive welding of stainless steel–carbon steel coaxial pipes, Journal of Materials Science 47(2) (2012) 685-695.
[232] K. Faes, A. Dhooge, P. De Baets, P. Afschrift, New friction welding process for pipeline girth welds—welding time optimisation, The International Journal of Advanced Manufacturing Technology 43(9) (2009) 982-992.
[233] T. Mura, Micromechanics of defects in solids, Springer Scince & Business Media1987.
[234] N.P. O'Dowd, C.F. Shih, Family of crack-tip fields characterized by a triaxiality parameter—II. Fracture applications, Journal of the Mechanics and Physics of Solids 40(5) (1992) 939-963.
[235] J.W. Hutchinson, Singular behaviour at the end of a tensile crack in a hardening material, Journal of the Mechanics and Physics of Solids 16(1) (1968) 13-31.
[236] J.R. Rice, G.F. Rosengren, Plane strain deformation near a crack tip in a power-law hardening material, Journal of the Mechanics and Physics of Solids 16(1) (1968) 1-12.
[237] Z.L. Zhang, C. Thaulow, M. Hauge, Effects of crack size and weld metal mismatch on the has cleavage toughness of wide plates, Engineering Fracture Mechanics 57(6) (1997) 653-664.
[238] Z. Zhang, M. Hauge, C. Thaulow, The effect of T -stress on the near tip stress field of an elastic-plastic interface crack, 1997.
[239] N.C. Broedling, A. Hartmaier, H. Gao, Fracture toughness of layered structures: Embrittlement due to confinement of plasticity, Engineering Fracture Mechanics 75(12) (2008) 3743-3754.
[240] N.C. Broedling, A. Hartmaier, H. Gao, A combined dislocation—cohesive zone model for fracture in a confined ductile layer, International Journal of Fracture 140(1) (2006) 169-181.
[241] X.H. Zeng, A. Hartmaier, Modeling size effects on fracture toughness by dislocation dynamics, Acta Materialia 58(1) (2010) 301-310.
[242] P. Shanthraj, M.A. Zikry, Dislocation density evolution and interactions in crystalline materials, Acta Materialia 59(20) (2011) 7695-7702.
[243] P. Shanthraj, M.A. Zikry, Dislocation-density mechanisms for void interactions in crystalline materials, International Journal of Plasticity 34 (2012) 154-163.

Appendix A Appended papers

Paper I

A.1 Paper 1

Constraint Effect on the Brittle-to-Ductile Transition of Single-crystal Iron Induced by Dislocation Mobility

Authors: Yang Li, Xiaobo Ren, Jianying He, Zhiliang Zhang

International Journal of Mechanical Sciences 149 (2018) 212–223

Constraint Effect on the Brittle-to-Ductile Transition of Single-crystal Iron Induced by Dislocation Mobility

Yang Li[1], Xiaobo Ren[2], Jianying He[1], Zhiliang Zhang[1,*]

1 NTNU Nanomechanical Lab, Department of Structural Engineering, Norwegian University of Science and Technology (NTNU), Richard Brikelandsvei 1A, N-7491Trondheim, Norway

2 SINTEF Industry, Richard Brikelandsvei 2B, N-7465 Trondheim, Norway

Abstract: *The brittle-to-ductile transition (BDT), no matter what the dominated mechanism is, dislocation nucleation or dislocation motion, is not an intrinsic phenomenon of material, and depends not only on the strain rate but also on the constraint at crack tip. However, few work has been performed on studying the effect of constraint on BDT. In this study, a dislocation mobility based continuum model is employed to model the BDT behavior of single-crystal iron under different loading rates. Two scenarios of T-stress implementation in the model has been adopted to investigate the effect of constraint on BDT. It is found that the change of the stress distribution ahead of crack tip due to the T-stress dictates the fracture toughness of single-crystal iron in the BDT transition region. Lower constraint leads to a higher fracture toughness in the transition region, a smoother transition curve and a lower critical BDT temperature, and also a higher fracture toughness at the critical BDT temperature. A quantitative relation between fracture toughness and T-stress has been established such that the BDT curve with constraint can be estimated from a reference BDT curve. Moreover, a solution to build a temperature-dependent effective surface energy law is also introduced, which could facilitate the cleavage fracture assessment.*

Keywords: Single-crystal iron; Brittle-to-ductile transition (BDT); Dislocation mobility; Loading rate; T-stress/constraint; viscoplastic

Nomenclature

a	notch depth of four point bend specimen
b	modulus of Burgers vector
B	thickness of four point bend specimen
E	Young's modulus
E_a	activation energy for the BDT
F	loading force of four point bend test

G_c	critical strain energy release rate
J	J-integral
K	stress intensity factor
K_I	mode I stress intensity factor applied to the outer boundary of the MBL model
K_{IC}	critical mode I stress intensity factor of material
K_I^a	applied mode I stress intensity factor
K_I^t	mode I stress intensity factor at crack tip
K_D	stress intensity factor generated by the image dislocations at the crack tip
$K_I^a(T=0)$	fracture toughness without T-stress
K_{I,Θ_C}^a	fracture toughness at critical BDT temperature
$K_{I,\Theta_C}^a(T=0)$	fracture toughness at critical BDT temperature without T-stress
$\dot{K}$	loading rate of applied stress intensity factor
$\dot{K}_I^a$	loading rate of mode I stress intensity factor applied to the MBL model
k_B	Boltzmann constant
m	temperature dependent stress exponent
Q	the activation energy for dislocation velocity
r_{el}	elastic zone size at crack tip
R	radius of MBL model
S_1	outer span of four point bend specimen
S_2	inner span of four point bend specimen
T	T-stress
$\dot{T}$	rate of T-stress
v	dislocation velocity
v_0	material specific reference dislocation velocity
v_0'	a constant
W	width of four point bend specimen
α	image stress parameter

β	proportionality constant
ξ	position of dislocation
ξ_i	position of the ith dislocation
ξ_0	distance from the crack tip where dislocation nucleation occurs
ν	Poisson's ratio
μ	shear modulus
φ	inclination angel of dislocation slip plane to the crack plane
Θ	absolute temperature in Kelvin
Θ_0	reference temperature to characterize ductile-to-brittle transition
Θ_c	critical BDT temperature
$\Theta_C(T=0)$	critical BDT temperature of material without T-stress
ρ	dislocation density
σ_{ij}	stress tensor
σ_{Mis}	von Mises equivalent stress
σ_h	hydrostatic stress
σ_y	average yield stress of single-crystal iron
σ_0	normalization stress
η	stress triaxiality
ε_{eq}	equivalent plastic strain
$\dot{\varepsilon}^p$	equivalent plastic strain rate
$\dot{\varepsilon}_0$	reference strain rate
$\dot{\varepsilon}_f$	outer-fiber strain rate of four point bend test
$\dot{\delta}$	cross head speed of four point bend test
γ_s	surface energy
γ_p	plastic work
γ_{eff}	effective surface energy
$\dot{\gamma}^p$	shear strain rate

τ	resolved shear stress
τ_0	normalization shear stress
τ_f	lattice friction stress
τ_{ξ_0}	resolved shear stress for dislocation nucleation with a distance ξ_0 from the crack tip
τ_{ξ_i}	shear stress acting on a dislocation at the position $\xi = \xi_i$
τ_{ij}	interaction shear stress of dislocations
$f_{ij}(\theta)$	dimensionless function of θ
$g(\varphi)$	function depending on φ
$g_1(\varphi)$	coefficient related to φ

1. Introduction

The transition of fracture mode from ductile to brittle is a crucial phenomenon of structural materials, e.g. body centered cubic (BCC) metals with strong interatomic forces which are normally brittle at low temperatures or high loading rates, become ductile at high temperatures or low loading rates. Although the general concern in engineering practice is ductile-to-brittle transition, the mechanism can be fundamentally revealed by studying the reverse process in which an intrinsically brittle material fractures in a ductile manner [1]. It has been indicated that BDT always involves a thermally-activated process of dislocations emission followed by their motion and multiplication near the crack tip [1]. To circumvent the complexity of problem, e.g. pre-existing dislocations, grain boundary or impurity in the material which affect dislocation activity near crack tip, single crystalline materials, e.g. Si [2-7], Tungsten [8-10], iron [11-13], etc. has been widely selected for experimental study of the mechanisms of BDT.

Many models have been developed to investigate the BDT behavior, and most of them address the intimate connection between the dislocation activity near the crack tip and fracture toughness. These models can be generally classified into two groups, e.g. dislocation nucleation controlled [14-17] and dislocation motion controlled [3, 5, 18, 19]. Models in the first category suggest that the competition between dislocation emission and atomic decohesion at crack tip is the controlling factor in the ductile versus brittle behavior of a material. The second category models suggest that the shielding on crack tip induced by thermal-activated dislocation motion is the dominated mechanism of BDT. Dislocation nucleation dominated BDT models can intrinsically distinguish the materials to be brittle or ductile, but fail to predict the temperature and loading rate dependence of the BDT behavior. On the contrary, the

dislocation mobility controlled BDT models are able to predict loading rate dependent BDT temperature based on the evaluation of the shielding effect of dislocation motion on the crack tip stress intensity factor at an atomistic level. Gradual and sharp BDT transition of single-crystal solids has been successfully predicted with detailed configurations of dislocation near the crack tip [3, 5, 19-21] based on dislocation mobility models. Further, a continuum model on the basis of dislocation mobility proposed by Nitzsche et al. [22] has been adopted to simulate the BDT of single-crystal Si [22] and single-crystal Tungsten by Hartmaier et al. [9].

Single parameter fracture criterion based on stress intensity factor K or J-integral has been widely adopted for engineering critical assessment (ECA). However, it is found that the constraint at crack tip resulted from geometry and loading strongly influences the crack-tip stress fields. In this regard, constraint analysis and multi-parameter crack-tip stress fields based fracture mechanics become necessary. Two-parameter approaches have been proposed to characterize crack-tip stress fields, e.g. J–T [23, 24], J–Q [25-27] , J–A2 [28] and J-M [29], by extending the HRR solution with higher-order terms. Ductile-to-brittle transition is not an intrinsic phenomenon of material and it depends not only on the temperature and strain rate but also on crack tip constraint. The effect of crack tip constraint on ductile brittle transition has been widely studied by both experiments and numerical simulation [30-37], e.g. the influence of T-stress on crack resistance curve at some specific temperature, the relation between reference temperature Θ_0 or fracture toughness and T-stress, etc. However, studies on the influence of constraint on the DBT in the transition region has not been performed by using a dislocation mobility based methodology.

The Griffith criterion has been broadly applied to study brittle fracture, which is expressed in terms of critical strain energy release rate, $G_c = 2\gamma_s$ (γ_s is the surface energy). Irwin [38] and Orowan [39] independently modified the Griffith theory to account for plastic work for fracture, e.g. in the transition region. Consequently, the modified Griffith criterion of cleavage can be written as $G_c = 2(\gamma_s + \gamma_p)$, in which a material's resistance to crack extension is determined by the sum of γ_s and the plastic work γ_p (both per unit crack surface area). However, how to quantitatively estimate plastic work γ_p during fracture of material is a challenge. McMahon and Vitek [40] and Jokl et al. [41] derived an exponential dependence of γ_p on γ_s so that a relatively small change in γ_s may lead to a large change in γ_p. Wallin et al. [42] proposed a simple equation to calculate plastic work related to temperature and the Peierls-Nabarro force. However, in their work the shielding effect of dislocation mobility on the crack tip is not considered. Linaza et al. [43] and San Martin et al[44] have found the temperature-dependent effective surface energy ($\gamma_{eff} = \gamma_s + \gamma_p$) of steel in experiments. However, the measured γ_{eff} is apparently geometry dependent and can not be generally applied in practice. An explicit function for the estimation of effective surface energy of LiF single-crystal was derived by Burns et al. [45] based

on the dynamic fracture in a double cantilever specimen. Among these work, few attention is paid on the constraint effect at crack tip on the effective surface energy.

In this paper, a continuum model for BDT controlled by dislocation mobility developed by Nitzshe et al. [22] is employed to investigate the effect of T-stress on the BDT of single-crystal iron. Parametric studies are carried out first to reveal the effects of various model parameters on the crack tip shielding. Then, a group of parameters obtained by comparing the computational results to the experimental results of Tanaka et al. [11] have been used to study the BDT of single-crystal iron under different loading rates. Local stress and triaxiality distribution ahead of the crack tip are analyzed also. Two scenarios of T-stress implementation has been adopted to investigate the effect of constraint on the BDT. Finally, an approach to build a temperature dependent effective surface energy of material is introduced and the influences of constraint on effective surface energy are also presented.

2. Shielding effect of dislocation motion on crack tip stress field

In the elastic field, crack and dislocations are treated as singularities of the material, whose collective response to the external applied stress can be addressed in elastic terms. It has been found that the toughness of the material against crack propagation is due to the shielding of dislocations on the crack from the external stress[46]. An isotropic elastic analysis of cracks and dislocations under general loading has been performed by Lin and Thomson [47], which includes theorems for the forces on interacting sharp cracks and dislocations. A local K-field of the crack tip can be expressed with the shielding contribution of the dislocations

$$K_I^t = K_I^a - K_D \tag{1}$$

where, K_I^t is the stress intensity factor at crack tip; K_I^a is the applied stress intensity factor; K_D is the shielding effect of dislocations [46, 47], for mode I and II fracture and in 2D plane strain, which can be expressed as

$$K_D = \sum_i \frac{\mu b g(\varphi)}{(1-\nu)\sqrt{2\pi\xi_i}} \tag{2}$$

where $g(\varphi)$ is a function depending on φ; φ is inclination angle of dislocation slip plane to the crack plane; μ and ν are shear modulus and Poisson's ratio respectively; b the modulus of Burgers vector; ξ_i is position of the ith dislocation. It has to be mentioned that the blunting effect of dislocation on the crack tip is neglected since that the analysis by Thomason et al. [46, 47] addresses only sharp cracks.

According to the formulation for the forces on the defect, e.g. dislocations, derived by Thomason et al. [46, 47], the shear stress on a dislocation with a position $\xi = \xi_i$ in the presence of a crack and embedded in a cloud of other dislocations can be expressed as:

$$\tau_{\xi_i} = \frac{K}{\sqrt{2\pi\xi_i}} g'(\varphi) - \alpha\frac{\mu b}{\xi_i} + \frac{\mu b}{2\pi}\sum_{ij}\left(\frac{\xi_j}{\xi_i}\right)^{\frac{1}{2}}\frac{1}{\xi_i - \xi_j} \tag{3}$$

where K is stress intensity factor of external loading; ξ_i or ξ_j is the position of the i[th] or j[th] dislocation; $g'(\varphi)$ is the coefficient related to φ; α is image stress parameter. The first term is the direct shear stress by the crack on the dislocation in a K dominated elastic field, the second term is the image stress that is always attractive toward the crack and the third term is the stress caused by interactions between dislocations.

The dynamics of dislocation emission and motion in the crack tip stress field is essential for the formation of dislocation clouds that result in the shielding effect on crack tip[19]. The dislocation velocity v can be described as function of resolved shear stress τ and temperature Θ by an empirical Arrhenius type law

$$v = v_0 exp\left(-\frac{Q}{k_B\Theta}\right)\left(\frac{\tau}{\tau_0}\right)^m \tag{4}$$

where Q is the activation energy for dislocation velocity; k_B is the Boltzmann constant; m is temperature dependent stress exponent; v_0 is material specific reference dislocation velocity; τ_0 is normalization shear stress; Θ is the absolute temperature in Kelvin. For a given material, the value of m can be measured through the relationship of dislocation velocity and applied stress (e.g. Fig. 3.11 [48]). The activation energy Q, for dislocation motion can be obtained from the relationship of loading rate and temperature [11, 12].

At a specific temperature, equation (4) can be written as $v = v_0'\left(\frac{\tau}{\tau_0}\right)^m$. If we write $v = \frac{d\xi}{dt} = \dot{K}\frac{d\xi}{dK}$, then the resolved shear stress on the dislocation can be expressed as [20]:

$$\tau = \tau_0\left(\frac{\dot{K}}{v_0'}\right)^{1/m}\left(\frac{d\xi_i}{dK}\right)^{1/m} \tag{5}$$

where $\dot{K}$ is loading rate of applied stress intensity factor, v_0' is a constant. Substituting τ in (5) for τ_{ξ_i} in (2), then

$$\tau_0\left(\frac{\dot{K}}{v_0'}\right)^{1/m}\left(\frac{d\xi_i}{dK}\right)^{1/m} = \frac{K}{\sqrt{2\pi\xi_i}} g'(\varphi) - \alpha\frac{\mu b}{\xi_i} + \frac{\mu b}{2\pi}\sum_{ij}\left(\frac{\xi_j}{\xi_i}\right)^{\frac{1}{2}}\frac{1}{\xi_i - \xi_j} \tag{6}$$

For a constant loading rate $\dot{K}$, the position of the dislocations ξ_i is a function of K. The initial condition for this function is that a dislocation emission occurs when $\tau_{\xi_0} = \tau_f$, τ_{ξ_0} is the resolved shear stress for dislocation nucleation with a distance ξ_0 from the crack tip. Then, at each time step, the positions ξ_i of the dislocations can be determined with the applied K. Accordingly, the shielding effect of dislocation on crack tip K_D and the local stress intensity factor at crack tip can be solved when the position of dislocations are determined. Here, it is assumed that emission of a dislocation occurs once that crack tip stress on a dislocation at a critical distance, e.g. ξ_0, exceeds the lattice friction stress τ_f, and also that dislocations emission from a source at or near the crack plane/tip have to move a certain distance before they can shield the crack[19]. If dislocation emission occurs involving an energy barrier by Rice-Thomason mechanism, this distance can be explained by that the critical loop configuration at the saddle point implies a critical stress at a certain finite distance from the crack tip [14]. The critical distance away from crack tip means a dislocation free zone will be formed near the crack tip [19]. And, the exponent m in equation (5) is assumed to be a constant. To circumvent the complexity, the interaction stress between dislocations from different sources is neglected.

3. The numerical model

The section 2 generally presents a dislocation mobility based theory of studying the BDT of single-crystal metals, which also provides a basic framework for studying the BDT with a numerical solution. Many studies on BDT of single-crystal metals have been carried out through a numerical solution based on the similar theory presented in section 2 [3, 19, 21]. On the other hand, it can be inferred from section 2 that the shielding effect of dynamics of dislocation on crack tip stress field is equivalent to that of rate-dependent plasticity in a finite region around the crack tip due to dislocation emission and motion. In this manner, the shielding effect of dislocation mobility on crack tip and the local stress intensity factor at crack tip can be resolved with a continuum method, which will be an alternative solution to replace the numerical solution.

Hereinafter, a modified boundary layer (MBL) model is adopted, in which the crack-tip region consists of an elastic zone surrounding the crack tip and an elastic-viscoplastic material outside of the elastic zone. The applied K with a constant loading rate $\dot{K}$ is implemented in this model through the nodal displacement on the outer boundary layer. The model used here was developed by Nitzsche et al. [22] to investigate the sharp BDT of single-crystal silicon, which was also adopted by Hartmaier et al. [9] to study the BDT of single-crystal Tunston. The configuration of this model is inspired by the concept proposed by Suo et al. [49], which states the fracture process can be divided into two elements in the transition region, atomic decohesion and background dislocation motion. The crack tip elastic zone is a dislocation free zone at a length scale (comparable to dislocation spacing) so that atomic decohesion

dominates the fracture process. The dislocation free zone near crack tip has also been proposed by Hirsch et al. [19] as mentioned in section 2. In order to describe the dislocation motion, two assumptions are made: the material is assumed to be isotropic even though single-crystals are usually anisotropic. The rate-dependent plastic deformation is only a result of dislocation motion.

To describe the plasticity generated by dislocation motion, according to Orowan law, the shear strain rate, $\dot{\gamma}^p$, can be written

$$\dot{\gamma}^p = \beta\rho b v \tag{7}$$

Where β is a proportionality constant; ρ is the dislocation density. The resolved shear stress τ in equation (4) and plastic shear strain rate $\dot{\gamma}^p$ in equation (7) can be replaced by the von Mises equivalent stress σ_{Mis} and the equivalent plastic strain rate $\dot{\varepsilon}^p$ since the isotropic material has no preferred slip plane. Therefore, insert the dislocation velocity according to equation (4) into equation (7), the viscoplastic response of the material can then be described as

$$\dot{\varepsilon} = \dot{\varepsilon}_0 \exp\left(-\frac{Q}{k_B\Theta}\right)\left(\frac{\sigma_{Mis}}{\sigma_0}\right)^m \tag{8}$$

where $\dot{\varepsilon}$ is equivalent plastic strain rate; $\dot{\varepsilon}_0$ is a reference strain rate, which incorporates the v_0, β, ρ and b, e.g. $\dot{\varepsilon}_0 = v_0\beta\rho b$; σ_0 is a normalization stress.

Since the shielding effect of dislocation mobility is localized in a finite region around crack tip, only the elastic zone and viscoplasctic zone near crack tip have been incorporated in this continuum model. While, for a semi-infinite crack the long range stress field in this model is still dominated at infinity by the K-field, because viscoplastic zone is restricted to a finite distances from the crack, i.e., small scale yielding approximation. Consistent simulation results have been achieved from the investigation of BDT of single-crystal Tungsten by both such a continuum elastic-vicoplastic model and discrete dislocation dynamics method by Hartmaier et al.[9]. Although such a continuum model has a certain of limitation in that the dislocation motion in various slip systems is not considered since the isotropic material is supposed, it still can be used to study how BDT is affected by the parameters, for instance, temperature, loading rate and constraint effect etc.

Only upper-half of the model is illustrated in Fig. 1 due to symmetry. The radius of model (R) is 20 times larger than the crack tip elastic zone size r_{el}, which is assumed to be a circle around the crack tip with a radius of 1μm. A crack with an initial radius of $1.15 \times 10^{-4}R$ is located in the center of model. Abaqus 6.14 is employed, and 4-node and plane strain elements (CPE4) are used in all simulation. The meshes are refined in the elastic region where the size of smallest elements is 10 nm. Following the work of Williams, the first two terms in the expansion of linear elastic crack-tip stress field can be written as [50]

$$\sigma_{ij} = \frac{K_I}{\sqrt{2\pi r}} f_{ij}(\theta) + T\delta_{1i}\delta_{1j} \tag{9}$$

where $f_{ij}(\theta)$ is dimensionless function of θ, T is regarded as a stress parallel to the crack flanks. Larsson and Carlsson [51] have demonstrated that the second term in the series has a significant effect on the shape and size of the plastic zone which develops at the crack tip. Therefore, T-stress has been widely used to describe the crack tip stress field in real flawed structures. A linear elastic K_I field is applied to the outer boundary of the model with nodal displacements controlled by the elastic asymptotic stress field of a crack

$$u(r,\theta) = K_I \frac{(1+\nu)}{E}\sqrt{\frac{r}{2\pi}}\, cos\left(\frac{\theta}{2}\right)(3-4\nu-cos\theta) + T\frac{1-\nu^2}{E} r cos\theta \tag{10a}$$

$$v(r,\theta) = K_I \frac{(1+\nu)}{E}\sqrt{\frac{r}{2\pi}}\, sin\left(\frac{\theta}{2}\right)(3-4\nu-cos\theta) - T\frac{\nu(1+\nu)}{E} r sin\theta \tag{10b}$$

where K_I is applied mode I stress intensity factor; E is Young's modulus, r and θ are polar coordinates centered at the crack tip. In the present study, only a stationary crack is investigated.

For a sharp crack tip, cleavage fracture is assumed to occur when the crack tip stress intensity factor reaches the critical value of material, i.e. $K_{\mathrm{I}}^t = K_{\mathrm{IC}}$. According to the Griffith criterion, K_{IC} depends only on the material's surface energy γ_s. The crack tip stress intensity factor is calculated from the J-integral through,

$$K_I^t = \sqrt{EJ/(1-\nu^2)} \tag{11}$$

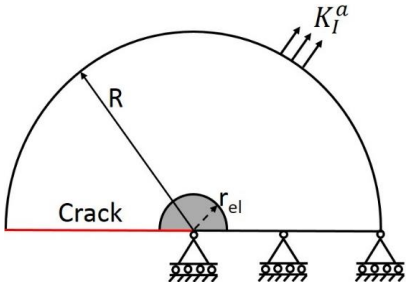

Fig.1 MBL model to describe BDT dominated by dislocation motion with a rate-dependent plasticity. The viscoplastic zone is white, the elastic zone dark gray.

4 Numerical results and discussion

4.1. General behavior

As mentioned in section 3, a small elastic zone around the crack tip with its size in the same scale as dislocation spacing in metals is assumed to be presented in the MBL model. According to equation (11), the stress intensity factor at crack tip is calculated from the J-integral at crack tip. The path independence of J-integral in the elastic region is shown in the Fig.2. The effect of the elastic zone size on the fracture toughness is presented in the Fig. 3(a), in which normalized crack tip stress intensity factor, $K_{\mathrm{I}}^{t}/K_{IC}$, are plotted against normalized applied stress intensity factor, $K_{\mathrm{I}}^{a}/K_{IC}$, for different elastic zone size at 178K and under a constant loading rate $\dot{K}_{I}^{a} = 10.0\mathrm{MPam}^{0.5}\mathrm{s}^{-1}$. It is shown that smaller size of elastic zone will result in a higher shielding effect on crack tip and thus a higher fracture toughness. According to Nitzsche et al. [22], the elastic zone can be comprehended as an obstacle to nucleation of dislocation, i.e., the larger size of elastic zone the harder to generate plastic deformation.

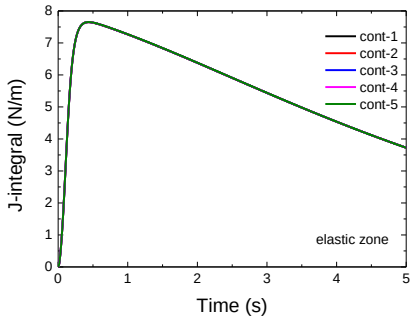

Fig.2 J-integral with variant contours at crack tip in the elastic region.

The dependence of the shielding effects of plastic deformation on crack tip stress intensity factor K_{I}^{t} are presented in Fig.3 (b) for different temperatures. A constant loading rate, $\dot{K}_{I}^{a} = 1.0\ \mathrm{MPam}^{0.5}\mathrm{s}^{-1}$, is applied. At the lowest temperature, there is a linear relation between the crack tip stress intensity factor and the applied stress intensity factor, and the two are equal when fracture occurs. Since dislocation motion is stimulated with the enhancement of temperature in terms of Arrhenius law, it can be found that the relation between the crack tip stress intensity factor and applied stress intensity factor gradually deviates from the linear line. A higher toughness can be achieved when the crack tip stress intensity factor reaches K_{IC} due to the stronger shielding effects as temperature increases. The crack tip stress intensity factor will never exceed K_{IC} when the temperature is beyond the critical temperature (for instance, $\Theta_c = 174.41K$). The BDT occurs at this circumstance and the temperature is called critical BDT temperature. The influence of stress exponent m and loading rate on the shielding effects of plastic deformation on crack tip stress intensity factor is also studied as shown in Fig. 3 (c) and (d). With the increase of m, the applied stress intensity factor gradually increases when $K_{\mathrm{I}}^{t} = K_{IC}$. As the loading rate increases, the applied stress intensity factor decreases when $K_{\mathrm{I}}^{t} = K_{IC}$. This means that a higher fracture toughness of material can be obtained with a higher m and a lower loading rate. The results

shown in Fig. 3 are very similar with the findings of Nitzsche et al. [22], which validates the model adopted in present work for studying the shielding effect of dislocation motion on crack tip and BDT induced by dislocation mobility.

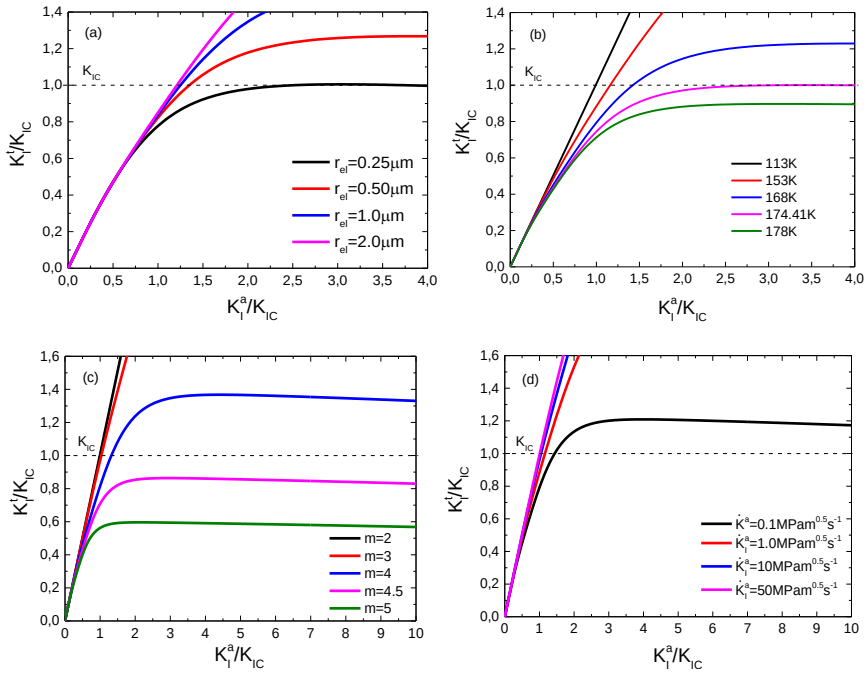

Fig.3 stress intensity factor at crack tip against applied stress intensity factor (a) for different elastic zone size under a loading rate $\dot{K}_I^a = 10.0 MPam^{0.5}s^{-1}$ *and at 178K, (b) for different temperature under a loading rate* $\dot{K}_I^a = 1.0 MPam^{0.5}s^{-1}$*, (c) for different m under a loading rate of* $\dot{K}_I^a = 10.0 MPam^{0.5}s^{-1}$ *and at 183K, (d) for different loading rates with m =4.0 and at 153K. The parameters used are* $\dot{\varepsilon}_0 = 3.968s^{-1}, Q = 0.33\ ev, r_{el} = 1\mu m$*. Critical stress intensity factor of iron,* $K_{IC} = 1 MPam^{0.5}$ *[11].*

4.2. Identification of the parameters for single-crystal iron

From equations (5) and (6), it can be observed that BDT is strain-rate dependent, e.g. in case of a specific K, the dislocation positions ξ_i, K_D and K_I^t depend on $\dot{K}$. Through experiments on single-crystals, a relation between loading rate $\dot{K}$ and Θ_c has been found [5]

$$ln\dot{K} = -E_a/k_B\Theta_c + const. \tag{12}$$

where E_a is the activation energy for the BDT, which has been found to be equal to the activation energy Q for dislocation velocity.

Tanaka et al. [11] has performed 4-point bend tests to measure the BDT temperature of single-crystal iron, in which different outer-fiber strain rates have been applied in their tests. The outer-fiber strain rate can be calculated with following equation [52],

$$\dot{\varepsilon}_f = \frac{4B}{S_1^2}\dot{\delta} \tag{13}$$

where $\dot{\varepsilon}_f$ is the outer-fiber strain rate and $\dot{\delta}$ is the cross head speed, B is the thickness of specimen and S_1 is the outer span of specimen. For a four point bend test, the applied stress intensity factor can be calculated by using the following equation [53],

$$K_I = \frac{3F(S_1 - S_2)}{2BW^2}\sqrt{a}Y \tag{14}$$

where $Y = \frac{1.1215\sqrt{\pi}}{(1-a/W)^{3/2}}\left[\frac{5}{8} - \frac{5}{12}\frac{a}{W} + \frac{1}{8}\left(\frac{a}{W}\right)^2 + 5\left(\frac{a}{W}\right)^2\left(1 - \frac{a}{W}\right)^6 + \frac{3}{8}\exp\left(-6.1342\frac{a}{W-a}\right)\right]$, F is loading force, S_2 is inner span, W is width of specimen and a is notch depth. Three-dimensional modelling of the four-point bend tests of single-crystal iron is carried out in present study, in which the cross head speed applied for modelling is converted from outer-fiber strain rates utilized by Tanaka et al. [11] according to equation (13) and only a stationary crack is studied. The Young's modulus E and poison's ratio ν of iron are 206GPa and 0.29 respectively [11]. Then, the rates of stress intensity factor applied on the four-point bend specimen can be calculated by equation (14). The outer-fiber strain rates and corresponding applied rates of stress intensity factor are listed in table 1. To obtain the BDT temperatures for each loading rate in table 1, several groups of parameters have been tried according to the method mentioned in 4.1. By doing this, one group of parameters is chosen, which are $r_{el} = 1\mu m, \dot{\varepsilon}_0 = 13044s^{-1}$, $m = 3.5$, $\sigma_0 = 1$ MPa and $Q = 0.33ev$. The computed BDT temperatures under different loading rates has been compared with experimental results by Tanaka et al. [11] in Fig. 4. It is shown that the computational results of single-crystal iron agree well with experimental results, which indicates that this group of parameters employed is reliable. Therefore, the parameters verified will be adopted in the following calculations.

Tab.1 The calculated applied rates of stress intensity factor from the outer-fiber strain rates of the four point bend tests for single-crystal iron [11].

$\dot{\varepsilon}, s^{-1}$	$\dot{K}_I^a$, MPam$^{0.5}s^{-1}$
4.46e-5	0.2579
4.46e-4	2.579
4.46e-3	25.79

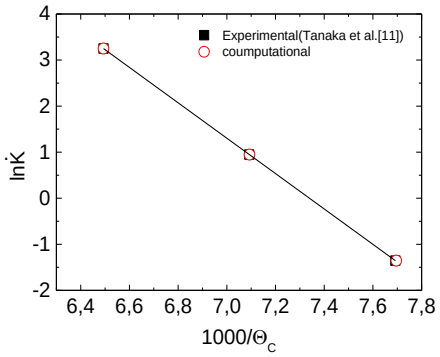

Fig.4 comparison of computed and experimental critical BDT temperature of single-crystal iron. The parameters in the model are $r_{el} = 1\mu m, \dot{\varepsilon}_0 = 13044s^{-1},\ m = 3.5, \sigma_0 = 1MPa, Q = 0.33ev.$

4.3. Brittle-to-ductile transition

The evolution of fracture toughness K_{I}^{a} is plotted against temperature under different loading rates in Fig. 5. The fracture toughness increases slowly over a relative long temperature range, and then sharply increases up to the BDT temperature. Generally, the transition curve shifts to the lower temperature when loading rate decreases, a lower loading rate leads to a smoother transition curve, and a higher toughness is expected for the occurrence of cleavage fracture under lower loading rate at the same temperature. These results are consistent with the observations of Nitzsche et al. [22] and Hartmaier et al. [9]. It is also illustrated in Fig. 5 that BDT temperature decreases as loading rate reduces. However the fracture toughness at the critical BDT temperature under different loading rates is almost the same, which is around $K_{\mathrm{I}}^{a} = 3.5K_{IC}$. This implies that loading rate only influences the critical BDT temperature, but has no effect on the fracture toughness of material at this critical BDT temperature.

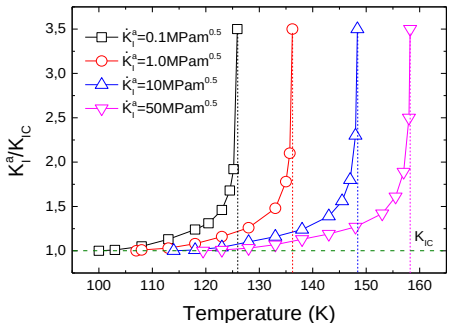

Fig.5 Fracture toughness K_I^a *normalized with* K_{IC} *vs. temperature for different loading rates. The critical BDT temperature is marked with dashed lines of each loading rate.*

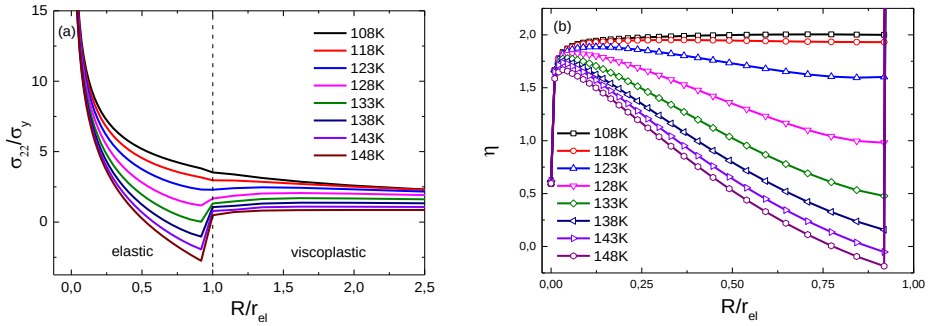

Fig. 6 distribution of (a) opening stress and (b) stress triaxiality ahead of crack front for different temperature under a loading rate $\dot{K}_I^a = 10.0 MPam^{0.5}s^{-1}$ when fracture happens, e.g. $K_I^t = K_{IC}$.

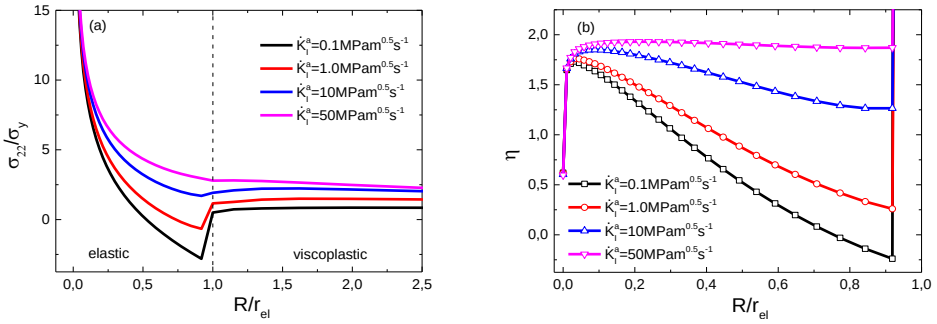

Fig. 7 distribution of (a) opening stress and (b) stress triaxiality ahead of crack front for different loading rate at Θ =125.8K when fracture happens, e.g. $K_I^t = K_{IC}$.

The distributions of the opening stress and stress triaxiality ahead of crack tip for different temperatures under a loading rate $\dot{K}_I^a = 10.0\text{MPam}^{0.5}\text{s}^{-1}$ are presented in Fig. 6 at the moment when fracture of material occurs. Opening stresses are normalized by the average yield stress of single-crystal iron at room temperature $\sigma_y = 110\text{MPa}$ [54] and the distance is normalized by r_{el}. Hereinafter, the stress triaxiality η is determined by the ratio of the hydrostatic stress σ_h and σ_{Mis}. Away from the crack tip, the opening stress for all temperatures decreases as shown in Fig. 6 (a). Upon approaching the interface between elastic and viscoplastic region, it even turns to be compressive at higher temperature, e.g. beyond 138 K. A turning point of stress distribution at the interface for each temperature can be observed because of the different properties of materials in the two regions. In Fig. 6 (b), a rapid rise of stress triaxiality on the first two nodes can be found at all temperatures. As the temperature increases, however, away from the first two nodes ahead of crack tip, the stress triaxiality for higher temperature decreases gradually. It is also found in Fig. 6 that the decrease of both opening stress and stress triaxiality ahead of crack tip becomes more pronounced at higher temperature. It is obvious that stress relaxation resulted by plastic deformation due to dislocation motion around crack tip is the reason for

the increase of fracture toughness as temperature raised and dictates the BDT as well. Opening stress and triaxiality ahead of crack tip under different loading rate and at the same temperature are presented in Fig. 7 at the moment when fracture occurs. It is found that stress relaxation occurs more apparently as loading rate decreases. Recall equation (4)-(5) and (7), at the same temperature, a lower dislocation velocity resulted by the higher loading rate generates a lower plastic deformation, which leads to a less stress relaxation and a lower fracture toughness (see Fig. 5). In short, the sensitivity of BDT on loading rate can be also ascribed to the stress relaxation resulted by plastic deformation.

4.4. Constraint effect on brittle-ductile transition

The T-stress is implemented linearly in the time-dependent process according to equation (10), in which the loading rate consists of two parts, the rate of stress intensity factor $\dot{K}_I^a$ and the rate of T-stress $\dot{T}$, see equation (9). The T-stress representing the constraint level at the crack tip, and is related to not only the geometry but also to the plastic deformation around the crack tip. In each case with a specific rate of stress intensity factor $\dot{K}_I^a$, there are two scenarios for exploring the influence of the rate of T-stress. Through changing the total amount of T-stress loaded, the first one generates a constant effective T-stress at the moment of the fracture of material at different temperature, e.g. -0.5σ_y, -0.25σ_y, 0.25$\sigma_y$and 0.5σ_y. Accordingly, this scenario will produce a non-constant $\dot{T}$ since that the stress relaxation at each temperature is different due to the thermal activated dislocation mobility as Fig.6 shown. The other scenario is keeping $\dot{T}$ as a constant value by fixing the total amount of T-stress loaded at each temperature, which makes the applied K and T proportional in the loading process as Jayadenvan et al.[55, 56] did for the quasistatic loading fracture. It will produce a non-constant T-stress at fracture due to the same reason of stress relaxation. In general, the first scenario facilitates the understanding the influence of T-stress on fracture at different temperature in BDT region. These scenarios to implement the rate of T-stress are illustrated in Fig. 8.

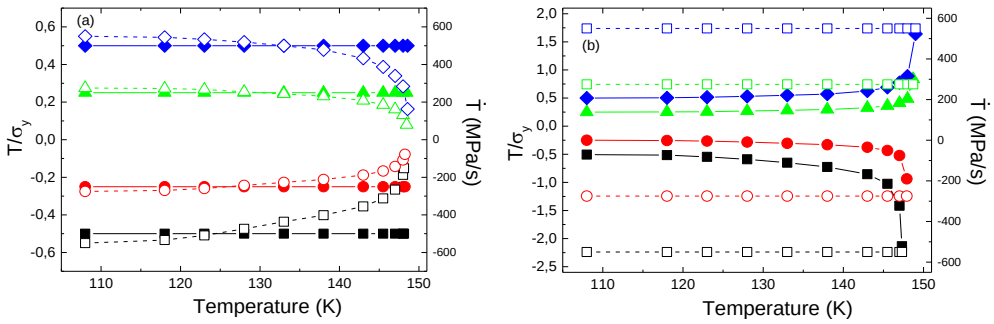

Fig. 8 Two scenarios of T-stress under a loading rate $\dot{K}_I^a = 10.0 MPam^{0.5}s^{-1}$: (a) a constant T-stress, (b) a constant rate of T-stress $\dot{T}$. Solid points represent T-stress at the fracture of material and open points represents the rate of T-stress.

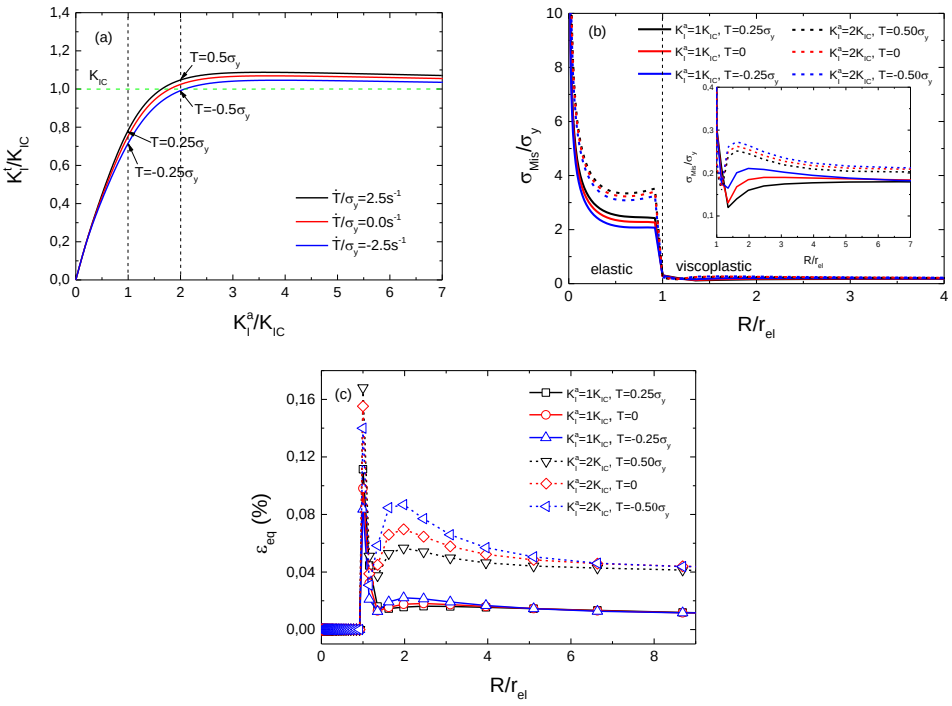

Fig. 9 The effect of T-stress on (a) stress intensity factor at crack tip, (b) Mises stress distribution ahead of crack tip, (c) the distribution of equivalent plastic strain ahead of crack tip. A loading rate $\dot{K}_I^a = 10.0 MPam^{0.5}s^{-1}$ is adopted, and temperature is 147K.

To analyze how the T-stress affects the fracture in the transition region, the second scenario is chosen to produce T-stresses at crack tip, see Fig. 9(a). It can be found that under the same applied K the stress intensity factor at crack tip with higher T-stress is always higher than that with lower T-stress. It also can be observed that a higher fracture toughness can be obtained as the T-stress decreases. The distribution of von Mises stress for different T-stresses is plotted against the distance ahead of crack tip in Fig. 9(b). In the elastic region, higher T-stress will result in higher von Mises stress. However, in the viscoplastic region, for each applied K, the von Mises stress ahead of crack tip for low T-stress is always higher than that for high T-stress, see the zoomed figure inside the Fig. 9(b). For the viscoplastic material, the negative T-stress (compressive) generates large shear deformation, which in turn will result in higher von Mises stress. The distribution of equivalent plastic strain ahead of crack tip is presented in Fig. 9(c). It can be found that large equivalent plastic strain occurs for the lower T-stress. Although the difference of von Mises stresses between different T-stresses is relatively small, the plastic deformation around the elastic region is very sensitive to the T-stress, especially at higher K_I^a. Recall equation (9), the stress field at crack tip is altered by the second term T-stress. Nevertheless, it plays a

different role in the elastic and viscoplastic region. Higher T-stress leads to a higher von Mises stress in the former, which naturally result in a higher stress intensity factor at crack tip (see Fig. 9(a)). On the contrary, higher T-stress generates a lower equivalent stress in viscoplastic region and lower plastic deformation (see Fig. 9(c)). Since higher T-stress leads to a higher stress intensity factor at crack tip, under the same fracture criterion, e.g. $K_I^t = K_{IC}$, lower applied K is obtained for higher T-stress and vice versa.

4.4.1. Effect of constant T-stress on BDT

The BDT transition curves with and without T-stress are presented in Fig.10. In the range of low temperature, e.g. below 118K, the T-stress has almost no effect on the BDT. When the temperature is higher than 118K, the influence of T-stress on BDT becomes apparent, higher T-stress leads to a lower fracture toughness and vice versa. A lower T-stress results in a smoother BDT curve. It is also observed that a lower critical BDT temperature Θ_C can be achieved with a lower T-stress or a higher T-stress leads to a higher Θ_C. However, the difference of Θ_C among different levels of T-stress is insignificant, e.g. $\Delta\Theta_C$ between T-stress=0.5σ_y and T-stress=-0.5σ_y is only 0.45K. Recall the influence of loading rate on BDT shown in Fig. 5, the loading rate affects only the critical BDT temperature. Nevertheless, the T-stress affects not only the critical BDT temperature but also the fracture toughness at the critical BDT temperature, for example, lower T-stress can result in a lower critical BDT temperature and higher fracture toughness at Θ_C.

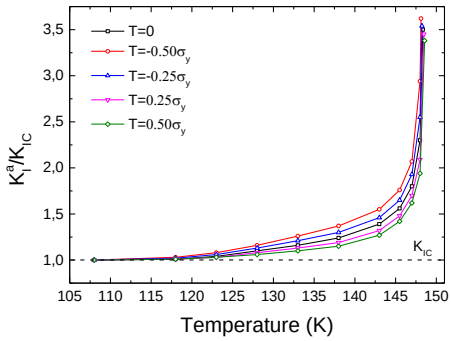

Fig. 10 the effect of T-stress on the brittle-to-ductile under a loading rate $\dot{K}_I^a = 10.0 MPam^{0.5}s^{-1}$.

In order to further investigate the effect of T-stress on the fracture toughness of single-crystal iron, the results of fracture toughness versus T-stress at different temperature are plotted in Fig. 11(a). The results show that the fracture toughness decreases with the increase of T-stress at all temperatures. As the temperature increases, the fracture toughness decreases more rapidly with the increase of T-stress. When comparing with the fracture toughness without T-stress, the increase of fracture toughness by

negative T-stress is always higher than the reduction by positive T-stress at each temperature, e.g. the amount of increase by T-stress -0.5σ_y is 0.27K_{IC} at 148K, while the amount of reduction by T-stress 0.5σ_y is only 0.18K_{IC}. In addition, an approximate linear relation between T-stress and fracture toughness can be observed at each temperature in Fig. 11(a), which also has been found in experimental results of steel reported by Meliani et al. [57] and Pluvinage et al. [37]. However, the slope of the linear relation gradually increase as the temperature increases. Recall the results in Fig.6, stress relaxation at crack tip occurs more obviously at higher temperature due to the higher plasticity around the crack tip induced by dislocation motion. The stress relaxation will reduce the constraint level at crack tip, which leads to a much higher fracture toughness as temperature increases for each level of T-stress. It implies that both T-stress and stress relaxation contribute to the variation of fracture toughness in the BDT regime, and that constraint effect on fracture in the transition region is temperature dependent. This phenomenon has been also found in the experiments by J Xu et al.[58] that the difference of fracture toughness of steel between low and high constraint level will be enlarged as temperature increases. Therefore, it is proposed that the correlation between fracture toughness, temperature and T-stress can be described by an equation:

$$K_I^a(\Theta, T) = [f(\Theta) * K_{IC}] * \left[c_0 + g(\Theta) * \left(T/\sigma_y\right)\right] \quad (15)$$

where constant c_0 equals to 1.01; $f(\Theta) = 0.97 + 0.134 * exp\ [(\ \Theta\ - 129.8)/11.5] + 3 * 10^{-9} * exp[(\Theta - 129.8)/0.942]$; $g(\Theta) = 0.009 * exp[(\Theta - 108)/10.9]$. In equation (15), the first term represents the only temperature-dependent fracture toughness without T-stress, e.g. $K_I^a(T = 0)$, which is obtained by fitting the data of zero T-stress in Fig. 10. The second term denotes the effect of T-stress on fracture toughness. For a specific temperature, a linear relation between T-stress and fracture toughness still can be achieved by the equation (15). The BDT of single-crystal iron with different level of T-stress calculated by equation (15) is presented in Fig. 11(b), and a comparison between calculated results and the predicted results shown in Fig. 10 is presented as well. In Fig. 11(b), color map is the calculated BDT curve varying with temperature and T-stress in the 3D space, and the pink map with mesh is the predicted BDT curve. It can observed that the two maps agree well with each other, which can be proved by the relative error of fracture toughness between results by the equation (15) and the predicted, see Fig. 11(c). It is found that the relative error is smaller than 5%. It is observed that large error occurs only at two higher temperatures for T-stress of both -0.5σ_y and 0.5σ_y, see Fig. 11(d). This implies that the equation (15) is able to describe the coupled relation of fracture toughness, temperature and T-stress. It also implies that a BDT transition with T-stress can be predicted under a specific loading rate by using such an equation once a BDT transition without T-stress has obtained and constraint at crack tip is known.

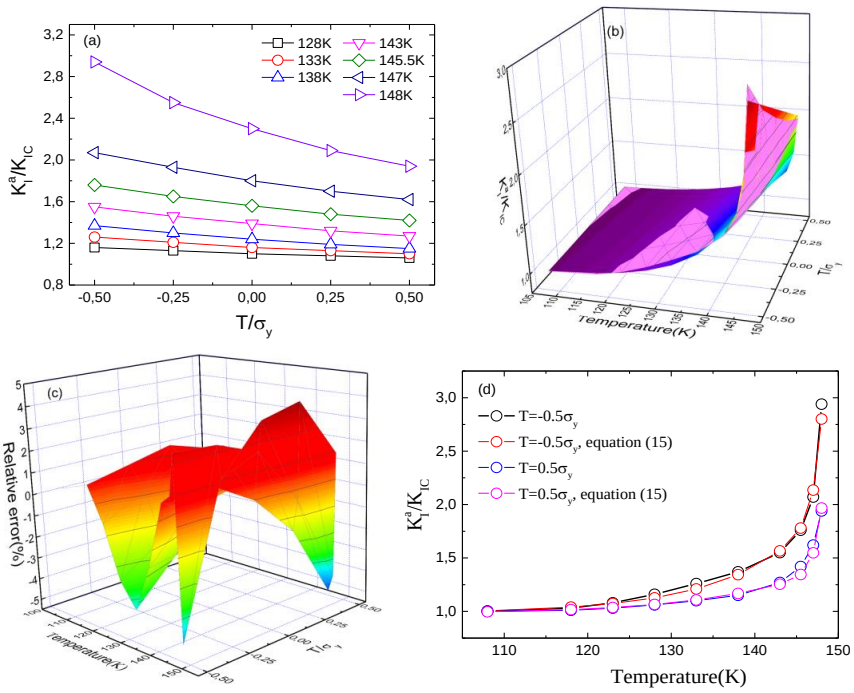

Fig. 11 the effect of T-stress on the fracture toughness of single-crystal iron under a loading rate $\dot{K}_I^a = 10.0MPam^{0.5}s^{-1}$: (a) at different temperatures, (b) comparison between the modelling results and results calculated by (15), (c) relative error of K_I^a between the modelling results and results calculated by (15), (d)BDT of material with two higher T-stress.

The critical BDT temperature Θ_C of single-crystal iron with different T-stress can be obtained from Fig. 10 under a loading rate $\dot{K}_I^a = 10.0$MPam$^{0.5}$s^{-1}. The effect of T-stress on the critical BDT temperature Θ_C and the fracture toughness at Θ_C is presented in Fig. 12. A linear relation can be achieved between $\Delta\Theta_C$ and T-tress as shown in Fig. 12(a), where $\Delta\Theta_C$ is the discrepancy of critical BDT temperature between the case with T-stress and that without T-stress. A similar linear relation between the reference transition temperature Θ_0 of 533B steel and the T-stress has been reported by Wallin [36]. Capelle et al. [34] also found such a linear relation for API X65 steel between reference transition temperature and effective T-stress. This implies that under a specific loading rate a new Θ_C with a certain level of crack tip constraint can be estimated with a Θ_C of the reference material without T-stress once the constraint at crack tip is known. Furthermore, a linear relation between Θ_C and $\Delta K_{\Theta_C}^a$ can be obtained in Fig. 12(b), here, $\Delta K_{\Theta_C}^a$ is the difference of fracture toughness at the critical BDT temperature between the case with T-stress and that without T-stress. Then substitute the Θ_C in the equation listed in Fig. 12(a) into the equation in Fig. 12(b), a new correlation between the fracture toughness at Θ_C and T-stress is built:

$$K^a_{I,\Theta_C} = K^a_{I,\theta_C}(T=0) - 0.509\theta_C(T=0) - 0.228\left(T/\sigma_y\right) + 75.51 \tag{16}$$

This relation implies that the fracture toughness at Θ_C can be estimated with both a measured Θ_C and corresponding fracture toughness at Θ_C of the reference case without T-stress when the constraint at crack tip is known. Combining equation in Fig. 12(b) and equation (16) a complete BDT curve of material can be estimated in the whole temperature range once a reference BDT curve without T-stress has been achieved:

$$K^a_I = \begin{cases} K^a_I(T=0) * \left[c_0 + g(\Theta) * \left(T/\sigma_y\right)\right], & \Theta < \Theta_C \\ K^a_I(T=0) + c_1 * \Theta_C(T=0) + c_2 * \left(T/\sigma_y\right) + c_3, & \Theta = \Theta_C \end{cases} \tag{17}$$

where c_0, c_1, c_2, and c_3 are constant can be obtained by fitting the predicted BDT curve with different T-stress in Fig.10.

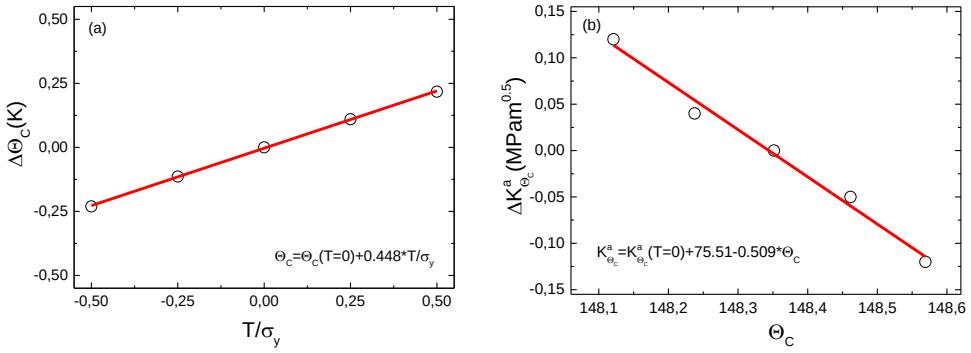

Fig. 12 the effect of T-stress on (a) critical BDT temperature, (b) fracture toughness at critical BDT temperature of single-crystal iron under a loading rate $\dot{K}^a_I = 10.0 MPam^{0.5}s^{-1}$. Here, $\Delta\Theta_C = \Theta_C - \Theta_C(T=0)$; $\Theta_C(T=0)$ is the critical BDT temperature of material without T-stress; $\Delta K^a_{I,\Theta_C} = K^a_{I,\Theta_C} - K^a_{I,\Theta_C}(T=0)$; K^a_{I,Θ_C} is fracture toughness at critical BDT temperature; $K^a_{I,\Theta_C}(T=0)$ is the fracture toughness at critical BDT temperature without T-stress.

4.4.2. Effect of constant rate of T-stress ($\dot{T}$) on BDT

Several constant rates of T-stress, $\dot{T}$, have been applied in the present model (see Fig. 8(b)) to investigate the influence of constant $\dot{T}$ on the BDT of single-crystal iron, see Fig. 13. It is observed that a lower $\dot{T}$ always induces a higher fracture toughness and a smoother BDT transition. A lower critical BDT temperature is obtained with a lower $\dot{T}$, and the corresponding fracture toughness at the critical BDT temperature for lower $\dot{T}$ is always higher. Although the two scenarios of implementation of $\dot{T}$ are different, e.g. constant T-stress and constant $\dot{T}$, the effect of T-stress is actually identical as discussed at the beginning of this section. Therefore, when comparing the Fig. 13(a) with Fig. 10, the same trend

of the effect of both constant $\dot{T}$ and constant T-stress on BDT is observed. A comparison of results between the two scenarios of implementation of T-stress on present model (see Fig. 8) is also presented in Fig. 13 (b). Although the BDT of two scenarios of T-stress implementation is similar, the influence of constant $\dot{T}$ on BDT is more significant than that of constant T-stress, especially for the negative $\dot{T}$ and negative T-stress. This is because that the T-stress produced by the negative $\dot{T}$ is always much larger than the negative constant T-stress, while, the T-stress produced by the positive $\dot{T}$ is comparable to the constant positive T-stress, see Fig. 8.

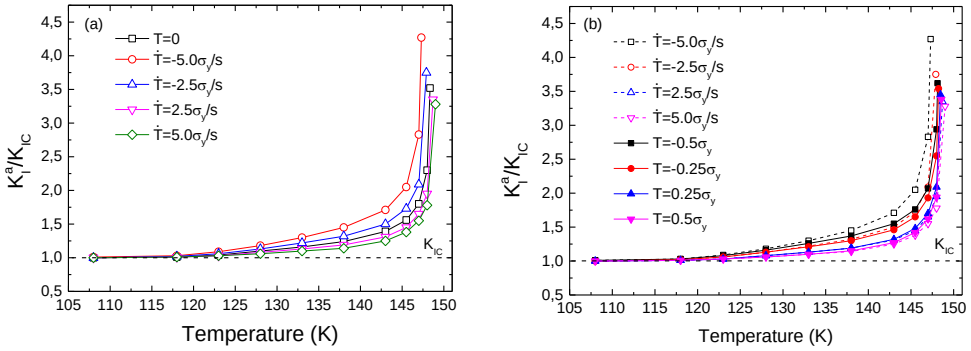

Fig. 13 the effect of rate of T-stress $\dot{T}$ on BDT under a loading rate $\dot{K}_I^a = 10.0 MPam^{0.5}s^{-1}$: (a) comparison between the BDT curves of different $\dot{T}$ and without T-stress, (b) comparison between the BDT curves of a constant $\dot{T}$ and a constant T-stress.

4.5. Effective surface energy for cleavage assessment

The modified Griffith criterion, $G_c = 2(\gamma_s + \gamma_p)$, can be adopted to assess the cleavage fracture in the transition region, where brittle fracture happens with plastic deformation in the vicinity of crack tip. However, it is difficult to directly evaluate the plastic work γ_p. Since the modified Griffith theory can also be written as $G_c = 2\gamma_{eff}$, the estimation of the effective surface energy can be an alternative solution for evaluation of plastic work during fracture. Consequently, the effective surface energy used for the description of cleavage fracture can be calculated by

$$\gamma_{eff} = \frac{(1-\nu^2)}{2E} K^2 \tag{18}$$

where K is calculated from section 4.3 and 4.4 for the material with and without T-stress. The evolution of effective surface energy during cleavage fracture of single-crystal iron with temperature is presented in Fig. 14, in which the constraint effect on the effective surface energy at different temperature is also presented. Since there is a quadratic relation between γ_{eff} and K, when comparing the transition of effective surface energy to the transition of fracture toughness, the change of effective surface energy

is very small in lower temperature range, e.g. below 145.5K, but is much larger at higher temperature. Following the same method and procedure introduced in 4.4.1, the complete relation of effective surface energy and T-stress in the whole BDT temperature range can be built with an equation like (17).

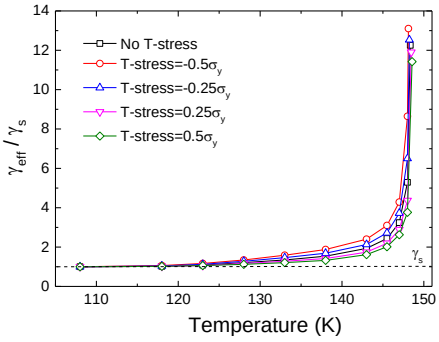

Fig. 14 constraint effect on the calculated effective surface energy γ_{eff} under a loading rate of $\dot{K}_I^a = 10.0 MPam^{0.5}s^{-1}$

Temperature dependent effective surface energy of steel has been found by Linaza et al. [43] and Martin et al. [44] by converting the measured the fracture stress of specimen to effective surface energy in terms of modified Griffith theory. However, the effective surface energy law obtained from experiment depends on the geometry of specimen, and can not be applied generally in practice. An explicit effective surface energy law has been derived by Burns et al. [45] to estimate the plastic contribution to the energy release rate during the cleavage fracture, which is function of temperature, geometry, crack speed, dislocation density at crack tip etc. This law has successfully adopted to the experimental studies of dynamic fracture on LiF single-crystal. However, since it can not explicitly predict the dislocation multiplication in the process of cleavage fracture, real-time measurement on dislocation density at propagating crack tip is necessary when using such law. The solution to estimate the effective surface energy law in BDT process proposed in present work is capable of integrating many influencing factors, e.g. temperature, loading rate and constraint, and has a potential application for components with any geometry. This temperature and constraint dependent effective surface energy law will benefit for the cleavage fracture criterion in the transition region, such as, using RKR model.

5. Conclusions

In the present study, a continuum model has been employed to model the BDT behavior of single-crystal iron based on dislocation mobility controlled BDT theory. Parametric studies have been carried

out and a group of parameters for BDT investigation has been obtained by comparing computational results to experimental results reported in the literature. BDT behavior under different loading rate has been studied. It can be observed that lower loading rate can produce a smoother BDT curve and a lower critical BDT temperature, however loading rate has no effect on the fracture toughness at the critical BDT temperature.

It is found that the change of the stress distribution ahead of crack tip due to the T-stress dictates the fracture toughness of single-crystal iron in the BDT transition region. Lower constraint leads to a higher fracture toughness in the transition region, a smoother transition curve and a lower critical BDT temperature, and also a higher fracture toughness at the critical BDT temperature. A correlation between the fracture toughness and T-stress has been found: below critical BDT temperature, the fracture toughness is related to the temperature dependent fracture toughness of a reference material without T-stress and the contribution of T-stress that relies on the temperature; at critical BDT temperature, the fracture toughness can be estimated with a linear function of T-stress, fracture toughness and critical BDT temperature of a reference material without T-stress. Therefore, a complete BDT curve can be predicted by the equation (17) created in present study once the amount of constraint and the BDT curve of a reference material without T-stress has been acquired.

A solution to estimate the temperature-dependent effective surface energy law in the brittle-to-ductile transition has been studied in present work, which will benefit for the assessment cleavage fracture in the transition region.

Acknowledgements

The authors wish to thank the Research Council of Norway for funding through the Petromaks 2 Programme, Contract No.228513/E30. The financial support from ENI, Statoil, Lundin, Total, JFE Steel Corporation, Posco, Kobe Steel, SSAB, Bredero Shaw, Borealis, Trelleborg, Nexans, Aker Solutions, FMC Kongsberg Subsea, Kværner Verdal, Marine Aluminium, Hydro and Sapa are also acknowledged.

References

[1] A.S. Argon, Mechanics and Physics of Brittle to Ductile Transitions in Fracture, Journal of Engineering Materials and Technology 123(1) (2000) 1-11.
[2] M. Brede, P. Haasen, The brittle-to-ductile transition in doped silicon as a model substance, Acta Metallurgica 36(8) (1988) 2003-2018.
[3] M. Brede, The brittle-to-ductile transition in silicon, Acta Metallurgica et Materialia 41(1) (1993) 211-228.
[4] J.S.a.S.G. Roberts, The brittle–ductile transition in silicon. I. Experiments, Proceedings of the Royal Society of London. A. Mathematical and Physical Sciences 421(1860) (1989) 1-23.

[5] P.B. Hirsch, S.G. Roberts, The brittle-ductile transition in silicon, Philosophical Magazine A 64(1) (1991) 55-80.
[6] B.J. Gally, A.S. Argon, Brittle-to-ductile transitions in the fracture of silicon single crystals by dynamic crack arrest, Philosophical Magazine A 81(3) (2001) 699-740.
[7] K.J. Hsia, A.S. Argon, Experimental study of the mechanisms of brittle-to-ductile transition of cleavage fracture in Si single crystals, Materials Science and Engineering: A 176(1) (1994) 111-119.
[8] P. Gumbsch, J. Riedle, A. Hartmaier, H.F. Fischmeister, Controlling Factors for the Brittle-to-Ductile Transition in Tungsten Single Crystals, Science 282(5392) (1998) 1293-1295.
[9] A. Hartmaier, P. Gumbsch, Thermal activation of crack-tip plasticity: The brittle or ductile response of a stationary crack loaded to failure, Physical Review B 71(2) (2005) 024108.
[10] A. Hartmaier, P. Gumbsch, The brittle-to-ductile transition and dislocation activity at crack tips, Journal of Computer-Aided Materials Design 6(2) (1999) 145-155.
[11] M. Tanaka, E. Tarleton, S.G. Roberts, The brittle–ductile transition in single-crystal iron, Acta Materialia 56(18) (2008) 5123-5129.
[12] M. Tanaka, A.J. Wilkinson, S.G. Roberts, Ductile–brittle transition of polycrystalline iron and iron–chromium alloys, Journal of Nuclear Materials 378(3) (2008) 305-311.
[13] A.P.L. Turner, T. Vreeland, The effect of stress and temperature on the velocity of dislocations in pure iron monocrystals, Acta Metallurgica 18(11) (1970) 1225-1235.
[14] J.R. Rice, R. Thomson, Ductile versus brittle behaviour of crystals, Philosophical Magazine 29(1) (1974) 73-97.
[15] J.R. Rice, Dislocation nucleation from a crack tip: An analysis based on the Peierls concept, Journal of the Mechanics and Physics of Solids 40(2) (1992) 239-271.
[16] G. Xu, A.S. Argon, M. Ortiz, Nucleation of dislocations from crack tips under mixed modes of loading: Implications for brittle against ductile behaviour of crystals, Philosophical Magazine A 72(2) (1995) 415-451.
[17] G.E. Beltz, D.M. Lipkin, L.L. Fischer, Role of Crack Blunting in Ductile Versus Brittle Response of Crystalline Materials, Physical Review Letters 82(22) (1999) 4468-4471.
[18] A.S. Argon, Brittle to ductile transition in cleavage fracture, Acta Metallurgica 35(1) (1987) 185-196.
[19] S.G.R.a.J.S. P. B. Hirsch, The brittle-ductile transition in silicon. II. Interpretation, Proceedings of the Royal Society of London. A. Mathematical and Physical Sciences 421(1860) (1989) 25-53.
[20] P.B. Hirsch, S.G. Roberts, Modelling plastic zones and the brittle-ductile transition, Philosophical Transactions of the Royal Society of London. Series A: Mathematical, Physical and Engineering Sciences 355(1731) (1997) 1991-2002.
[21] Y.-B. Xin, K.J. Hsia, Simulation of the brittle-ductile transition in silicon single crystals using dislocation mechanics, Acta Materialia 45(4) (1997) 1747-1759.
[22] V.R. Nitzsche, K.J. Hsia, Modelling of dislocation mobility controlled brittle-to-ductile transition, Materials Science and Engineering: A 176(1) (1994) 155-164.
[23] C. Betegón, J.W. Hancock, Two-Parameter Characterization of Elastic-Plastic Crack-Tip Fields, Journal of Applied Mechanics 58(1) (1991) 104-110.
[24] M.H. ZL Zhang, C Thaulow, The effect of T stress on the near tip stress field of an elastic-plastic interface crack, ICF 9, Sydney, Australia, 1997.
[25] N.P. O'Dowd, C.F. Shih, Family of crack-tip fields characterized by a triaxiality parameter—I. Structure of fields, Journal of the Mechanics and Physics of Solids 39(8) (1991) 989-1015.
[26] J. Xu, Z.L. Zhang, E. Østby, B. Nyhus, D.B. Sun, Effects of crack depth and specimen size on ductile crack growth of SENT and SENB specimens for fracture mechanics evaluation of pipeline steels, International Journal of Pressure Vessels and Piping 86(12) (2009) 787-797.
[27] C. Thaulow, E. Østby, B. Nyhus, Z.L. Zhang, B. Skallerud, Constraint correction of high strength steel: Selection of test specimens and application of direct calculations, Engineering Fracture Mechanics 71(16) (2004) 2417-2433.
[28] Y.J. Chao, S. Yang, M.A. Sutton, On the fracture of solids characterized by one or two parameters: Theory and practice, Journal of the Mechanics and Physics of Solids 42(4) (1994) 629-647.
[29] Z.L. Zhang, M. Hauge, C. Thaulow, Two-parameter characterization of the near-tip stress fields for a bi-material elastic-plastic interface crack, International Journal of Fracture 79(1) (1996) 65-83.

[30] X. Gao, C.F. Shih, V. Tvergaard, A. Needleman, Constraint effects on the ductile-brittle transition in small scale yielding, Journal of the Mechanics and Physics of Solids 44(8) (1996) 1255-1282.
[31] X. Gao, R.H. Dodds, Constraint effects on the ductile-to-brittle transition temperature of ferritic steels: a Weibull stress model, International Journal of Fracture 102(1) (2000) 43-69.
[32] X. Gao, R.H. Dodds Jr, An engineering approach to assess constraint effects on cleavage fracture toughness, Engineering Fracture Mechanics 68(3) (2001) 263-283.
[33] C. Yan, Y.W. Mai, Effect of constraint on ductile crack growth and ductile-brittle fracture transition of a carbon steel, International Journal of Pressure Vessels and Piping 73(3) (1997) 167-173.
[34] J. Capelle, J. Furtado, Z. Azari, S. Jallais, G. Pluvinage, Design based on ductile–brittle transition temperature for API 5L X65 steel used for dense CO2 transport, Engineering Fracture Mechanics 110(Supplement C) (2013) 270-280.
[35] J. Capelle, M. Ben Amara, G. Pluvinage, Z. Azari, Role of constraint on the shift of ductile–brittle transition temperature of subsize Charpy specimens, Fatigue & Fracture of Engineering Materials & Structures 37(12) (2014) 1367-1376.
[36] K. Wallin, Structural integrity assessment aspects of the Master Curve methodology, Engineering Fracture Mechanics 77(2) (2010) 285-292.
[37] G. Pluvinage, J. Capelle, M. Hadj Méliani, A review of fracture toughness transferability with constraint and stress gradient, Fatigue & Fracture of Engineering Materials & Structures 37(11) (2014) 1165-1185.
[38] G.R. Irwin, Fracture dynamics, Fracture of metals, American Society for Metals, Cleveland, OH, 1948, pp. 147-166.
[39] E. Orown, Fracture and Strength of Solids, Reports on Progress in Physics 12 (1948) 185.
[40] C.J. McMahon, V. Vitek, The effects of segregated impurities on intergranular fracture energy, Acta Metallurgica 27(4) (1979) 507-513.
[41] M.L. Jokl, V. Vitek, C.J. McMahon, A microscopic theory of brittle fracture in deformable solids: A relation between ideal work to fracture and plastic work, Acta Metallurgica 28(11) (1980) 1479-1488.
[42] K. Wallin, T. Saario, K. Törrönen, Statistical model for carbide induced brittle fracture in steel, Metal Science 18(1) (1984) 13-16.
[43] M.A. Linaza, J.M. Rodriguez-Ibabe, J.J. Urcola, DETERMINATION OF THE ENERGETIC PARAMETERS CONTROLLING CLEAVAGE FRACTURE INITIATION IN STEELS, Fatigue & Fracture of Engineering Materials & Structures 20(5) (1997) 619-632.
[44] J.I. San Martin, J.M. Rodriguez-Ibabe, Determination of energetic parameters controlling cleavage fracture in a Ti-V microalloyed ferrite-pearlite steel, Scripta Materialia 40(4) (1999) 459-464.
[45] S.J. Burns, W.W. Webb, Fracture Surface Energies and Dislocation Processes during Dynamical Cleavage of LiF. I. Theory, Journal of Applied Physics 41(5) (1970) 2078-2085.
[46] R.M. Thomson, J.E. Sinclair, Mechanics of cracks screened by dislocations, Acta Metallurgica 30(7) (1982) 1325-1334.
[47] I.H. Lin, R. Thomson, Cleavage, dislocation emission, and shielding for cracks under general loading, Acta Metallurgica 34(2) (1986) 187-206.
[48] D.J.B. D. Hull, introduction to dislocations, Fifth Edition, Elsevier Ltd, Oxford, 2011.
[49] Z. Suo, C.F. Shih, A.G. Varias, A theory for cleavage cracking in the presence of plastic flow, Acta Metallurgica et Materialia 41(5) (1993) 1551-1557.
[50] M.L. Williams, On the Stress Distribution at the Base of a Stationary Crack, Journal of Applied Mechanics 24(1) (1956) 109-114.
[51] S.G. Larsson†, A.J. Carlsson, Influence of non-singular stress terms and specimen geometry on small-scale yielding at crack tips in elastic-plastic materials, Journal of the Mechanics and Physics of Solids 21(4) (1973) 263-277.
[52] G.W. Hollenberg, G.R. Terwilliger, R.S. Gordon, Calculation of Stresses and Strains in Four-Point Bending Creep Tests, Journal of the American Ceramic Society 54(4) (1971) 196-199.
[53] T. Fett, Stress Intensity Factors – T-Stresses – Weight Functions, Supplement Volume, KIT Scientific Publishing, 2009.
[54] N.P. Allen, B.E. Hopkins, J.E. McLennan, The Tensile Properties of Single Crystals of High-Purity Iron at Temperatures from 100 to -253 degrees C, Proceedings of the Royal Society of London. Series A, Mathematical and Physical Sciences 234(1197) (1956) 221-246.

[55] K.R. Jayadevan, R. Narasimhan, T.S. Ramamurthy, B. Dattaguru, A numerical study of T-stress in dynamically loaded fracture specimens, International Journal of Solids and Structures 38(28) (2001) 4987-5005.
[56] K.R. Jayadevan, R. Narasimhan, T.S. Ramamurthy, B. Dattaguru, Effect of T-stress and loading rate on crack initiation in rate sensitive plastic materials, International Journal of Solids and Structures 39(7) (2002) 1757-1775.
[57] M.H. Meliani, Y.G. Matvienko, G. Pluvinage, Two-parameter fracture criterion (K ρ,c -T ef,c) based on notch fracture mechanics, International Journal of Fracture 167(2) (2011) 173-182.
[58] Z.L.Z. J Xu, E Østby, B Nyhus, D B Sun, Effects of Temperature and Crack Tip Constraint on Cleavage Fracture Toughness in the Weld Thermal Simulated X80 Pipeline Steel, The Twentieth (2010) International Offshore and Polar Engineering Conference, Shanghai, China, 2010.

Paper II

A.2 Paper 2

CAFE based Multi-scale Modelling of Ductile-to-Brittle Transition of Steel with a Temperature Dependent Effective Surface Energy

Authors: Yang Li, Anton Shterenlikht, Xiaobo Ren, Jianying He, Zhiliang Zhang

Materials Science and Engineering: A 755 (2019) 220-230.

CAFE based Multi-scale Modelling of Ductile-to-Brittle Transition of Steel with a Temperature Dependent Effective Surface Energy

Yang Li[1], Anton Shterenlikht[2], Xiaobo Ren[3], Jianying He[1], Zhiliang Zhang[1,*]

[1] NTNU Nanomechanical Lab, Department of Structural Engineering, Norwegian University of Science and Technology (NTNU), Richard Brikelands vei 1A, N-7491Trondheim, Norway

[2] Department of Mechanical Engineering, University of Bristol, University Walk, Bristol

[3] SINTEF Industry, Richard Brikelands vei 2B, N-7465 Trondheim, Norway

Abstract: *It is still a challenge to numerically achieve the interactive competition between ductile damage and brittle fracture in ductile-to-brittle transition (DBT) region. In addition, since two types of fracture occur at two independent material length scales, it is difficult to process them with the same mesh size by using finite element method. In this study, a framework of modelling DBT of a thermal mechanical controlled-rolling (TMCR) steel is explored by using the cellular automata finite element (CAFE) method. The statistical feature of material's microstructure is incorporated in the modelling. It is found that DBT curve cannot be reproduced with only one temperature dependent flow property, for which another temperature dependent variable must be considered. A temperature dependent effective surface energy based on typical cleavage fracture stage is proposed and obtained through a continuum approach in present work. The DBT of TMCR steel is simulated by using CAFE method implemented with a temperature dependent effective surface energy. It is found that numerical simulation is able to produce a full transition curve, especially with scattered absorbed energies in the transition region represented. It is also observed that simulation results can reproduce a comparable DBT curve contrasting to the experimental results.*

Keywords: Cellular Atoumata Finite Element (CAFE); Ductile-to-Brittle Transition (DBT); Cleavage; Effective surface energy; TMCR steel

1. Introduction

Ductile-to-brittle transition (DBT) is normally found in the BCC materials, e.g., steel, due to temperature decreasing and loading rate elevation. Ductile fracture usually occurs at higher temperature, e.g. the upper-shelf, with a damage mechanism of void nucleation, growth and coalescence. The well-known Gurson type of model [1-4] and Rousselier model [5] have been widely used to describe ductile fracture accompanying with plastic deformation, in which the critical void volume fraction f_c has been proposed as the failure criterion. While, unstable cleavage fracture is commonly initiated by second-

phase particle cracking due to dislocation pile-up, which refers to the sequence of three steps: particle breakage, transgranular fracture within a single grain and overcoming of the grain boundary [6]. A simple model proposed by Ritchie, Knott and Rice [7], so called RKR model, assumes that cleavage failure occurs when the maximum principle stress ahead of the crack tip exceeds the fracture stress σ_f over a characteristic distance. In order to describe the statistical nature of micro-cracks in the stress field, micromechanical models [8-10] following the weakest link philosophy have been reformulated based on RKR model, which provide a promising local approach to understand the essentials of cleavage. One of the most widely used approaches is Beremin model [8], in which a simple expression for macroscopic failure probability can be derived involving a scalar measure of the crack-front loading, the so-called Weibull stress σ_w. Consequently, two main types of the failure criterion for cleavage have been established, critical fracture stress σ_f or Weibull stress σ_w. Whereas, in the DBT regime, two fracture modes coexist, and the final rupture of materials occurs as a consequence of the competition between two failure mechanisms.

Modelling of DBT of steel has aroused great interest in past decades. Ductile damage models (e.g., GTN, Rousselier) combined with RKR criterion model or local approach (e.g. Beremen model) has been widely applied to model the DBT of steel under quasi-static load [11, 12] or dynamic load [13-18]. However, it is basically a post-processing solution to evaluate the occurrence of cleavage after stress field ahead of crack tip obtained from the constitutive equation of ductile model. The competition between two failure mechanisms and the interaction between two failure modes in the transition region are not involved indeed. Furthermore, the fracture in the transition region occurs on two independent scales of microstructure size, ductile fracture related to the spacing of the dominant void initiated from particles, while the brittle fracture related to the grain or cleavage facet size. It is difficult to handle two fracture modes with only one mesh size using the finite element method. Although attempts have been conducted to overcome this problem by using non-local approaches [11, 12, 19], it is still a challenge to represent the competition between two failure mechanisms and the interaction between two failure modes in the transition region. However, one approach coupled cellular automata (CA) and finite element (FE), so-called CAFE method, provides a practical solution to solve these two challenges simultaneously [20]. In addition, the statistical feature of microstructure of material can also be represented in this method, e.g. initial void distribution, grain size distribution, misoriention of grain boundaries etc., such that the scatter of toughness in the transition region can be captured. The principle and implementation of CAFE method have been thoroughly described in the ref. [20-25].

It is known that the flow properties, e.g., yield stress and strain hardening, will be altered as temperature decreases, which could be a significant factor resulting in the occurrence of DBT. However, only temperature-dependent flow stress is not enough to predict the transition behavior of materials when comparing with the test data reported by Rossoll et al [16], Tanguy et al [18] and Shterenlikht et al [20]. Many efforts have been made to describe temperature dependence of fracture toughness in the DBT

transition region. A global approach, Master curve method has been adopted in ASTM E1921 [26], in which the variation of fracture toughness with temperature in DBT region can be described with a reference temperature T_0. Although the Master curve method is very convenient to apply in practice since only few tests are needed for calibration, it requires high constraint and small scale yielding conditions. Tanguy et al [18] has simulated the DBT of A508 steel with a temperature-dependent σ_u rather than a constant value when modelling the Charpy impact test. By using Master curve method [26] to calibrate the parameters of Beremin model, Petti et al [27], Wasiluk et al [28], Cao et al [29] and Qian et al [30] have also found that σ_u is increasing with temperature in the transition region. Gao et al [31] has found that σ_u increased with temperature reflecting the combined effects of temperature on material flow properties and toughness. Moattari et al[32] accurately predicted the fracture toughness in DBT transition region by introducing a temperature-dependent σ_u described with a summation of athermal and thermally activated stress contribution. A temperature dependent misorientation of grain boundary proposed by Shterenlikht et al [20] has been implemented into the CAFE method to model the DBT of Charpy test of TMCR steel. It has to be noticed that either the temperature dependent σ_u or misorientation proposed in the literature is just a phenomenological parameter for DBT modelling. Therefore, exploring a physical-based variable to disclose the nature of temperature dependent fracture toughness in the transition region is not only significant but also necessary. In this work, on the basis of our previous work [33], a continuum approach is developed to estimate the effective surface energy in the DBT transition region of a TMCR steel. Then, we attempt to establish a framework of numerical prediction of the DBT in steel by utilizing the CAFE method implemented with the temperature dependent effective surface energy.

The present paper is organized as the followings. Section 2 reviews the CAFE method and discusses the parameters of the model. Section 3 introduces a continuum solution to determine the temperature dependent effective surface energy of TMCR steel. Section 4 describes the finite element procedures and models used to predict the DBT of steels. Section 5 presents the main modelling results of DBT of Charpy tests by using CAFE method implemented with a temperature dependent effective surface energy. The physical nature of the competition between particle size dominated and grain size dominated cleavage propagation is also discussed. The feasibility of CAFE method implemented with temperature dependent effective surface energy is validated by comparing the predicted results to experimental results in the literature [20]. Section 6 ends the paper with a short summary and conclusions.

2. The CAFE Method

The motivation of the CAFE method is to combine the structural and microstructural interactions by finite element method [20-22]. The method is divided into two phases: one is finite elements to capture the stresses or strains at the structural level, the other is to catch the mechanical essentials of the microstructural behavior and its development in a set of CA arrays. Fig.1 shows the implementation of the above strategy to deal with the fracture in the transition region where both ductile and brittle micro-mechanisms work simultaneously [20]. In each material integration point, the microstructure is represented by two CA arrays, where the brittle array represents the cleavage behavior while the ductile array processes ductile damage. Structural information, for example, stress/strain and damage variable, processed in FE level inputs to CA levels, meanwhile, the microstructural evolution and the failure are integrated and send back to the FEs. To achieve the implementation of CAFE method in finite element, the explicit dynamic process has been chosen to develop a VUMAT by Shterenlikht et al [20-22] so that crack can propagate along a natural failure path through element removal.

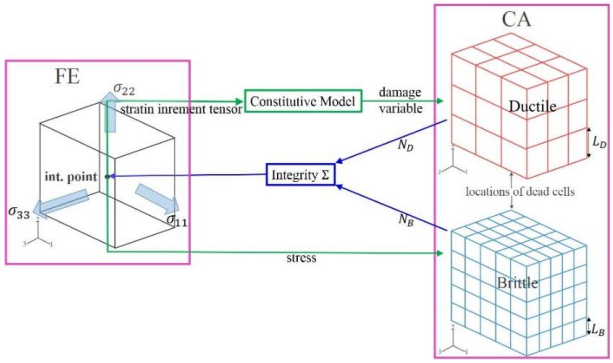

Fig.1 the illustration of the mechanism of CAFE method in which ductile damage and cleavage fracture have been coupled through two different CA arrays. Here, N_D and N_B are the number of 'dead' cell of ductile CA arrays and brittle CA arrays respectively; Σ is integration indicator; L_D and L_B are the size of cells in brittle and ductile CA arrays.

The Roussellier ductile damage model [5] is adopted to describe the constitutive response at the integration point. Equation (1) describes the plastic potential of this model

$$\frac{\sigma_{eq}}{\rho} - H(\varepsilon_{eq}) + B(\beta)Dexp\left(\frac{\sigma_m}{\rho\sigma_1}\right) = 0 \tag{1}$$

where $H(\varepsilon_{eq})$ is the hardening property of material; σ_1 and D are material constants that need to be tuned; σ_{eq}, σ_m and ε_{eq} are equivalent stress, mean stress and equivalent strain; $B(\beta)$ is the function of damage variable β; ρ is relative density, which can be described by

$$\rho = \frac{1}{1 - f_0 + f_0 exp\beta} \tag{2}$$

where f_0 is initial void volume fraction. In ductile CA arrays, cell size L_D is used to characterize the unit cell size of ductile damage of material with a single void, which normally relates to the spacing of inclusions or large carbides in steel.

According to modified Griffith theory, the critical fracture stress for cleavage can be calculated by

$$\sigma_F = \sqrt{\frac{\pi E \gamma_{eff}}{(1-\nu^2)d}} \tag{3}$$

where γ_{eff} is effective surface energy for the cleavage fracture; E and ν are Young's modulus and Poisson's ratio respectively; d is grain size. In present work, a temperature dependent effective surface energy for cleavage will be applied in the CAFE method to calculate critical fracture stress of cleavage. A fraction of brittle cells, η, in each brittle CA array, is adopted to represent grains with adjacent grain boundary carbides, where micro-crack has already nucleated. In brittle CA arrays, the cleavage facet size (d_{CFS}) is applied as the size of cells in brittle CA arrays, e.g. L_B, which can be measured through fractographic analysis on the fracture surface of specimen [20]. Since the misorientation between grains is naturally the barrier of cleavage crack propagation crossing the grain boundary [34], a random orientation is assigned to each cell in brittle CA arrays, and a misorientation threshold, e.g., θ_{th}, is assumed so that crack can propagate from one cell to the other.

The property of CA depends on the state of cells. The state of each cell in next time increment is determined by its state and the states of neighboring cells at the previous time increment. Once that the cell is failed due to the fracture propagation, the state of cell will be changed from 'alive', e.g., initial state, to 'dead'. Then, the closing neighborhood of 'dead' cell will be stress-concentrated since the 'dead' cell lost its load-bearing capacity. A framework [22, 25] has described in detail how to locate such a closing neighborhood around the 'dead' cell. The local concentration factors are utilized to solve this problem, which are C_D for ductile CA array and C_B for brittle CA array. Thus, at the next time increment, the states of concentrated cells (either ductile or brittle) are determined by the results of comparison between the product of damage variable and concentration factors and failure criteria mentioned above. An integrity indicator, Σ, is used to count the 'dead' cells of both ductile and brittle CA arrays by which the potential fracture at every current time increment is evaluated. The Σ whose initial value is 1.0, decreases continuously with the accumulation of damage until N_D or N_B reaches its maximum value N_{D-max} or N_{B-max}. At this moment, the Σ turns to be zero, which means material inside the integration point is failed and the integration point does not have loading-bearing capacity any more. The FE will then be removed from the mesh when the zero Σ is transferred to FE. The Σ can be calculated by

$$\Sigma = 1 - \max\left(\frac{N_D}{N_{D-max}}, \frac{N_B}{N_{B-max}}\right) \tag{4}$$

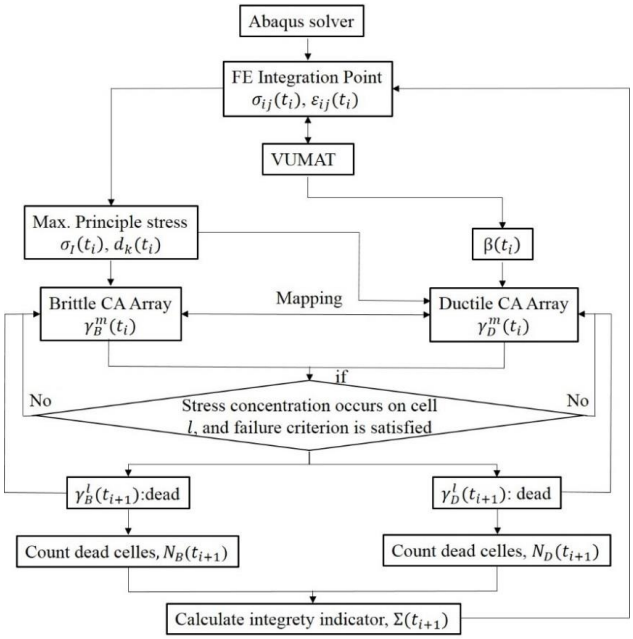

Fig.2 flow chart of the CAFE method. Here, $\sigma_{ij}(t_i)$ and $\varepsilon_{ij}(t_i)$ are stress and strain tensors at time t_i provided by Abaqus solver; and $\beta(t_i)$ is damage variable of cells given by constitutive model to ductile CA array at time t_i; $\sigma_I(t_i)$ is the maximum principle stress of each element calculated from $\sigma_{ij}(t_i)$; $d_k(t_i)$ is the direction cosines of $\sigma_I(t_i)$; $\gamma_D^m(t_i)$ or $\gamma_B^m(t_i)$ is state of cell m in ductile or brittle CA arrays t_i; $\gamma_D^l(t_{i+1})$ or $\gamma_B^l(t_{i+1})$ is state of cell l where stress concentration occurs and failure criterion is satisfied in ductile or brittle cell arrays at time t_{i+1}; $N_D(t_{i+1})$ or $N_B(t_{i+1})$ is numbers of dead cells in ductile or brittle CA arrays at time t_{i+1}; $\Sigma(t_{i+1})$ is the integrity indicator at time at time t_{i+1}.

The calculation process of the CAFE method is presented in Fig.2. It has to be mentioned that in order to reduce the calculation time, the damage variable $\beta(t_i)$ is given to the ductile CA array instead of the strain increment tensor $\Delta\varepsilon_{ij}(t_i)$, and accordingly only the solution dependent variable Σ is returned to the FE from CA array. Both ductile and brittle CA arrays are used only for the simulation of fracture propagation at each CA scale, while, the constitutive response is calculated at FE level. In addition, for the easy achievement of convergence, in ductile CA array a normal distribution of damage value β_F rather than that of f_0 is adopted. At each increment of deformation, the model compares the present damage variable β with the failure value β_F until the material failed. Since two CA arrays occupy the same physical space, the evaluation of the cells shall be synchronized in both CA arrays. Thus, a mapping rule has been introduced in the CAFE method to reflect dead cells in ductile CA array into the corresponding brittle CA array, and vice versa [21]. After stress concentration occurred on the cell *m*

in either CA arrays, it becomes dead when failure criteria are satisfied. A more detailed description about the CAFE method can be found in literature [21].

3. The Temperature dependent effective surface energy

Based on the theory of shielding effect of dislocation mobility on crack tip, a method has been proposed [33] to predict the temperature dependent effective surface energy of single-crystal iron in the ductile-to-brittle transition (DBT) region. In the present work, this method will be extended to calculate the effective surface energy of steel in the transition region.

The shielding effect of the dynamics of dislocation on crack tip stress field can be assessed with a continuum method [33, 35, 36]. It is assumed that the material is isotropic, and that the rate-dependent plastic deformation is induced by dislocation emission and motion. According to Orowan law, the shear strain rate, $\dot{\gamma}^p$, can be used to describe the plasticity caused by the dislocation mobility

$$\dot{\gamma}^p = \alpha \rho_d b v \tag{5}$$

Where α is a proportionality constant; ρ_d is the dislocation density; b is Burgers vector; v is dislocation velocity. The dislocation velocity v can be obtained from the function of resolved shear stress τ and temperature Θ, e.g., the empirical Arrhenius type law

$$v = v_0 exp\left(-\frac{Q}{k_B \Theta}\right)\left(\frac{\tau}{\tau_0}\right)^m \tag{6}$$

where Q is the activation energy for dislocation velocity; k_B is the Boltzmann constant; m is a material constant for wide range of stress level; v_0 is material specific reference dislocation velocity; τ_0 is normalization shear stress; here Θ is the absolute temperature in Kelvin. Since the material is assumed to be isotropic, the von Mises equivalent stress σ_{Mis} and the equivalent plastic strain rate $\dot{\varepsilon}^p$ can be used to replace the plastic shear strain rate $\dot{\gamma}^p$ in equation (5) and the resolved shear stress τ in equation (6). Then, after inserting the equation (6) into equation (5), the equivalent plastic strain rate $\dot{\varepsilon}$ to describe the rate-dependent plasticity induced by the dislocation mobility can be derived

$$\dot{\varepsilon} = \dot{\varepsilon}_0 \exp\left(-\frac{Q}{k_B \Theta}\right)\left(\frac{\sigma_{Mis}}{\sigma_0}\right)^m \tag{7}$$

where $\dot{\varepsilon}_0$ is a reference strain rate; σ_0 is a normalization stress.

It is known that DBT normally occurs in body centered cubic (BCC) metals, e.g., single-crystal iron, Fe alloys and steel, due to the thermal-activated dislocation emission and motion [37]. The difference between single-crystal iron and steel is the presence of impurities (e.g., particles), grain boundary and

preexisting dislocations in the latter, which affects the dislocation behavior, for instance, nucleation, motion, multiplication etc. If their effect on the fracture of the latter can be described by the change of dislocation density near crack tip comparing with that of former, see equation (5), the model developed for single-crystal iron is possible to be applied to the steel according to the theory of the of shielding effect of dislocation mobility on crack tip. To do this, several assumptions have to be made. Firstly, a micro-crack is assumed to be initiated within a grain boundary particle, e.g., carbide or inclusion, at a position x_c ahead of the notch/crack tip where the local tensile stress equals to the maximum principle stress, see Fig.3 (a). Then, the nucleated micro-crack will penetrate the interface between particle and matrix once that local tensile stress at the interface exceeds the fracture stress. Secondly, we postulate that the penetration of the micro-crack into the interface leads to the final unstable cleavage fracture, namely the crack resistance of grain boundary is not taken into account. Further, it is assumed that the crack penetration from particle into matrix is dominated by a local *K*-field. Then, the elastic zone (dislocation free zone) in the continuum model for single-crystal material [33] is replaced with an elastic particle, and the viscoplasitic material outside the elastic region is defined as the ferrite, e.g., a time-dependent plastic matrix. Thus, a new continuum model can be adopted to estimate the fracture toughness of steel in the transition region, see Fig.3 (b).

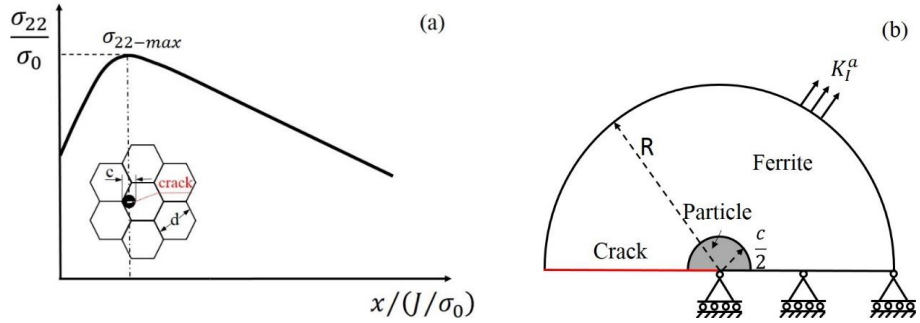

Fig.3 the continuum model: (a) the schematic illustration of the micro-crack initiation and propagation across the interface and grain boundary, c is the particle diameter, and d is grain size; (b) MBL model to calculate the effective surface energy for cleavage extension across the interface between particle and matrix [33]. c is particle size.

Only the upper-half of model is presented due to symmetry, see Fig.3 (b). A small circle around the crack tip with a radius $c/2$ is the elastic zone, e.g., particle. The radius of model R is 20 times larger than the elastic zone size. Outside the elastic zone, there is the matrix, e.g., ferrite, which is time-dependent plastic material described by the equation (7). A crack with an initial radius of $1.15 \times 10^{-4}R$ is located in the center of model. Abaqus 6.14 is employed, and 4-node and plane strain elements (CPE4) are used in all simulations. Through the nodal displacement on the outer boundary layer in the MBL

model, a linear elastic K_I field, e.g., the applied stress intensity factor K_{I}^{a}, with a constant loading rate $\dot{K}$ is implemented. To calculate the effective surface energy, only a stationary crack is studied.

For a sharp crack tip, cleavage fracture occurs once the crack tip stress intensity factor equals to the critical value, i.e. $K_{\mathrm{I}}^{t} = K_{\mathrm{IC}}$. The critical stress intensity factor K_{IC} depends only on the material's surface energy γ_s in terms of the Griffith criterion. Due to the shielding effect of plastic deformation on the crack tip stress field, the local stress intensity factor K_I^t at crack tip is always lower than the applied stress intensity factor K_I^a, particularly at higher temperature. The applied stress intensity factor K_{I}^{a} at the moment of failure, e.g. $K_{\mathrm{I}}^{t} = K_{\mathrm{IC}}$ is regarded as the fracture toughness of material. According to modified Griffith theory, $G_c = 2(\gamma_s + \gamma_p)$, if let $\gamma_s + \gamma_p = \gamma_{eff}$, the effective surface energy can be obtained by

$$\gamma_{eff} = \frac{(1-\nu^2)}{2E} K^2 \tag{8}$$

Thus, the applied stress intensity factor K_I^a at cleavage fracture can be calculated, and accordingly the effective surface energy for cleavage extension across the particle-matrix interface of steel in the transition region can also be obtained from equation (8).

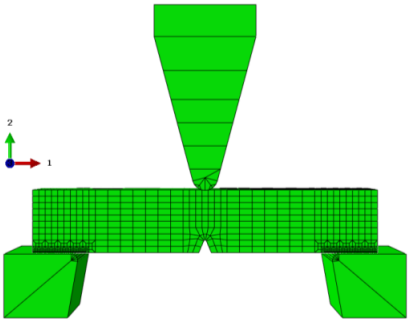

Fig.4 Finite element model of the Charpy test.

4. Numerical simulation

An explicit dynamic process is adopted to model the Charpy test by using an explicit code with CAFE strategy implemented, which has been introduced in Section 2. The geometry of Charpy V-notch specimen is 55mm*10mm*10mm according to the standard ASTM E23 16b [38], the notch radius and notch depth are 0.25mm and 2.0mm respectively. The striker and anvils size and geometry are also those of the standard ASTM E23 16b [38]. The finite element model of Charpy test is shown in Fig.4, in which the full Charpy specimen is meshed with 8 nodes and reduced integration elements (C3D8R). Cells are assembled only to those elements in a small region in the center of specimen with a mesh size

around 1mm, so-called damage zone, where damages in a real Charpy specimen is expected. The striker and two anvils are modelled as elastic body, and are meshed with C3D8R and C3D6 type of elements. The total number of elements in this model is 8250, in which damage zone composes of 700 elements. The contact between the Charpy specimen and striker and anvils is modeled with a friction coefficient 0.15. The initial velocity of striker is 5.5 m/s.

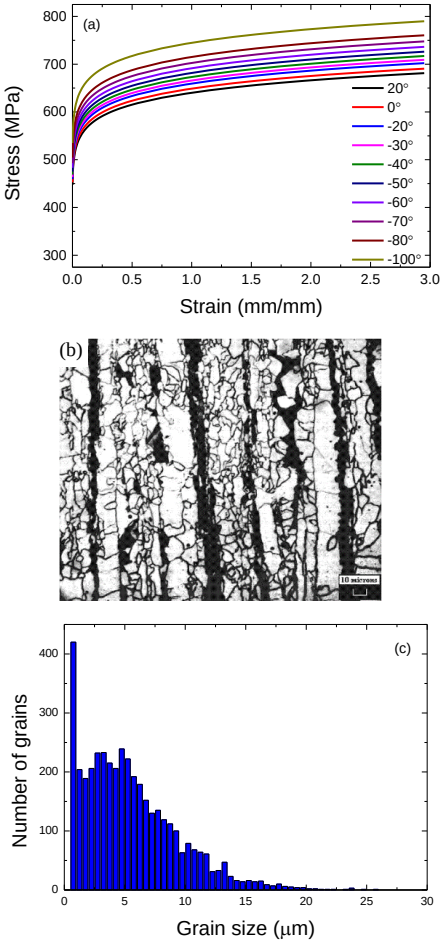

Fig. 5 The properties and microstructure of TMCR steel: (a) flow stress and strain curve at different test temperatures[21], (b) the microstructure of TMCR steel [20] and (c) the histogram of grain size distribution [20].

It is assumed that L_D and L_B are 200μm and 100 μm respectively. Then, in the ductile CA arrays, each cubic array has 5 cells per linear dimension, namely $m_D = 5$. Likewise, in the brittle CA arrays, each cubic has 10 cells per linear dimension, namely $m_B = 10$. Therefore, in each element or integration

point, there are 125 ductile cells and 1000 brittle cells. Accordingly, the damage zone is composed of 87500 ductile cells and 700000 brittle cells. It is assumed that the CA array either ductile or brittle loses the load-bearing capacity when the cells in one orthogonal section of CA array are failed [21]. Therefore, the maximum numbers of the dead cells in each CA array are taken as $N_{D-max} = m_D^2 = 25$ for ductile CA arry and $N_{B-max} = m_B^2 = 100$ for the brittle CA array. The concentration factor for ductile CA, e.g., C_D, is 1.4 and that for brittle CA, e.g., C_B, is 1.4 and 11.0 respectively [20].

The initial void volume fraction f_0 is assumed to be 0.0001. The statistical feature of damage failure value β_F conforms to a normal distribution, in which the mean value β_{F-mean} is 8.0 and the standard deviation β_{F-std} is 1.2. The material constant D and σ_1 are 1.65 and 400MPa respectively. These values of ductile damage variables used in the present work has been calibrated with experimental results of pure ductile fracture, for example the upper shelf energy (USE) of Charpy test. The flow property of the TMCR steel at different temperature is presented in Fig.5 (a). The microstructure of this TMCR steel is presented in the Fig.5 (b), which consists mainly of ferrite and some banded pearlites. Based on the measurement of grain size of this TMCR steel, the histogram of grain size distribution is obtained as shown in the Fig.5 (c), which presents a bimodal distribution. Since these tiny grains will never fracture as they have very high fracture strength, the modelling results are not affected by omitting this small volume of tiny grains. Hence, an equivalent unimodal three-parameter Weibull distribution is applied to characterize the grain size distribution of this material, in which the scale, shape and location parameter are 1.223, 5.392 and 0.516 respectively. The fraction of brittle CA cells that cleavage is nucleated, η, is assumed to be 0.01, which has been adopted by Shterenlikht et al [20] as well. The misorientation threshold θ_{th} is assumed to be 40°. The effective surface energy for the fracture stress of cleavage will be calculated in the section 5.

5. Numerical results and discussion

In the following, we firstly present the predicted results of DBT by using a constant effective surface energy. To reproduce the transition by using the CAFE method, another temperature dependent variable, e.g., the temperature dependent effective surface energy, is calculated via the continuum approach introduced in the Section 3. Although being improved, the DBT predicted with the calculated temperature dependent effective surface energy indicates that the role of grain boundary in the cleavage propagation in the transition region cannot be neglected. As such, the lower limit of effective surface energy for overcoming the barrier of grain boundary in the transition region is estimated based on both the temperature dependent effective surface energy for unstable cleavage formation and the size ratio of cleavage facet (unit) to critical particle. In the end, an accurate prediction of DBT of TMCR steel is

achieved by using the lower limit of effective surface energy for crack propagating across the grain boundary.

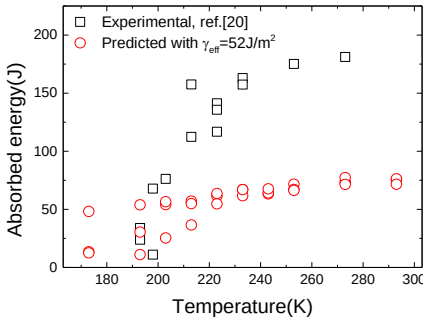

Fig.6 absorbed energy of Charpy impact test in the transition region predicted by CAFE method with a constant effective surface energy, e.g., $\gamma_{eff} = 52\,J/m^2$.

5.1 DBT prediction by using a constant effective surface energy

Firstly, a constant value of the effective surface energy γ_{eff}, $52\,J/m^2$, which has been adopted in the study on the DBT of TMCR steel by Wu et al [23] and Shterenlikht et al [20], is used in the CAFE method to calculate the fracture stress of cleavage according to equation (3). The other parameters to model the DBT of TMCR steel have been introduced in the Section 4. The absorbed energy of standard Charpy tests in the transition region vs. temperature is plotted in the Fig.6, in which the predicted results by CAFE method with constant effective surface energy compare with the experimental results by Shterenlikht et al [20]. At each temperature, three runs have been performed. Since the statistical nature of material has been incorporated in the model, results present a scattered feature as shown in the Fig.6. It can be found that the predicted absorbed energy at higher temperature is not as scattered as that at lower temperature since the fewer cleavage happens at higher temperature. The predicted absorbed energy at lower temperature, e.g., 193K, is comparable to the experimental results. However, the predicted absorbed energy is dramatically underestimated comparing to the experimental results. It implies that only temperature-dependent flow stress of material shown in Fig.5 (a) is not adequate to obtain an ideal DBT behavior, which has been similarly reported by Rossoll et al [16], Tanguy et al [18] and Shterenlikht et al [20]. Thus, the second temperature-dependent parameter has to be searched so as to accurately represent the DBT behavior of materials.

5.2 The effective surface energy of TMCR steel

5.2.1 Identification of the parameters

It is found that the variation of activation energy of DBT among single-crystal iron, poly-crystal iron and Fe-alloys is relatively minor [39, 40], e.g., in the range of 0.2-0.5. This implies that the minor

difference between parameters calibrated from the activation energies of DBT of different steels can be expected. In addition, there are still some resemblances between low carbon steel studied by Tanaka et al [40] and the TMCR steel investigated in the present work, e.g., the ferritic type of microstructure and controlled-rolling process of production. Since the absence of the test results of activation energy of DBT of the TMCR steel, a low carbon steel experimentally obtained by Tanaka et al [40] is utilized to approximately identify the parameters for the calculation of effective surface energy of the TMCR steel. In the aim of exploring a solution to estimate the effective surface energy in transition region, the gap between two materials, e.g., low carbon steel and the TMCR steel can be ignored.

As reported in the literature, a relation between loading rate $\dot{K}$ and Θ_c has been found through experiments [41]

$$ln\dot{K} = -E_a/k_B\Theta_c + const. \tag{9}$$

where E_a is the activation energy for the DBT, which equals to the activation energy Q for dislocation velocity; Θ_c is critical DBT temperature at which ductile fracture changes to be brittle fracture [33, 35, 36]. Based on the theory of shielding effect of dislocation mobility on crack tip, equation (9) has also been used to depict the correlation of loading rate and Θ_c of low carbon steel by Tanaka et al [40]. The critical transition temperatures of low carbon steel have been measured through four point bending tests under different outer-fiber strain rates by Tanaka et al [40]. The outer-fiber strain rate can be calculated by [42]

$$\dot{\varepsilon}_f = \frac{4B}{S_1^2}\dot{\delta} \tag{10}$$

where $\dot{\varepsilon}_f$ is the outer-fiber strain rate and $\dot{\delta}$ is the cross head speed, B is the thickness of specimen and S_1 is the outer span of specimen. The applied stress intensity factor of four point bending test can be calculated by using the equation [43]

$$K_I = \frac{3F(S_1 - S_2)}{2BW^2}\sqrt{a}Y \tag{11}$$

where $Y = \frac{1.1215\sqrt{\pi}}{(1-a/W)^{3/2}}\left[\frac{5}{8} - \frac{5}{12}\frac{a}{W} + \frac{1}{8}\left(\frac{a}{W}\right)^2 + 5\left(\frac{a}{W}\right)^2\left(1 - \frac{a}{W}\right)^6 + \frac{3}{8}\exp\left(-6.1342\frac{a}{W-a}\right)\right]$, F is loading force, S_2 is inner span, W is width of specimen and a is notch depth. To obtain the loading rate of four point bending test, three-dimensional analysis with a quasi-static process is carried out in the present study. The cross head speed applied for modelling is converted from outer-fiber strain rates used by Tanaka et al. [40] in terms of the equation (10). It has to be mentioned that only a stationary crack is studied. The Young's modulus E and poison's ratio ν of steel are 206 GPa and 0.29 respectively. The loading rate, e.g., the rates of stress intensity factor, applied on the four-point bending specimen is calculated by equation (11). The outer-fiber strain rates and calculated loading rate, e.g., the applied rates of stress intensity factor are listed in table 1.

Tab.1 The outer-fiber strain rates of the four point bend tests on fully annealed low carbon steel [43] and the calculated applied rates of stress intensity factor.

$\dot{\varepsilon}(s^{-1})$	$\dot{K}_I^a$(MPam$^{0.5}s^{-1}$)
4.46e-4	2.5790
2.23e-4	12.897
1.12e-2	64.774

The critical DBT temperature under a specific loading rate can be predicted by using the continuum approach introduced in section 3. Different elastic zone size (e.g., particle size) of the model is also studied. To obtain the critical DBT temperatures under the loading rates listed in table 1, for each elastic zone size, several groups of parameters have been tried following the method introduced previously by the authors [33]. By doing this, groups of parameters are optimized for each elastic zone size, which are listed in the table 2. The computed DBT temperatures under different loading rates are compared with experimental results by Tanaka et al [40] in Fig.7. It is shown that the computational results of low carbon steel agree well with experimental results, which indicates that the group of parameters for each elastic zone size is reliable. Meanwhile, the influence of the elastic zone size on the fracture toughness in the transition region is also studied under the loading rate *10 MPam$^{0.5}$s^{-1}*. The applied stress intensity factor K_I^a normalized with the critical stress intensity factor K_{IC} vs. temperature are plotted in the Fig.8 for each elastic zone size. Here, $K_{IC} = 1.77MPam^{0.5}$ is calculated from the widely used effective surface energy for cleavage of steel, e.g., $7\,J/m^2$, tested by Bowen et al [44] according to Griffith theory. It is shown in Fig.8 that to achieve an identical DBT temperature Θ_c the minor difference among the fracture toughness for different elastic zone sizes is presented in the whole temperature range by using the parameters identified above. Recall the equation (5)-(7), at a specific temperature and under same stress level, when activation energy Q is determined, with the combination of parameter of $\dot{\varepsilon}_0$ and m, the similar amount of shielding effect of dislocation dynamics and DBT behavior can be always achieved no matter how large the elastic zone size (particle size) is. To this end, it can be concluded that the predicted DBT of low carbon steel by using the continuum model is elastic zone size independent. In the later simulation, the parameters verified for elastic zone size 1 μm will be adopted.

Tab.2 Parameters for different elastic zone size.

c/2(μm)	$\dot{\varepsilon}_0(s^{-1})$	$Q(ev)$	m	σ_0
0.25	29934.39	0.236	1.45	1.0
0.50	11307.01	0.236	1.70	1.0
1.0	3898.48	0.236	2.00	1.0
2.0	1717.67	0.236	2.30	1.0

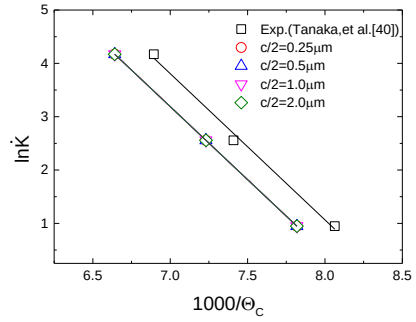

Fig.7 comparison of computed and experimental critical DBT temperature of low-carbon steel.

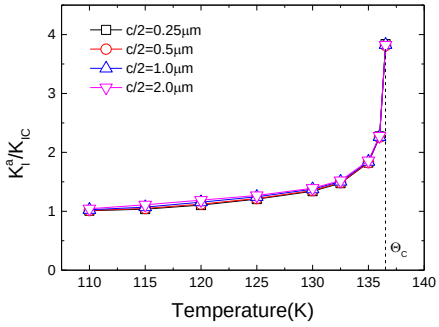

Fig.8 the DBT curve of steel predicted by the continuum model with different elastic zone size. The loading rate is 10 MPam$^{0.5}$s^{-1}.

5.2.2 The temperature dependent effective surface energy

As mentioned above, the shielding effect of dislocation mobility on crack tip is loading rate dependent. To obtain the loading rate of Charpy impact test, the three-dimensional analysis of Charpy test is conducted. The geometry of Charpy V-notch specimen is identical to that introduced in the section 4. To model the transient process of impact and obtain the J-integral from Abaqus, a dynamic implicit process is utilized. However, only a stationary crack is studied here. The V-notch Charpy impact specimen is actually replaced by U-notch specimen in the calculation of J-integral since that the identical J-integrals calculated by Abaqus have been obtained from both notch-type specimen with same radius in present study. A path-independence pattern is presented in the Fig.9 (a) in a relative far field (beyond the 5 contours) near notch root. A notch radius independence of J-integrals is presented in Fig.9 (b). The loading rate $\dot{K}$ of Charpy impact test, 4.0386×10^4MPam$^{0.5}$s^{-1}, is achieved by fitting the linear part of the curve of J-integral vs. time as shown in Fig.9 (c).

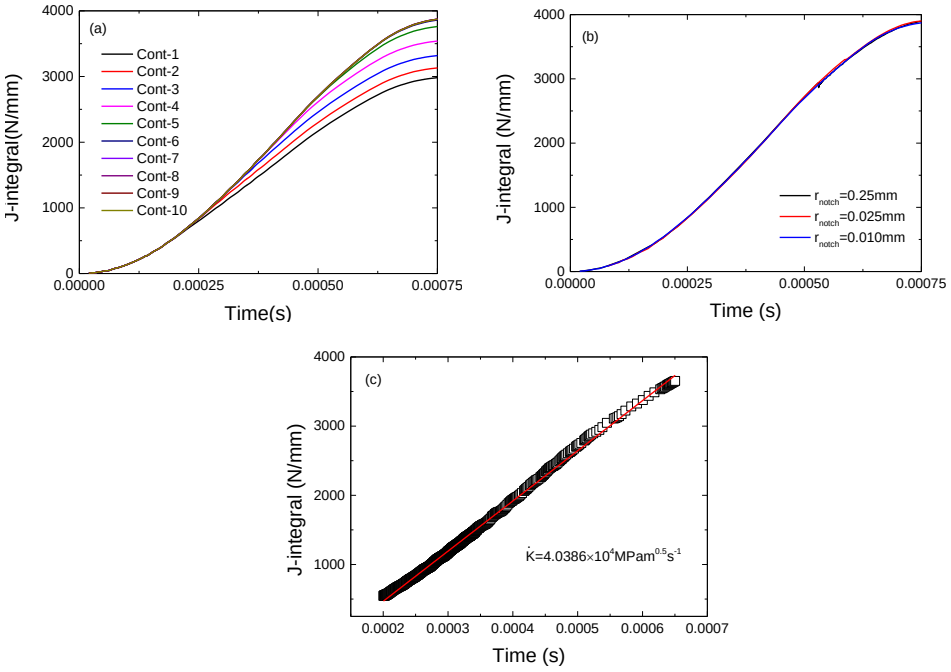

Fig.9 Charpy impact test modelling results: (a) path-independence of J-integral of U-notch specimen with notch radius 0.25mm, (b) J-integral of Charpy impact tests with different notch radius, (c) the loading rate of Charpy impact test. Here, r_{notch} is the notch radius of Charpy specimen.

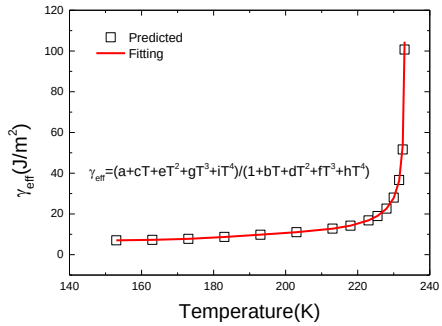

Fig.10 the calculated effective surface energy in the transition region by using continuum model, where a, b, c, d, e, f, g, h, i are constant.

By applying continuum approach shown in Section 3, the fracture toughness of the TMCR steel in the DBT region is calculated with parameters identified in section 5.2.1 and the loading rate of Charpy impact test calculated above. According to equation (8), the effective surface energy of TMCR steel in the transition region is calculated as shown in Fig.10. It can be found that the effective surface energy of steel in the lower temperature, e.g. below 200K, is very stable and comparatively low. However, it

increase rapidly until the critical DBT temperature when temperature beyond 220K. In addition, an equation for describing the correlation between the effective surface energy and temperature is obtained by fitting the calculated effective surface energy at different temperature, see Fig.10. This equation for temperature dependent effective surface energy will be adopted in the later simulation of DBT of TMCR steel.

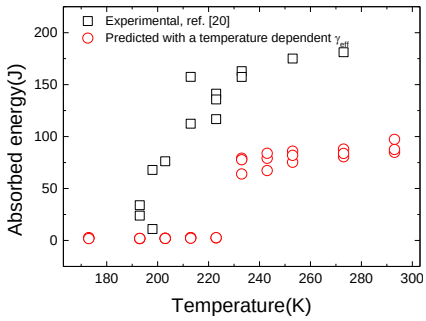

Fig.11 absorbed energy of Charpy impact test in the transition region predicted by CAFE method with a temperature-dependent effective surface energy.

5.3 DBT of TMCR steel modeled with an effective surface energy

A temperature-dependent effective surface energy law obtained in Section 5.2 (see Fig.10) is applied to the CAFE method to simulate the DBT of TMCR steel. Here, the procedure and parameters used for the modelling are identical to those utilized in the Section 5.1 except that a constant value of the effective surface energy is replaced by the temperature-dependent effective surface energy. The predicted absorbed Charpy energy vs. temperature is plotted in the Fig.11, in which the experimental results are also presented for comparison. It can be observed that the DBT transition happens in a very narrow temperature range and a dramatic steep transition are obtained comparing with the experimental results. In addition, both lower shelf and upper shelf of DBT are obviously underestimated.

In the process of the unstable cleavage propagation of steel, the second step is critical in terms of the formation of unstable fracture [45], otherwise the crack stops or be blunted at the interface, and then the cracked particle may act as the nuclei for void growth when ductile fracture intervenes. The critical fracture stress for the crack propagation across the interface between the particle and matrix, e.g., particle cleavage strength σ_{pm} [46] , can be calculated by

$$\sigma_{pm} = \left(\frac{\pi E \gamma_{pm}}{(1-\nu^2)c}\right)^{1/2} \tag{12}$$

where γ_{pm} is the effective surface energy to propagate the micro-crack across particle-matrix interface; c is the particle size. Once unstable fracture formatted, e.g., micro-crack initiation from the particle and penetration into the matrix, the first grain boundary could be the barrier for unstable cleavage crack to

trespass, see Fig.3 (a).The critical fractures stress, e.g. grain strength σ_{mm} [46], becomes a criterion for the extension of the crack across the grain boundary, which can be described as

$$\sigma_{mm} = \left(\frac{\pi E \gamma_{mm}}{(1-\nu^2)d}\right)^{1/2} \tag{13}$$

where γ_{mm} is the effective surface energy for crack propagation across the grain boundary; d is grain size. Comparing with the equation (14), it indicates that

$$\frac{\sigma_{mm}}{\sigma_{pm}} = \frac{\gamma_{mm}}{\gamma_{pm}}\frac{c}{d} \tag{14}$$

When the local stress near the particle $\sigma_L = \sigma_{mm} < \sigma_{pm}$, the micro-crack could propagate across the grain boundary, and unstable cleavage fracture would be ensured by the particle cracking. It implies that the unstable fracture is dominated by the particle size, e.g., cleavage at the lower shelf, where the local stress near the particle is high enough due to the higher yield stress. However, when $\sigma_L = \sigma_{mm} > \sigma_{pm}$, the crack arrests at the grain boundary, resulting in the appearance of stable and grain-sized micro-crack. It means that the propagation of unstable fracture is dominated by the grain size, e.g., cleavage occurring in the transition region, where the local stress near the particle is not adequate to overcome the grain strength. Therefore, it can be concluded that the role of grain boundary on the unstable cleavage propagation should not be neglected, and that the cleavage propagation in the transition region depends on the competition between σ_{mm} and σ_{pm}, e.g., particle dominated or grain size dominated [46-50].

A critical condition for crack propagating across the first grain boundary can be deduced from the equation (14) when σ_{mm} equals to σ_{pm}, from which the lower limit of the effective surface energy for crack extension across the grain boundary can be achieved

$$\gamma_{mm} = \gamma_{pm}\frac{d}{c} \tag{15}$$

It implies that the minimum of γ_{mm} is solely related the size ratio of grain and particle when the effective surface energy of cleavage formation of the material, e.g., γ_{pm}, has been obtained. As such, the γ_{pm} can be transferred to γ_{mm}, by using equation (15). Recall the equation (3), the γ_{mm} is exactly required to calculate the fracture stress of cleavage in CAFE method. While, the effective surface energy obtained in the section 5.2, it is actually not the γ_{mm} but the γ_{pm}, which is the reason why the absorbed energies in the full temperature range is underestimated as shown in the Fig.11.

Based on the γ_{pm} obtained in Section 5.2, DBT of the TMCR steel is predicted with the variable ratio of d/c as shown in the Fig.12. It can be observed that different ratio of d/c can achieve a similar upper shelf, while the lower shelf and the absorbed energy in transition region are quite different. Since complete ductile fracture happens on the upper shelf, the ratio of d/c presents no effect on the absorbed

energy, which is usually only relevant to the cleavage fracture. It is also found that the larger ratio of d/c enables a higher absorbed energy of steel in the temperature range below the upper shelf. Meanwhile, a lower transition temperature, Θ_T, is achieved for the larger ratio of d/c. San Martin et al. [47] has studied the cleavage fracture in the transition region of Ti-V alloyed steel, in which some isolated cleavage islands could be formed surrounded by ductile fracture. They have measured the sizes of cleavage islands, e.g., d_{CL} and the sizes of cleavage initiators, e.g. $c_{crit.}$. The effective surface energy γ_{mm} has been calculated by using a similar transferring rule (e.g., equation (15)), in which the effective surface energy $\gamma_{pm} = 7\ J/m^2$ has been adopted. It has been found that the γ_{mm} lineally increases with the ratio of $d_{CL}/c_{crit.}$ measured at all temperatures in DBT regime. This proves that the ratio d/c in equation (15) can physically reflect the toughness of material as shown in Fig.12.

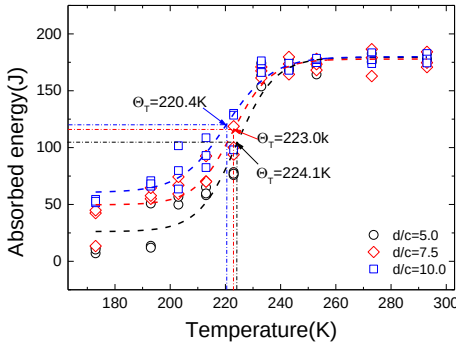

Fig.12 the predicted DBT of TMCR steel with different ratios of d/c. Here, data is fitted by the sigmoidal method. The transition temperature Θ_T is defined as the temperature corresponding to the impact energy halfway between the lower shelf energy (LSE) and USE [49].

It is well known that the particle precipitated in the steel is non-uniformly distributed for both size and spacing. Ahead of the crack/notch tip, the particle is sampled as the cleavage nucleate once the maximum principle stress ahead of the crack/notch tip is higher than σ_{pm}, see equation (12). However, the stress ahead of the crack/notch tip generally decreases with the temperature, which means that accordingly the size of qualified particle to be sampled as the initiator of cleavage decreases with the decrease of temperature. A linear relation between temperature and critical particle size has been found in SA 508 steel by Lee et al [51]. Since the grain size is temperature independent, it implies that the ratio of d/c is not a constant value in the transition regime but a variable relevant to the temperature. In addition, the crystallographic unit of cleavage could not be the grain size, since crack deflection or arrest usually does not happens at the lower grain boundary. Whilst, it has been pointed out that the cleavage fracture unit (facet) size or the effective grain size is more suitable to describe the cleavage fracture unit, and that both of them match each other very well in Mn-Mo-Ni low alloy steel [52]. To

accurately describe the competition between σ_{pm} and σ_{mm} of cleavage fracture in the transition region, the grain size *d* in equation (15) should be modified to the cleavage facet (unit) size $d_{CF(U)S}$ or effective grain size d_{EGS}. According to the findings by Lee et al [51], a linear relation between the ratio of $d_{CF(U)S}/c_{crit.}$ or $d_{EGS}/c_{crit.}$ and temperature could be expected since that the $d_{CF(U)S}$ is generally temperature independent. To this end, a linear correlation between $d_{CF(U)S}/c_{crit.}$ and temperature is assumed

$$\frac{d_{CF(U)S}}{c_{crit.}} = -0.025(\Theta - 273) + 4.0 \tag{16}$$

where Θ is temperature. Then, the effective surface energy obtained in section 5.2 as shown in Fig.10 is corrected by the ratio of $d_{CF(U)S}/c_{crit.}$ in equation (16) according to the equation (15), from which the γ_{mm} can be obtained. Then, the calculated γ_{mm} is implemented in CAFE method to predict the DBT of TMCR steel. The predicted absorbed energy vs. temperature is plotted in the Fig.13, in which the experimental results of TMCR steel is also presented for comparison. It is observed that simulation is able to produce a full transition curve with a scatter pattern of absorbed energies in the transition region. Generally, the predicted transition curve is comparative to the experimental results. The simulation can reproduce a similar LSE and USE comparing with the experimental results, while the absorbed energy in transition region is slightly underestimated comparing with the experimental results.

It is not surprising for the underestimation of the absorbed energy in the transition region as shown in Fig.13 because that the γ_{mm} estimated from equation (15) is just its lower limit. Actually, it is very difficult to precisely measure or predict the effective surface energy for crack propagating across the grain boundary [47, 50]. In the section 5.2, a constant exponent *m* that describes the correlation between dislocation velocity and resolved shear stress is used to estimate the effective surface energy of unstable cleavage formation (e.g., the second step) in the transition region, see equation (6) and (7). However, it has been found that *m* decreases with the increase of temperature [53, 54], which means that the fracture toughness in transition region could be underestimated since the lower *m* can lead to a higher toughness [35] in the transition region. Accordingly, the γ_{pm} for cleavage penetration into matrix could be under-predicted as well. This could be a reason why the predicted absorbed energies in the transition region are lower than those of experimental results as shown in Fig.13. Since the lacking of the experimental correlation between the ratio of $d_{CF(U)S}/c_{crit.}$ and temperature for this TMCR steel, an artificial linear relation between them is assumed to transfer the γ_{pm} to γ_{mm}, which is inspired by the study in ref. [51]. Therefore, measurements on the critical particle size and the cleavage facet (unit) size of steel have to be conducted so as to find a more reliable temperature dependent ratio of $d_{CF(U)S}/c_{crit.}$.

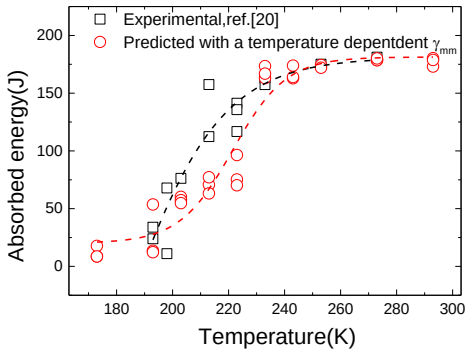

Fig.13 absorbed energy of Charpy impact test in the transition region predicted by CAFE method with a temperature-dependent effective surface energy corrected by a temperature dependent ratio of $d_{CF(U)S}/c_{crit.}$*. Here, data is fitted by the sigmoidal method.*

6. Conclusions

In this study the CAFE method developed by Shterenlikht et al [20-22] has been applied to mitigate some of the computational challenges in modelling of DBT and incorporate the statistical nature of microstructure at the same time. In order to realistically capture the temperature dependent fracture toughness in the transition region, a physical based variable has to be searched, which is also one of the motivations of this work. On the basis of our previous work [33] a continuum approach has been developed to estimate the effective surface energy for unstable cleavage formation, e.g., γ_{pm}. Further, to describe the essence of the competition between particle size and grain size controlled propagation of unstable cleavage, a more robust variable, effective surface energy for overcoming the barrier of grain boundary, e.g., γ_{mm}, was proposed. Finally, a framework for the modelling of DBT is explored through implementing the γ_{mm} into the CAFE method. Some important findings obtained in present work can be summarized as followings:

- It is proved that a second temperature dependent variable has to be found to reproduce the DBT curve, in addition to the temperature dependent flow properties. In present work, a continuum approach has been developed to establish the second temperature dependent variable, e.g., γ_{pm}.
- It is observed that the role of grain boundary on the unstable cleavage propagation cannot be ignored. Through analyzing the competition between the particle size and grain size dominated unstable cleavage propagation, a method to quantify the lower limit of γ_{mm} has been built.

- Due to the fact that cleavage facet (unit) size or effective grain size, e.g., $d_{CF(U)S}$, rather than the grain size is more appropriate for characterizing the cleavage fracture unit, the ratio of grain size to critical particle size has been replaced by $d_{CF(U)S}/c_{crit.}$ in the estimation of γ_{mm}.
- It is found that numerical simulation by using the CAFE method implemented with γ_{mm} is able to produce a full transition curve, especially with scattered absorbed energies in the transition region represented.

Although a framework of modelling DBT of steel is explored in this work, it still has some limitations. More experimental results are required for the calibration of parameters to calculate the temperature effective surface energy adopted in present work, for instance, the activation energy for the DBT and the temperature dependent ratio of $d_{CF(U)S}/c_{crit.}$ of the TMCR steel. In addition, the adiabatic heating effect and viscoplastic of material is not considered in Charpy impact modelling.

Acknowledgements

The authors wish to thank the Research Council of Norway for funding through the Petromaks 2 Programme, Contract No.228513/E30. The financial support from Eni, Statoil, Lundin, Total, JFE Steel Corporation, Posco, Kobe Steel, SSAB, Bredero Shaw, Borealis, Trelleborg, Nexans, Aker Solutions, FMC Kongsberg Subsea, Kværner Verdal, Marine Aluminium, Hydro and Sapa are also acknowledged.

References

[1] A.L. Gurson, Continuum Theory of Ductile Rupture by Void Nucleation and Growth: Part I—Yield Criteria and Flow Rules for Porous Ductile Media, Journal of Engineering Materials and Technology 99(1) (1977) 2-15.
[2] V. Tvergaard, A. Needleman, Analysis of the cup-cone fracture in a round tensile bar, Acta Metallurgica 32(1) (1984) 157-169.
[3] Z.L. Zhang, C. Thaulow, J. Ødegård, A complete Gurson model approach for ductile fracture, Engineering Fracture Mechanics 67(2) (2000) 155-168.
[4] T. Pardoen, J.W. Hutchinson, An extended model for void growth and coalescence, Journal of the Mechanics and Physics of Solids 48(12) (2000) 2467-2512.
[5] G. Rousselier, Ductile fracture models and their potential in local approach of fracture, Nuclear Engineering and Design 105(1) (1987) 97-111.
[6] A. Pineau, A.A. Benzerga, T. Pardoen, Failure of metals I: Brittle and ductile fracture, Acta Materialia 107 (2016) 424-483.
[7] R.O. Ritchie, J.F. Knott, J.R. Rice, On the relationship between critical tensile stress and fracture toughness in mild steel, Journal of the Mechanics and Physics of Solids 21(6) (1973) 395-410.
[8] F.M. Beremin, A. Pineau, F. Mudry, J.-C. Devaux, Y. D'Escatha, P. Ledermann, A local criterion for cleavage fracture of a nuclear pressure vessel steel, Metallurgical Transactions A 14(11) (1983) 2277-2287.

[9] T. Lin, A.G. Evans, R.O. Ritchie, A statistical model of brittle fracture by transgranular cleavage, Journal of the Mechanics and Physics of Solids 34(5) (1986) 477-497.
[10] K. Wallin, T. Saario, K. Törrönen, Statistical model for carbide induced brittle fracture in steel, Metal Science 18(1) (1984) 13-16.
[11] M.K. Samal, M. Seidenfuss, E. Roos, B.K. Dutta, H.S. Kushwaha, Experimental and numerical investigation of ductile-to-brittle transition in a pressure vessel steel, Materials Science and Engineering: A 496(1) (2008) 25-35.
[12] M.K. Samal, J.K. Chakravartty, M. Seidenfuss, E. Roos, Evaluation of fracture toughness and its scatter in the DBTT region of different types of pressure vessel steels, Engineering Failure Analysis 18(1) (2011) 172-185.
[13] V. Tvergaard, A. Needleman, An analysis of the temperature and rate dependence of Charpy V-notch energies for a high nitrogen steel, International Journal of Fracture 37(3) (1988) 197-215.
[14] V. Tvergaard, A. Needleman, An analysis of the brittle-ductile transition in dynamic crack growth, International Journal of Fracture 59(1) (1993) 53-67.
[15] A. Needleman, V. Tvergaard, Numerical modeling of the ductile-brittle transition, International Journal of Fracture 101(1) (2000) 73.
[16] A. Rossoll, C. Berdin, C. Prioul, Determination of the Fracture Toughness of a Low Alloy Steel by the Instrumented Charpy Impact Test, International Journal of Fracture 115(3) (2002) 205-226.
[17] B. Tanguy, J. Besson, R. Piques, A. Pineau, Ductile to brittle transition of an A508 steel characterized by Charpy impact test: Part I: experimental results, Engineering Fracture Mechanics 72(1) (2005) 49-72.
[18] B. Tanguy, J. Besson, R. Piques, A. Pineau, Ductile to brittle transition of an A508 steel characterized by Charpy impact test: Part II: modeling of the Charpy transition curve, Engineering Fracture Mechanics 72(3) (2005) 413-434.
[19] G. Hütter, T. Linse, S. Roth, U. Mühlich, M. Kuna, A modeling approach for the complete ductile–brittle transition region: cohesive zone in combination with a non-local Gurson-model, International Journal of Fracture 185(1) (2014) 129-153.
[20] A. Shterenlikht, I.C. Howard, The CAFE model of fracture—application to a TMCR steel, Fatigue & Fracture of Engineering Materials & Structures 29(9-10) (2006) 770-787.
[21] A. Shterenlikht, 3D CAFE modelling of transitional ductile-brittle fracture in steel, The University of Sheffield, UK, 2003.
[22] A. Shterenlikht, I.C. Howard, Cellular Automata Finite Element (CAFE) modelling of transitional ductile-brittle fracture in steel, The 15th European Conference of Fracture (ECF15), KTH, Stockholm, Sweden, 2004.
[23] S.J. Wu, C.L. Davis, A. Shterenlikht, I.C. Howard, Modeling the ductile-brittle transition behavior in thermomechanically controlled rolled steels, Metall and Mat Trans A 36(4) (2005) 989-997.
[24] S. Das, A. Shterenlikht, I.C. Howard, E.J. Palmiere, A general method for coupling microstructural response with structural performance, Proceedings of the Royal Society A: Mathematical, Physical and Engineering Science 462(2071) (2006) 2085-2096.
[25] A. Shterenlikht, L. Margetts, Three-dimensional cellular automata modelling of cleavage propagation across crystal boundaries in polycrystalline microstructures, Proceedings of the Royal Society of London A: Mathematical, Physical and Engineering Sciences 471(2177) (2015).
[26] Standard Test Method for Determination of Reference Temperature, T0, for Ferritic Steels in the Transition Range (ASTM E1921-18), American Society for Testing and Materials, 2018.
[27] J.P. Petti, R.H. Dodds, Calibration of the Weibull stress scale parameter, σu, using the Master Curve, Engineering Fracture Mechanics 72(1) (2005) 91-120.
[28] B. Wasiluk, J.P. Petti, R.H. Dodds, Temperature dependence of Weibull stress parameters: Studies using the Euro-material, Engineering Fracture Mechanics 73(8) (2006) 1046-1069.
[29] Y. Cao, H. Hui, G. Wang, F.-Z. Xuan, Inferring the temperature dependence of Beremin cleavage model parameters from the Master Curve, Nuclear Engineering and Design 241(1) (2011) 39-45.
[30] G. Qian, V.F. González-Albuixech, M. Niffenegger, Calibration of Beremin model with the Master Curve, Engineering Fracture Mechanics 136 (2015) 15-25.
[31] X. Gao, G. Zhang, T.S. Srivatsan, A probabilistic model for prediction of cleavage fracture in the ductile-to-brittle transition region and the effect of temperature on model parameters, Materials Science and Engineering: A 415(1) (2006) 264-272.

[32] M. Moattari, I. Sattari-Far, I. Persechino, N. Bonora, Prediction of fracture toughness in ductile-to-brittle transition region using combined CDM and Beremin models, Materials Science and Engineering: A 657 (2016) 161-172.
[33] Y. Li, X. Ren, J. He, Z. Zhang, Constraint effect on the brittle-to-ductile transition of single-crystal iron induced by dislocation mobility, International Journal of Mechanical Sciences 149 (2018) 212-223.
[34] M. Stec, J. Faleskog, Micromechanical modeling of grain boundary resistance to cleavage crack propagation in ferritic steels, International Journal of Fracture 160(2) (2009) 151.
[35] V.R. Nitzsche, K.J. Hsia, Modelling of dislocation mobility controlled brittle-to-ductile transition, Materials Science and Engineering: A 176(1) (1994) 155-164.
[36] A. Hartmaier, P. Gumbsch, Thermal activation of crack-tip plasticity: The brittle or ductile response of a stationary crack loaded to failure, Physical Review B 71(2) (2005) 024108.
[37] A.S. Argon, Mechanics and Physics of Brittle to Ductile Transitions in Fracture, Journal of Engineering Materials and Technology 123(1) (2000) 1-11.
[38] ASTM E23-18 Standard Test Methods for Notched Bar Impact Testing of Metallic Materials, 2018.
[39] A. Giannattasio, M. Tanaka, T.D. Joseph, S.G. Roberts, An empirical correlation between temperature and activation energy for brittle-to-ductile transitions in single-phase materials, Physica Scripta 2007(T128) (2007) 87.
[40] M. Tanaka, K. Higashida, T. Shimokawa, T. Morikawa, Brittle-Ductile Transition in Low Carbon Steel Deformed by the Accumulative Roll Bonding Process, MATERIALS TRANSACTIONS 50(1) (2009) 56-63.
[41] P.B. Hirsch, S.G. Roberts, The brittle-ductile transition in silicon, Philosophical Magazine A 64(1) (1991) 55-80.
[42] G.W. Hollenberg, G.R. Terwilliger, R.S. Gordon, Calculation of Stresses and Strains in Four-Point Bending Creep Tests, Journal of the American Ceramic Society 54(4) (1971) 196-199.
[43] T. Fett, Stress Intensity Factors – T-Stresses – Weight Functions, Supplement Volume, KIT Scientific Publishing, 2009.
[44] P. Bowen, S.G. Druce, J.F. Knott, Effects of microstructure on cleavage fracture in pressure vessel steel, Acta Metallurgica 34(6) (1986) 1121-1131.
[45] M. Kroon, J. Faleskog, Micromechanics of cleavage fracture initiation in ferritic steels by carbide cracking, Journal of the Mechanics and Physics of Solids 53(1) (2005) 171-196.
[46] T. Lin, A.G. Evans, R.O. Ritchie, Stochastic modeling of the independent roles of particle size and grain size in transgranular cleavage fracture, Metall and Mat Trans A 18(4) (1987) 641-651.
[47] J.I. San Martin, J.M. Rodriguez-Ibabe, Determination of energetic parameters controlling cleavage fracture in a Ti-V microalloyed ferrite-pearlite steel, Scripta Materialia 40(4) (1999) 459-464.
[48] L. Rancel, M. Gómez, S.F. Medina, I. Gutierrez, Measurement of bainite packet size and its influence on cleavage fracture in a medium carbon bainitic steel, Materials Science and Engineering: A 530 (2011) 21-27.
[49] A. Ghosh, A. Ray, D. Chakrabarti, C.L. Davis, Cleavage initiation in steel: Competition between large grains and large particles, Materials Science and Engineering: A 561 (2013) 126-135.
[50] M.A. Linaza, J.M. Rodriguez-Ibabe, J.J. Urcola, DETERMINATION OF THE ENERGETIC PARAMETERS CONTROLLING CLEAVAGE FRACTURE INITIATION IN STEELS, Fatigue & Fracture of Engineering Materials & Structures 20(5) (1997) 619-632.
[51] S. Lee, S. Kim, B. Hwang, B.S. Lee, C.G. Lee, Effect of carbide distribution on the fracture toughness in the transition temperature region of an SA 508 steel, Acta Materialia 50(19) (2002) 4755-4762.
[52] S. Kim, S. Lee, B.S. Lee, Effects of grain size on fracture toughness in transition temperature region of Mn–Mo–Ni low-alloy steels, Materials Science and Engineering: A 359(1) (2003) 198-209.
[53] H.W. Schadler, Mobility of edge dislocations on {110} planes in tungsten single crystals, Acta Metallurgica 12(8) (1964) 861-870.
[54] H.A. Khater, D.J. Bacon, Dislocation core structure and dynamics in two atomic models of α-zirconium, Acta Materialia 58(8) (2010) 2978-2987.

Paper III

A.3 Paper 3

The Effect of Thermal Residual Stresses on Ductile-to-Brittle Transition of a Bi-material Specimen by Using CAFE Method

Authors: Yang Li, Xiaobo Ren, Jianying He, Zhiliang Zhang

Submitted to European Journal of Mechanics – A/Solids.

Appendix B

List of previous PhD Theses at Department of Structural Engineering

Appendix

DEPARTMENT OF STRUCTURAL ENGINEERING
NORWEGIAN UNIVERSITY OF SCIENCE AND TECHNOLOGY

N–7491 TRONDHEIM, NORWAY
Telephone: +47 73 59 47 00

"Reliability Analysis of Structural Systems using Nonlinear Finite Element Methods",
C. A. Holm, 1990:23, ISBN 82-7119-178-0.

"Uniform Stratified Flow Interaction with a Submerged Horizontal Cylinder",
Ø. Arntsen, 1990:32, ISBN 82-7119-188-8.

"Large Displacement Analysis of Flexible and Rigid Systems Considering
Displacement-Dependent Loads and Nonlinear Constraints",
K. M. Mathisen, 1990:33, ISBN 82-7119-189-6.

"Solid Mechanics and Material Models including Large Deformations",
E. Levold, 1990:56, ISBN 82-7119-214-0, ISSN 0802-3271.

"Inelastic Deformation Capacity of Flexurally-Loaded Aluminium Alloy Structures",
T. Welo, 1990:62, ISBN 82-7119-220-5, ISSN 0802-3271.

"Visualization of Results from Mechanical Engineering Analysis",
K. Aamnes, 1990:63, ISBN 82-7119-221-3, ISSN 0802-3271.

"Object-Oriented Product Modeling for Structural Design",
S. I. Dale, 1991:6, ISBN 82-7119-258-2, ISSN 0802-3271.

"Parallel Techniques for Solving Finite Element Problems on Transputer Networks",
T. H. Hansen, 1991:19, ISBN 82-7119-273-6, ISSN 0802-3271.

"Statistical Description and Estimation of Ocean Drift Ice Environments",
R. Korsnes, 1991:24, ISBN 82-7119-278-7, ISSN 0802-3271.

“Properties of concrete related to fatigue damage: with emphasis on high strength concrete”,
G. Petkovic, 1991:35, ISBN 82-7119-290-6, ISSN 0802-3271.

"Turbidity Current Modelling",
B. Brørs, 1991:38, ISBN 82-7119-293-0, ISSN 0802-3271.

"Zero-Slump Concrete: Rheology, Degree of Compaction and Strength. Effects of Fillers as Part Cement-Replacement",
C. Sørensen, 1992:8, ISBN 82-7119-357-0, ISSN 0802-3271.

"Nonlinear Analysis of Reinforced Concrete Structures Exposed to Transient Loading",
K. V. Høiseth, 1992:15, ISBN 82-7119-364-3, ISSN 0802-3271.

"Finite Element Formulations and Solution Algorithms for Buckling and Collapse Analysis of Thin Shells",
R. O. Bjærum, 1992:30, ISBN 82-7119-380-5, ISSN 0802-3271.

"Response Statistics of Nonlinear Dynamic Systems",
J. M. Johnsen, 1992:42, ISBN 82-7119-393-7, ISSN 0802-3271.

"Digital Models in Engineering. A Study on why and how engineers build and operate digital models for decisison support",
J. Høyte, 1992:75, ISBN 82-7119-429-1, ISSN 0802-3271.

"Sparse Solution of Finite Element Equations",
A. C. Damhaug, 1992:76, ISBN 82-7119-430-5, ISSN 0802-3271.

"Some Aspects of Floating Ice Related to Sea Surface Operations in the Barents Sea",
S. Løset, 1992:95, ISBN 82-7119-452-6, ISSN 0802-3271.

"Modelling of Cyclic Plasticity with Application to Steel and Aluminium Structures",
O. S. Hopperstad, 1993:7, ISBN 82-7119-461-5, ISSN 0802-3271.

"The Free Formulation: Linear Theory and Extensions with Applications to Tetrahedral Elements
with Rotational Freedoms",
G. Skeie, 1993:17, ISBN 82-7119-472-0, ISSN 0802-3271.

"Høyfast betongs motstand mot piggdekkslitasje. Analyse av resultater fra prøving i Veisliter'n",
T. Tveter, 1993:62, ISBN 82-7119-522-0, ISSN 0802-3271.

"A Nonlinear Finite Element Based on Free Formulation Theory for Analysis of Sandwich Structures",
O. Aamlid, 1993:72, ISBN 82-7119-534-4, ISSN 0802-3271.

"The Effect of Curing Temperature and Silica Fume on Chloride Migration and Pore Structure of High Strength Concrete",
C. J. Hauck, 1993:90, ISBN 82-7119-553-0, ISSN 0802-3271.

"Failure of Concrete under Compressive Strain Gradients",
G. Markeset, 1993:110, ISBN 82-7119-575-1, ISSN 0802-3271.

"An experimental study of internal tidal amphidromes in Vestfjorden",
J. H. Nilsen, 1994:39, ISBN 82-7119-640-5, ISSN 0802-3271.

"Structural analysis of oil wells with emphasis on conductor design",
H. Larsen, 1994:46, ISBN 82-7119-648-0, ISSN 0802-3271.

"Adaptive methods for non-linear finite element analysis of shell structures",
K. M. Okstad, 1994:66, ISBN 82-7119-670-7, ISSN 0802-3271.

"On constitutive modelling in nonlinear analysis of concrete structures",
O. Fyrileiv, 1994:115, ISBN 82-7119-725-8, ISSN 0802-3271.

"Fluctuating wind load and response of a line-like engineering structure with emphasis on motion-induced wind forces",
J. Bogunovic Jakobsen, 1995:62, ISBN 82-7119-809-2, ISSN 0802-3271.

"An experimental study of beam-columns subjected to combined torsion, bending and axial actions",
A. Aalberg, 1995:66, ISBN 82-7119-813-0, ISSN 0802-3271.

"Scaling and cracking in unsealed freeze/thaw testing of Portland cement and silica fume concretes",
S. Jacobsen, 1995:101, ISBN 82-7119-851-3, ISSN 0802-3271.

"Damping of water waves by submerged vegetation. A case study of laminaria hyperborea",
A. M. Dubi, 1995:108, ISBN 82-7119-859-9, ISSN 0802-3271.

"The dynamics of a slope current in the Barents Sea",
Sheng Li, 1995:109, ISBN 82-7119-860-2, ISSN 0802-3271.

"Modellering av delmaterialenes betydning for betongens konsistens",
Ernst Mørtsell, 1996:12, ISBN 82-7119-894-7, ISSN 0802-3271.

"Bending of thin-walled aluminium extrusions",
Birgit Søvik Opheim, 1996:60, ISBN 82-7119-947-1, ISSN 0802-3271.

"Material modelling of aluminium for crashworthiness analysis",
Torodd Berstad, 1996:89, ISBN 82-7119-980-3, ISSN 0802-3271.

"Estimation of structural parameters from response measurements on submerged floating tunnels",
Rolf Magne Larssen, 1996:119, ISBN 82-471-0014-2, ISSN 0802-3271.

“Numerical modelling of plain and reinforced concrete by damage mechanics”,
Mario A. Polanco-Loria, 1997:20, ISBN 82-471-0049-5, ISSN 0802-3271.

“Nonlinear random vibrations - numerical analysis by path integration methods”,
Vibeke Moe, 1997:26, ISBN 82-471-0056-8, ISSN 0802-3271.

"Numerical prediction of vortex-induced vibration by the finite element method",
Joar Martin Dalheim, 1997:63, ISBN 82-471-0096-7, ISSN 0802-3271.

"Time domain calculations of buffeting response for wind sensitive structures",
Ketil Aas-Jakobsen, 1997:148, ISBN 82-471-0189-0, ISSN 0802-3271.

"A numerical study of flow about fixed and flexibly mounted circular cylinders",
Trond Stokka Meling, 1998:48, ISBN 82-471-0244-7, ISSN 0802-3271.

"Estimation of chloride penetration into concrete bridges in coastal areas",
Per Egil Steen, 1998:89, ISBN 82-471-0290-0, ISSN 0802-3271.

"Stress-resultant material models for reinforced concrete plates and shells",
Jan Arve Øverli, 1998:95, ISBN 82-471-0297-8, ISSN 0802-3271.

"Chloride binding in concrete. Effect of surrounding environment and concrete composition",
Claus Kenneth Larsen, 1998:101, ISBN 82-471-0337-0, ISSN 0802-3271.

"Rotational capacity of aluminium alloy beams",
Lars A. Moen, 1999:1, ISBN 82-471-0365-6, ISSN 0802-3271.

"Stretch Bending of Aluminium Extrusions",
Arild H. Clausen, 1999:29, ISBN 82-471-0396-6, ISSN 0802-3271.

"Aluminium and Steel Beams under Concentrated Loading",
Tore Tryland, 1999:30, ISBN 82-471-0397-4, ISSN 0802-3271.

"Engineering Models of Elastoplasticity and Fracture for Aluminium Alloys",
Odd-Geir Lademo, 1999:39, ISBN 82-471-0406-7, ISSN 0802-3271.

"Kapasitet og duktilitet av dybelforbindelser i trekonstruksjoner",
Jan Siem, 1999:46, ISBN 82-471-0414-8, ISSN 0802-3271.

"Etablering av distribuert ingeniørarbeid; Teknologiske og organisatoriske erfaringer fra en norsk ingeniørbedrift",
Lars Line, 1999:52, ISBN 82-471-0420-2, ISSN 0802-3271.

"Estimation of Earthquake-Induced Response",
Símon Ólafsson, 1999:73, ISBN 82-471-0443-1, ISSN 0802-3271.

"Coastal Concrete Bridges: Moisture State, Chloride Permeability and Aging Effects"
Ragnhild Holen Relling, 1999:74, ISBN 82-471-0445-8, ISSN 0802-3271.

"Capacity Assessment of Titanium Pipes Subjected to Bending and External Pressure",
Arve Bjørset, 1999:100, ISBN 82-471-0473-3, ISSN 0802-3271.

“Validation of Numerical Collapse Behaviour of Thin-Walled Corrugated Panels”,
Håvar Ilstad, 1999:101, ISBN 82-471-0474-1, ISSN 0802-3271.

“Strength and Ductility of Welded Structures in Aluminium Alloys”,
Miroslaw Matusiak, 1999:113, ISBN 82-471-0487-3, ISSN 0802-3271.

“Thermal Dilation and Autogenous Deformation as Driving Forces to Self-Induced Stresses in High Performance Concrete”,
Øyvind Bjøntegaard, 1999:121, ISBN 82-7984-002-8, ISSN 0802-3271.

“Some Aspects of Ski Base Sliding Friction and Ski Base Structure”,
Dag Anders Moldestad, 1999:137, ISBN 82-7984-019-2, ISSN 0802-3271.

"Electrode reactions and corrosion resistance for steel in mortar and concrete",
Roy Antonsen, 2000:10, ISBN 82-7984-030-3, ISSN 0802-3271.

"Hydro-Physical Conditions in Kelp Forests and the Effect on Wave Damping and Dune Erosion. A case study on Laminaria Hyperborea",
Stig Magnar Løvås, 2000:28, ISBN 82-7984-050-8, ISSN 0802-3271.

"Random Vibration and the Path Integral Method",
Christian Skaug, 2000:39, ISBN 82-7984-061-3, ISSN 0802-3271.

"Buckling and geometrical nonlinear beam-type analyses of timber structures",
Trond Even Eggen, 2000:56, ISBN 82-7984-081-8, ISSN 0802-3271.

”Structural Crashworthiness of Aluminium Foam-Based Components”,
Arve Grønsund Hanssen, 2000:76, ISBN 82-7984-102-4, ISSN 0809-103X.

“Measurements and simulations of the consolidation in first-year sea ice ridges, and some aspects of mechanical behaviour”,
Knut V. Høyland, 2000:94, ISBN 82-7984-121-0, ISSN 0809-103X.

”Kinematics in Regular and Irregular Waves based on a Lagrangian Formulation”,
Svein Helge Gjøsund, 2000-86, ISBN 82-7984-112-1, ISSN 0809-103X.

”Self-Induced Cracking Problems in Hardening Concrete Structures”,
Daniela Bosnjak, 2000-121, ISBN 82-7984-151-2, ISSN 0809-103X.

"Ballistic Penetration and Perforation of Steel Plates",
Tore Børvik, 2000:124, ISBN 82-7984-154-7, ISSN 0809-103X.

"Freeze-Thaw resistance of Concrete. Effect of: Curing Conditions, Moisture Exchange and Materials",
Terje Finnerup Rønning, 2001:14, ISBN 82-7984-165-2, ISSN 0809-103X

"Structural behaviour of post tensioned concrete structures. Flat slab. Slabs on ground",
Steinar Trygstad, 2001:52, ISBN 82-471-5314-9, ISSN 0809-103X.

"Slipforming of Vertical Concrete Structures. Friction between concrete and slipform panel",
Kjell Tore Fosså, 2001:61, ISBN 82-471-5325-4, ISSN 0809-103X.

"Some numerical methods for the simulation of laminar and turbulent incompressible flows",
Jens Holmen, 2002:6, ISBN 82-471-5396-3, ISSN 0809-103X.

“Improved Fatigue Performance of Threaded Drillstring Connections by Cold Rolling”,
Steinar Kristoffersen, 2002:11, ISBN: 82-421-5402-1, ISSN 0809-103X.

"Deformations in Concrete Cantilever Bridges: Observations and Theoretical Modelling",
Peter F. Takâcs, 2002:23, ISBN 82-471-5415-3, ISSN 0809-103X.

"Stiffened aluminium plates subjected to impact loading",
Hilde Giæver Hildrum, 2002:69, ISBN 82-471-5467-6, ISSN 0809-103X.

"Full- and model scale study of wind effects on a medium-rise building in a built up area",
Jónas Thór Snæbjørnsson, 2002:95, ISBN82-471-5495-1, ISSN 0809-103X.

“Evaluation of Concepts for Loading of Hydrocarbons in Ice-infested water”,
Arnor Jensen, 2002:114, ISBN 82-417-5506-0, ISSN 0809-103X.

”Numerical and Physical Modelling of Oil Spreading in Broken Ice”,
Janne K. Økland Gjøsteen, 2002:130, ISBN 82-471-5523-0, ISSN 0809-103X.

”Diagnosis and protection of corroding steel in concrete”,
Franz Pruckner, 20002:140, ISBN 82-471-5555-4, ISSN 0809-103X.

“Tensile and Compressive Creep of Young Concrete: Testing and Modelling”,
Dawood Atrushi, 2003:17, ISBN 82-471-5565-6, ISSN 0809-103X.

“Rheology of Particle Suspensions. Fresh Concrete, Mortar and Cement Paste with Various Types of Lignosulfonates”,
Jon Elvar Wallevik, 2003:18, ISBN 82-471-5566-4, ISSN 0809-103X.

“Oblique Loading of Aluminium Crash Components”,
Aase Reyes, 2003:15, ISBN 82-471-5562-1, ISSN 0809-103X.

“Utilization of Ethiopian Natural Pozzolans”,
Surafel Ketema Desta, 2003:26, ISSN 82-471-5574-5, ISSN:0809-103X.

“Behaviour and strength prediction of reinforced concrete structures with discontinuity regions”, Helge Brå, 2004:11, ISBN 82-471-6222-9, ISSN 1503-8181.

“High-strength steel plates subjected to projectile impact. An experimental and numerical study”, Sumita Dey, 2004:38, ISBN 82-471-6282-2 (printed version), ISBN 82-471-6281-4 (electronic version), ISSN 1503-8181.

“Alkali-reactive and inert fillers in concrete. Rheology of fresh mixtures and expansive reactions.”
Bård M. Pedersen, 2004:92, ISBN 82-471-6401-9 (printed version), ISBN 82-471-6400-0 (electronic version), ISSN 1503-8181.

“On the Shear Capacity of Steel Girders with Large Web Openings”.
Nils Christian Hagen, 2005:9 ISBN 82-471-6878-2 (printed version), ISBN 82-471-6877-4 (electronic version), ISSN 1503-8181.

”Behaviour of aluminium extrusions subjected to axial loading”.
Østen Jensen, 2005:7, ISBN 82-471-6873-1 (printed version), ISBN 82-471-6872-3 (electronic version), ISSN 1503-8181.

”Thermal Aspects of corrosion of Steel in Concrete”.
Jan-Magnus Østvik, 2005:5, ISBN 82-471-6869-3 (printed version), ISBN 82-471-6868 (electronic version), ISSN 1503-8181.

”Mechanical and adaptive behaviour of bone in relation to hip replacement.” A study of bone remodelling and bone grafting.
Sébastien Muller, 2005:34, ISBN 82-471-6933-9 (printed version), ISBN 82-471-6932-0 (electronic version), ISSN 1503-8181.

“Analysis of geometrical nonlinearities with applications to timber structures”.
Lars Wollebæk, 2005:74, ISBN 82-471-7050-5 (printed version), ISBN 82-471-7019-1 (electronic version), ISSN 1503-8181.

“Pedestrian induced lateral vibrations of slender footbridges”,
Anders Rönnquist, 2005:102, ISBN 82-471-7082-5 (printed version), ISBN 82-471-7081-7 (electronic version), ISSN 1503-8181.

“Initial Strength Development of Fly Ash and Limestone Blended Cements at Various Temperatures Predicted by Ultrasonic Pulse Velocity”,
Tom Ivar Fredvik, 2005:112, ISBN 82-471-7105-8 (printed version), ISBN 82-471-7103-1 (electronic version), ISSN 1503-8181.

“Behaviour and modelling of thin-walled cast components”,
Cato Dørum, 2005:128, ISBN 82-471-7140-6 (printed version), ISBN 82-471-7139-2 (electronic version), ISSN 1503-8181.

“Behaviour and modelling of selfpiercing riveted connections”,
Raffaele Porcaro, 2005:165, ISBN 82-471-7219-4 (printed version), ISBN 82-471-7218-6 (electronic version), ISSN 1503-8181.

”Behaviour and Modelling og Aluminium Plates subjected to Compressive Load”,
Lars Rønning, 2005:154, ISBN 82-471-7169-1 (printed version), ISBN 82-471-7195-3 (electronic version), ISSN 1503-8181.

”Bumper beam-longitudinal system subjected to offset impact loading”,
Satyanarayana Kokkula, 2005:193, ISBN 82-471-7280-1 (printed version), ISBN 82-471-7279-8 (electronic version), ISSN 1503-8181.

“Control of Chloride Penetration into Concrete Structures at Early Age”,
Guofei Liu, 2006:46, ISBN 82-471-7838-9 (printed version), ISBN 82-471-7837-0 (electronic version), ISSN 1503-8181.

“Modelling of Welded Thin-Walled Aluminium Structures”,
Ting Wang, 2006:78, ISBN 82-471-7907-5 (printed version), ISBN 82-471-7906-7 (electronic version), ISSN 1503-8181.

”Time-variant reliability of dynamic systems by importance sampling and probabilistic analysis of ice loads”,
Anna Ivanova Olsen, 2006:139, ISBN 82-471-8041-3 (printed version), ISBN 82-471-8040-5 (electronic version), ISSN 1503-8181.

“Fatigue life prediction of an aluminium alloy automotive component using finite element analysis of surface topography”.
Sigmund Kyrre Ås, 2006:25, ISBN 82-471-7791-9 (printed version), ISBN 82-471-7791-9 (electronic version), ISSN 1503-8181.

”Constitutive models of elastoplasticity and fracture for aluminium alloys under strain path change”,
Dasharatha Achani, 2006:76, ISBN 82-471-7903-2 (printed version), ISBN 82-471-7902-4 (electronic version), ISSN 1503-8181.

“Simulations of 2D dynamic brittle fracture by the Element-free Galerkin method and linear fracture mechanics”,
Tommy Karlsson, 2006:125, ISBN 82-471-8011-1 (printed version), ISBN 82-471-8010-3 (electronic version), ISSN 1503-8181.

“Penetration and Perforation of Granite Targets by Hard Projectiles”,
Chong Chiang Seah, 2006:188, ISBN 82-471-8150-9 (printed version), ISBN 82-471-8149-5 (electronic version), ISSN 1503-8181.

"Deformations, strain capacity and cracking of concrete in plastic and early hardening phases",
Tor Arne Hammer, 2007:234, ISBN 978-82-471-5191-4 (printed version), ISBN 978-82-471-5207-2 (electronic version), ISSN 1503-8181.

"Crashworthiness of dual-phase high-strength steel: Material and Component behaviour", Venkatapathi Tarigopula, 2007:230, ISBN 82-471-5076-4 (printed version), ISBN 82-471-5093-1 (electronic version), ISSN 1503-8181.

"Fibre reinforcement in load carrying concrete structures",
Åse Lyslo Døssland, 2008:50, ISBN 978-82-471-6910-0 (printed version), ISBN 978-82-471-6924-7 (electronic version), ISSN 1503-8181.

"Low-velocity penetration of aluminium plates",
Frode Grytten, 2008:46, ISBN 978-82-471-6826-4 (printed version), ISBN 978-82-471-6843-1 (electronic version), ISSN 1503-8181.

"Robustness studies of structures subjected to large deformations",
Ørjan Fyllingen, 2008:24, ISBN 978-82-471-6339-9 (printed version), ISBN 978-82-471-6342-9 (electronic version), ISSN 1503-8181.

"Constitutive modelling of morsellised bone",
Knut Birger Lunde, 2008:92, ISBN 978-82-471-7829-4 (printed version), ISBN 978-82-471-7832-4 (electronic version), ISSN 1503-8181.

"Experimental Investigations of Wind Loading on a Suspension Bridge Girder",
Bjørn Isaksen, 2008:131, ISBN 978-82-471-8656-5 (printed version), ISBN 978-82-471-8673-2 (electronic version), ISSN 1503-8181.

"Cracking Risk of Concrete Structures in The Hardening Phase",
Guomin Ji, 2008:198, ISBN 978-82-471-1079-9 (printed version), ISBN 978-82-471-1080-5 (electronic version), ISSN 1503-8181.

"Modelling and numerical analysis of the porcine and human mitral apparatus",
Victorien Emile Prot, 2008:249, ISBN 978-82-471-1192-5 (printed version), ISBN 978-82-471-1193-2 (electronic version), ISSN 1503-8181.

"Strength analysis of net structures",
Heidi Moe, 2009:48, ISBN 978-82-471-1468-1 (printed version), ISBN 978-82-471-1469-8 (electronic version), ISSN1503-8181.

"Numerical analysis of ductile fracture in surface cracked shells",
Espen Berg, 2009:80, ISBN 978-82-471-1537-4 (printed version), ISBN 978-82-471-1538-1 (electronic version), ISSN 1503-8181.

"Subject specific finite element analysis of bone – for evaluation of the healing of a leg lengthening and evaluation of femoral stem design",
Sune Hansborg Pettersen, 2009:99, ISBN 978-82-471-1579-4 (printed version), ISBN 978-82-471-1580-0 (electronic version), ISSN 1503-8181.

"Evaluation of fracture parameters for notched multi-layered structures",
Lingyun Shang, 2009:137, ISBN 978-82-471-1662-3 (printed version), ISBN 978-82-471-1663-0 (electronic version), ISSN 1503-8181.

"Modelling of Dynamic Material Behaviour and Fracture of Aluminium Alloys for Structural Applications"
Yan Chen, 2009:69, ISBN 978-82-471-1515-2 (printed version), ISBN 978-82 471-1516-9 (electronic version), ISSN 1503-8181.

"Nanomechanics of polymer and composite particles"
Jianying He 2009:213, ISBN 978-82-471-1828-3 (printed version), ISBN 978-82-471-1829-0 (electronic version), ISSN 1503-8181.

"Mechanical properties of clear wood from Norway spruce"
Kristian Berbom Dahl 2009:250, ISBN 978-82-471-1911-2 (printed version) ISBN 978-82-471-1912-9 (electronic version), ISSN 1503-8181.

"Modeling of the degradation of TiB_2 mechanical properties by residual stresses and liquid Al penetration along grain boundaries"
Micol Pezzotta 2009:254, ISBN 978-82-471-1923-5 (printed version) ISBN 978-82-471-1924-2 (electronic version) ISSN 1503-8181.

"Effect of welding residual stress on fracture"
Xiabo Ren 2010:77, ISBN 978-82-471-2115-3 (printed version) ISBN 978-82-471-2116-0 (electronic version), ISSN 1503-8181.

"Pan-based carbon fiber as anode material in cathodic protection system for concrete structures"
Mahdi Chini 2010:122, ISBN 978-82-471-2210-5 (printed version) ISBN 978-82-471-2213-6 (electronic version), ISSN 1503-8181.

"Structural Behaviour of deteriorated and retrofitted concrete structures"
Irina Vasililjeva Sæther 2010:171, ISBN 978-82-471-2315-7 (printed version) ISBN 978-82-471-2316-4 (electronic version) ISSN 1503-8181.

"Prediction of local snow loads on roofs"
Vivian Meløysund 2010:247, ISBN 978-82-471-2490-1 (printed version) ISBN 978-82-471-2491-8 (electronic version) ISSN 1503-8181.

"Behaviour and modelling of polymers for crash applications"
Virgile Delhaye 2010:251, ISBN 978-82-471-2501-4 (printed version) ISBN 978-82-471-2502-1 (electronic version) ISSN 1503-8181.

"Blended cement with reducted CO_2 emission – Utilizing the Fly Ash-Limestone Synergy",
Klaartje De Weerdt 2011:32, ISBN 978-82-471-2584-7 (printed version) ISBN 978-82-471-2584-4 (electronic version) ISSN 1503-8181.

"Chloride induced reinforcement corrosion in concrete" Concept of critical chloride content – methods and mechanisms.
Ueli Angst 2011:113, ISBN 978-82-471-2769-9 (printed version) ISBN 978-82-471-2763-6 (electronic version) ISSN 1503-8181.

"A thermo-electric-Mechanical study of the carbon anode and contact interface for Energy savings in the production of aluminium".
Dag Herman Andersen 2011:157, ISBN 978-82-471-2859-6 (printed version) ISBN 978-82-471-2860-2 (electronic version) ISSN 1503-8181.

"Structural Capacity of Anchorage Ties in Masonry Veneer Walls Subjected to Earthquake". The implications of Eurocode 8 and Eurocode 6 on a typical Norwegain veneer wall.
Ahmed Mohamed Yousry Hamed 2011:181, ISBN 978-82-471-2911-1 (printed version) ISBN 978-82-471-2912-8 (electronic ver.) ISSN 1503-8181.

"Work-hardening behaviour in age-hardenable Al-Zn-Mg(-Cu) alloys".
Ida Westermann , 2011:247, ISBN 978-82-471-3056-8 (printed ver.) ISBN 978-82-471-3057-5 (electronic ver.) ISSN 1503-8181.

"Behaviour and modelling of selfpiercing riveted connections using aluminium rivets".
Nguyen-Hieu Hoang, 2011:266, ISBN 978-82-471-3097-1 (printed ver.) ISBN 978-82-471-3099-5 (electronic ver.) ISSN 1503-8181.

"Fibre reinforced concrete".
Sindre Sandbakk, 2011:297, ISBN 978-82-471-3167-1 (printed ver.) ISBN 978-82-471-3168-8 (electronic ver) ISSN 1503:8181.

"Dynamic behaviour of cablesupported bridges subjected to strong natural wind".
Ole Andre Øiseth, 2011:315, ISBN 978-82-471-3209-8 (printed ver.) ISBN 978-82-471-3210-4 (electronic ver.) ISSN 1503-8181.

"Constitutive modeling of solargrade silicon materials"
Julien Cochard, 2011:307, ISBN 978-82-471-3189-3 (printed ver). ISBN 978-82-471-3190-9 (electronic ver.) ISSN 1503-8181.

"Constitutive behavior and fracture of shape memory alloys"
Jim Stian Olsen, 2012:57, ISBN 978-82-471-3382-8 (printed ver.) ISBN 978-82-471-3383-5 (electronic ver.) ISSN 1503-8181.

"Field measurements in mechanical testing using close-range photogrammetry and digital image analysis"
Egil Fagerholt, 2012:95, ISBN 978-82-471-3466-5 (printed ver.) ISBN 978-82-471-3467-2 (electronic ver.) ISSN 1503-8181.

"Towards a better under standing of the ultimate behaviour of lightweight aggregate concrete in compression and bending",
Håvard Nedrelid, 2012:123, ISBN 978-82-471-3527-3 (printed ver.) ISBN 978-82-471-3528-0 (electronic ver.) ISSN 1503-8181.

"Numerical simulations of blood flow in the left side of the heart"
Sigrid Kaarstad Dahl, 2012:135, ISBN 978-82-471-3553-2 (printed ver.) ISBN 978-82-471-3555-6 (electronic ver.) ISSN 1503-8181.

"Moisture induced stresses in glulam"
Vanessa Angst-Nicollier, 2012:139, ISBN 978-82-471-3562-4 (printed ver.) ISBN 978-82-471-3563-1 (electronic ver.) ISSN 1503-8181.

"Biomechanical aspects of distraction osteogensis"
Valentina La Russa, 2012:250, ISBN 978-82-471-3807-6 (printed ver.) ISBN 978-82-471-3808-3 (electronic ver.) ISSN 1503-8181.

"Ductile fracture in dual-phase steel. Theoretical, experimental and numerical study"
Gaute Gruben, 2012:257, ISBN 978-82-471-3822-9 (printed ver.) ISBN 978-82-471-3823-6 (electronic ver.) ISSN 1503-8181.

"Damping in Timber Structures"
Nathalie Labonnote, 2012:263, ISBN 978-82-471-3836-6 (printed ver.) ISBN 978-82-471-3837-3 (electronic ver.) ISSN 1503-8181.

"Biomechanical modeling of fetal veins: The umbilical vein and ductus venosus bifurcation"
Paul Roger Leinan, 2012:299, ISBN 978-82-471-3915-8 (printed ver.) ISBN 978-82-471-3916-5 (electronic ver.) ISSN 1503-8181.

"Large-Deformation behaviour of thermoplastics at various stress states"
Anne Serine Ognedal, 2012:298, ISBN 978-82-471-3913-4 (printed ver.) ISBN 978-82-471-3914-1 (electronic ver.) ISSN 1503-8181.

"Hardening accelerator for fly ash blended cement"
Kien Dinh Hoang, 2012:366, ISBN 978-82-471-4063-5 (printed ver.) ISBN 978-82-471-4064-2 (electronic ver.) ISSN 1503-8181.

"From molecular structure to mechanical properties"
Jianyang Wu, 2013:186, ISBN 978-82-471-4485-5 (printed ver.) ISBN 978-82-471-4486-2 (electronic ver.) ISSN 1503-8181.

"Experimental and numerical study of hybrid concrete structures"
Linn Grepstad Nes, 2013:259, ISBN 978-82-471-4644-6 (printed ver.) ISBN 978-82-471-4645-3 (electronic ver.) ISSN 1503-8181.

"Mechanics of ultra-thin multi crystalline silicon wafers"
Saber Saffar, 2013:199, ISBN 978-82-471-4511-1 (printed ver.) ISBN 978-82-471-4513-5 (electronic ver). ISSN 1503-8181.

"Through process modelling of welded aluminium structures"
Anizahyati Alisibramulisi, 2013:325, ISBN 978-82-471-4788-7 (printed ver.) ISBN 978-82-471-4789-4 (electronic ver.) ISSN 1503-8181.

"Combined blast and fragment loading on steel plates"
Knut Gaarder Rakvåg, 2013:361, ISBN978-82-471-4872-3 (printed ver.) ISBN 978-82-4873-0 (electronic ver.). ISSN 1503-8181.

"Characterization and modelling of the anisotropic behaviour of high-strength aluminium alloy"
Marion Fourmeau, 2014:37, ISBN 978-82-326-0008-3 (printed ver.) ISBN 978-82-326-0009-0 (electronic ver.) ISSN 1503-8181.

"Behaviour of threated steel fasteners at elevated deformation rates"
Henning Fransplass, 2014:65, ISBN 978-82-326-0054-0 (printed ver.) ISBN 978-82-326-0055-7 (electronic ver.) ISSN 1503-8181.

"Sedimentation and Bleeding"
Ya Peng, 2014:89, ISBN 978-82-326-0102-8 (printed ver.) ISBN 978-82-326-0103-5 (electric ver.) ISSN 1503-8181.

"Impact against X65 offshore pipelines"
Martin Kristoffersen, 2014:362, ISBN 978-82-326-0636-8 (printed ver.) ISBN 978-82-326-0637-5 (electronic ver.) ISSN 1503-8181.

"Formability of aluminium alloy subjected to prestrain by rolling"
Dmitry Vysochinskiy, 2014:363,, ISBN 978-82-326-0638-2 (printed ver.) ISBN 978-82-326-0639-9 (electronic ver.) ISSN 1503-8181.

"Experimental and numerical study of Yielding, Work-Hardening and anisotropy in textured AA6xxx alloys using crystal plasticity models"
Mikhail Khadyko, 2015:28, ISBN 978-82-326-0724-2 (printed ver.) ISBN 978-82-326-0725-9 (electronic ver.) ISSN 1503-8181.

"Behaviour and Modelling of AA6xxx Aluminium Alloys Under a Wide Range of Temperatures and Strain Rates"
Vincent Vilamosa, 2015:63, ISBN 978-82-326-0786-0 (printed ver.) ISBN 978-82-326-0787-7 (electronic ver.) ISSN 1503-8181.

"A Probabilistic Approach in Failure Modelling of Aluminium High Pressure Die-Castings"
Octavian Knoll, 2015:137, ISBN 978-82-326-0930-7 (printed ver.) ISBN 978-82-326-0931-4 (electronic ver.) ISSN 1503-8181.

"Ice Abrasion on Marine Concrete Structures"
Egil Møen, 2015:189, ISBN 978-82-326-1034-1 (printed ver.) ISBN 978-82-326-1035-8 (electronic ver.) ISSN 1503-8181.

"Fibre Orientation in Steel-Fibre-Reinforced Concrete"
Giedrius Zirgulis, 2015:229, ISBN 978-82-326-1114-0 (printed ver.) ISBN 978-82-326-1115-7 (electronic ver.) ISSN 1503-8181.

"Effect of spatial variation and possible interference of localised corrosion on the residual capacity of a reinforced concrete beam"
Mohammad Mahdi Kioumarsi, 2015:282, ISBN 978-82-326-1220-8 (printed ver.) ISBN 978-82-1221-5 (electronic ver.) ISSN 1503-8181.

"The role of concrete resistivity in chloride-induced macro-cell corrosion"
Karla Horbostel, 2015:324, ISBN 978-82-326-1304-5 (printed ver.) ISBN 978-82-326-1305-2 (electonic ver.) ISSN 1503-8181.

"Flowable fibre-reinforced concrete for structural applications"
Elena Vidal Sarmiento, 2015-335, ISBN 978-82-326-1324-3 (printed ver.) ISBN 978-82-326-1325-0 (electronic ver.) ISSN 1503-8181.

"Development of chushed sand for concrete production with microproportioning"
Rolands Cepuritis, 2016:19, ISBN 978-82-326-1382-3 (printed ver.) ISBN 978-82-326-1383-0 (electronic ver.) ISSN 1503-8181.

"Withdrawal properties of threaded rods embedded in glued-laminated timer elements"
Haris Stamatopoulos, 2016:48, ISBN 978-82-326-1436-3 (printed ver.) ISBN 978-82-326-1437-0 (electronic ver.) ISSN 1503-8181.

"An Experimental and numerical study of thermoplastics at large deformation"
Marius Andersen, 2016:191, ISBN 978-82-326-1720-3 (printed ver.) ISBN 978-82-326-1721-0 (electronic ver.) ISSN 1503-8181.

"Modeling and Simulation of Ballistic Impact"
Jens Kristian Holmen, 2016:240, ISBN 978-82-326-1818-7 (printed ver). ISBN 978-82-326-1819-4 (electronic ver.) ISSN 1503-8181.

"Early age crack assessment of concrete structures"
Anja B. Estensen Klausen, 2016:256, ISBN 978-82-326-1850-7 (printed ver). ISBN 978-82-326-1851-4 (electronic ver.) ISSN 1503-8181.

"Uncertainty quantification and sensitivity analysis for cardiovascular models"
Vinzenz Gregor Eck, 2016:234, ISBN 978-82-326-1806-4 (printed ver.) ISBN 978-82-326-1807-1 (electronic ver.) ISSN 1503-8181.

"Dynamic behaviour of existing and new railway catenary systems under Norwegain conditions"
Petter Røe Nåvik, 2016:298, ISBN 978-82-326-1935-1 (printed ver.) ISBN 978-82-326-1934-4 (electronic ver.) ISSN 1503-8181.

"Mechanical behaviour of particle-filled elastomers at various temperatures"
Arne Ilseng, 2016-295, ISBN978-82-326-1928-3 (printed ver.) ISBN 978-82-326-1929-0 (electronic ver.) ISSN 1503-8181.

"Nanotechnology for Anti-Icing Application"
Zhiwei He, 2016:348, ISBN 978-82-326-2038-8 (printed ver.) ISBN 978-82-326-2019-5 (electronic ver.) ISSN 1503-8181.

"Conduction Mechanisms in Conductive Adhesives with Metal-Coated Polyer Spheres"
Sigurd Rolland Pettersen, 2016:349, ISBN 978-326-2040-1 (printed ver,) ISBN 978-82-326-2041-8 (electronic ver.) ISSN 1503-8181.

"The interaction between calcium lignosulfonate and cement"
Alessia Colombo, 2017:20, ISBN 978-82-326-2122-4 (printed ver.) ISBN 978-82-326-2123-1 (electronic ver.) ISSN 1503-8181.

"Behaviour and Modelling of Flexible Structures Subjected to Blast Loading"
Vegard Aune, 2017:101, ISBN 978-82-326-2274-0 (printed ver.) ISBN 978-82-326-2275-7 (electronic ver.) ISSN 1503-8181.

"Behaviour of steel connections under quasi-static and impact loading"
Erik Løhre Grimsmo, 2017:159, ISBN 978-82-326-2390-7 (printed ver.) ISBN 978-82-326-2391-4 (electronic ver.) ISSN 1503-8181.

"An experimental and numerical study of cortical bone at he macro and Nano-scale"
Masoud Ramenzanzadehkoldeh,, 2017:208, ISBN 978-82-326-2488-1 (printed ver.) ISBN 978-82-326-2489-8 (electronic ver.) ISSN 1503-8181.

"Optoelectrical Properties of a Novel Organic Semiconductor: 6,13-Dichloropentacene"
Mao Wang, 2017:130, ISBN 978-82-326-2332-7 (printed ver.) ISBN 978-82-326-2333-4) (electronic ver.) ISSN 1503-8181.

"Core-shell structured microgels and their behavior at oil and water interface"
Yi Gong, 2017:182, ISBN 978-82-326-2436-2 (printed. ver.) ISBN 978-82-326-2437-9 (electronic ver.) ISSN 1503-8181.

"Aspects of design of reinforced concrete structures using nonliear finite element analyses"
Morten Engen, 2017:149, ISBN 978-82-326-2370-9 (printed ver.) ISBN 978-82-326-2371-6 (electronic ver.) ISSN 1503-8181.

"Numerical studies on ductile failure of aluminium alloys"
Lars Edvard Dæhli, 2017:284, ISBN 978-82-326-2636-6 (printed ver.) ISBN 978-82-326-2637-3 (electronic ver.) ISSN 1503-8181.

"Modelling and Assessment of Hydrogen Embrittlement in Steels and Nickel Alloys"
Haiyang Yu, 2017:278, ISBN 978-82-326-2624-3 (printed. ver.) ISBN 978-82-326-2625-0 (electronic ver.) ISSN 1503-8181.

"Network arch timber bridges with light timber deck on transverse crossbeams"
Anna Weronika Ostrycharczyk, 2017:318, ISBN 978-82-326-2704-2 (printed ver.) ISBN 978-82-326-2705-9 (electronic ver.) ISSN 1503-8181.

"Splicing of Large Glued Laminated Timber Elements by Use of Long Threated Rods"
Martin Cepelka, 2017:320, ISBN 978-82-326-2708-0 (printed ver.) ISBN 978-82-326-2709-7 (electronic ver.) ISSN 1503-8181.

"Thermomechanical behaviour of semi-crystalline polymers: experiments, modelling and simulation"
Joakim Johnsen, 2017-317, ISBN 978-82-326-2702-8 (printed ver.) ISBN 978-82-326-2703-5 (electronic ver.) ISSN 1503-8181.

"Small-Scale Plasiticity under Hydrogen Environment"
Kai Zhao, 2017:356, ISBN 978-82-326-2782-0 (printed ver.) ISBN 978-82-326-2783-7 (electronic er.) ISSN 1503-8181.

"Risk and Reliability Based Calibration of Structural Design Codes"
Michele Baravalle, 2017:342, ISBN 978-82-326-2752-3 (printed ver,) ISBN 978-82-326-2753-0 (electronic ver.) ISSN 1503-8181.

"Dynamic behaviour of floating bridges exposed to wave excitation"
Knut Andreas Kvåle, 2017:365, ISBN 978-82-326-2800-1 (printed ver.) ISBN 978-82-326-2801-8 (electronic ver.) ISSN 1503-8181.

"Dolomite calcined clay composite cement – hydration and durability"
Alisa Lydia Machner, 2018:39, ISBN 978-82-326-2872-8 (printed ver.). ISBN 978-82-326-2873-5 (electronic ver.) ISSN 1503-8181.

"Modelling of the self-excited forces for bridge decks subjected to random motions: an experimental study"
Bartosz Siedziako, 2018:52, ISBN 978-82-326-2896-4 (printed ver.). ISBN 978-82-326-2897-1 (electronic ver.) ISSN 1503-8181.

"A probabilistic-based methodology for evaluation of timber facade constructions"
Klodian Gradeci, 2018:69, ISBN 978-82-326-2928-2 (printed ver.) ISBN 978-82-326-2929-9 (electronic ver.) ISSN 1503-8181.

"Behaviour and modelling of flow-drill screw connections"
Johan Kolstø Sønstabø, 2018:73, ISBN 978-82-326-2936-7 (printed ver.) ISBN 978-82-326-2937-4 (electronic ver.) ISSN 1503-8181.

"Full-scale investigation of the effects of wind turbulence characteristics on dynamic behavior of long-span cable-supported bridges in complex terrain"
Aksel Fenerci, 2018 100, ISBN 9978-82-326-2990-9 (printed ver.) ISBN 978-82-326-2991-6 (electronic ver.) ISSN 1503-8181.

"Modeling and simulation of the soft palate for improved understanding of the obstructive sleep apnea syndrome"
Hongliang Liu, 2018:101, ISBN 978-82-326-2992-3 (printed ver.) ISBN 978-82-326-2993-0 (electronic ver.) ISSN 1503-8181.

"Long-term extreme response analysis of cable-supported bridges with floating pylons subjected to wind and wave loads".
Yuwang Xu, 2018:229, ISBN 978-82-326-3248-0 (printed ver.) ISBN 978-82-326-3249-7 (electronic ver.) ISSN 1503-8181.

"Reinforcement corrosion in carbonated fly ash concrete"
Andres Belda Revert, 2018:230, ISBN 978-82-326-3250-3 (printed ver.) ISBN 978-82-326-3251-0 (electronic ver.) ISSN 1503-8181.

"Direct finite element method for nonliear earthquake analysis of concrete dams including dam-water-foundation rock interaction"
Arnkjell Løkke, 2018:252, ISBN 978-82-326-3294-7 (printed ver.) ISBN 978-82-326-3295-4 (electronic ver.) ISSN 1503-8181.

"Electromechanical characterization of metal-coated polymer spheres for conductive adhesives"
Molly Strimbeck Bazilchuk, 2018:295, ISBN 978-82-326-3380-7 (printed. ver.) ISBN 978-82-326-3381-4 (electrical ver.) ISSN 1503-8181.

"Determining the tensile properties of Artic materials and modelling their effects on fracture"
Shengwen Tu, 2018:269, ISBN 978-82-326-3328-9 (printed ver.) ISBN 978-82-326-3329-6 (electronic ver.) ISSN 1503-8181.

"Atomistic Insigth into Tranportation of Nanofluid in Ultra-confined Channel"
Xiao Wang, 2018:334, ISBN978-82-326-3456-9 (printed ver.) ISBN 978-82-326-3457-6 (electronic ver.) ISSN 1503-8181.

“An experimental and numerical study of the mechanical behaviour of short glass-fibre reinforced thermoplastics”.
Jens Petter Henrik Holmstrøm, 2019:79, ISBN 978-82-326-3760-7 (printed ver.) ISBN 978-82-326-3761-4 (electronic ver.) ISSN 1503-8181.

“Uncertainty quantification and sensitivity analysis informed modeling of physical systems”
Jacob Sturdy, 2019:115, ISBN 978-82-326-3828-4 (printed ver.) ISBN 978-82-326-3829-1 (electric ver.) ISSN 1503-8181.

“Load model of historic traffic for fatigue life estimation of Norwegian railway bridges”
Gunnstein T. Frøseth, 2019:73, ISBN 978-82-326-3748-5 (printed ver.) ISBN 978-82-326-3749-2 (electronic ver.) ISSN 1503-8181.

“Force identification and response estimation in floating and suspension bridges using measured dynamic response”
Øyvind Wiig Petersen, 2019:88, ISBN 978-82-326-3778-2 (printed ver.) ISBN 978-82-326-377-9 (electronic ver.) ISSN 1503-8181.

“Consistent crack width calculation methods for reinforced concrete elements subjected to 1D and 2D stress states”
Reignard Tan, 2019:147, ISBN 978-82-326-3892-5 (printed ver.) ISBN 978-82-326-3893-2 (electronic ver.) ISSN 1503-8181.

“Nonlinear static and dynamic isogeometric analysis of slender spatial and beam type structures”
Siv Bente Raknes, 2019:181, ISBN 978-82-326-3958-8 (printed ver.) ISBN 978-82-326-3959-5 (electronic ver.) ISSN 1503-8181.

“Experimental study of concrete-ice abrasion and concrete surface topography modification”
Guzel Shamsutdinova, 2019:182, ISBN978-82-326-3960-1 (printed ver.) ISBN 978-82-326-3961-8 (electronic ver.) ISSN 1503-8181.

“Wind forces on bridge decks using state-of-the art FSI methods”
Tore Andreas Helgedagsrud, 2019:180, ISBN 978-82-326-3956-4 (printed ver.) ISBN 978-82-326-3957-1 (electronic ver.) ISSN 1503-8181.